

# Control of Alkali Species in Gasification Systems

## Final Report

S. Turn, C. Kinoshita, D. Ishimura, J. Zhou,  
T. Hiraki, and S. Masutani  
*Hawaii Natural Energy Institute  
Honolulu, Hawaii*



**NREL**

**National Renewable Energy Laboratory**

1617 Cole Boulevard  
Golden, Colorado 80401-3393

NREL is a U.S. Department of Energy Laboratory  
Operated by Midwest Research Institute • Battelle • Bechtel

Contract No. DE-AC36-99-GO10337

# Control of Alkali Species in Gasification Systems

## Final Report

S. Turn, C. Kinoshita, D. Ishimura, J. Zhou,  
T. Hiraki, and S. Masutani  
*Hawaii Natural Energy Institute  
Honolulu, Hawaii*

NREL Technical Monitor: Richard Bain

Prepared under Subcontract No. YCV-7-16662-01



# NREL

**National Renewable Energy Laboratory**

1617 Cole Boulevard  
Golden, Colorado 80401-3393

NREL is a U.S. Department of Energy Laboratory  
Operated by Midwest Research Institute • Battelle • Bechtel

Contract No. DE-AC36-99-GO10337

## NOTICE

This report was prepared as an account of work sponsored by an agency of the United States government. Neither the United States government nor any agency thereof, nor any of their employees, makes any warranty, express or implied, or assumes any legal liability or responsibility for the accuracy, completeness, or usefulness of any information, apparatus, product, or process disclosed, or represents that its use would not infringe privately owned rights. Reference herein to any specific commercial product, process, or service by trade name, trademark, manufacturer, or otherwise does not necessarily constitute or imply its endorsement, recommendation, or favoring by the United States government or any agency thereof. The views and opinions of authors expressed herein do not necessarily state or reflect those of the United States government or any agency thereof.

Available electronically at <http://www.doe.gov/bridge>

Available for a processing fee to U.S. Department of Energy  
and its contractors, in paper, from:

U.S. Department of Energy  
Office of Scientific and Technical Information  
P.O. Box 62  
Oak Ridge, TN 37831-0062  
phone: 865.576.8401  
fax: 865.576.5728  
email: [reports@adonis.osti.gov](mailto:reports@adonis.osti.gov)

Available for sale to the public, in paper, from:

U.S. Department of Commerce  
National Technical Information Service  
5285 Port Royal Road  
Springfield, VA 22161  
phone: 800.553.6847  
fax: 703.605.6900  
email: [orders@ntis.fedworld.gov](mailto:orders@ntis.fedworld.gov)  
online ordering: <http://www.ntis.gov/ordering.htm>



## ABSTRACT

Gas-phase alkali metal compounds contribute to fouling, slagging, corrosion, and agglomeration problems in energy conversion facilities. One mitigation strategy applicable at high temperature is to pass the gas stream through a fixed bed of sorbent or getter material, which preferentially adsorbs alkali via physical adsorption or chemisorption. This report presents results of an experimental investigation of high-temperature (600° to 700°C) alkali removal from a hot filtered gasifier product gas stream using a packed bed of sorbent material. Two getter materials, activated bauxite and emathlite, were tested at two levels of space time (0.7 and 1.5 s) by using two interchangeable reactors of different internal diameters (51 and 76 mm). The effect of getter particle size was also investigated.

The experimental apparatus consisted of a bench-scale fluidized bed gasifier, a hot ceramic filter unit, and a packed bed alkali getter reactor. Banagrass, a candidate crop for tropical and subtropical dedicated feedstock supply systems, was used as fuel. Banagrass's high K and Cl content facilitates experimental measurement of these trace elements at levels well above analytical detection limits. Potassium, Na, and Cl concentrations in the gas stream exiting the filter were 28, 11, and 1,300 ppmw, respectively, with total alkali to Cl ratios of ~0.03, indicating that Cl is present in forms other than alkali chlorides. Potassium and Na removal efficiencies by the getter beds were >99% and >92%, respectively, for all tests, with no apparent differences attributable to the variables tested: getter material, space time, or getter particle size. The highest concentrations of K and Na in the getter materials were measured in the sorbent recovered from the top 5 cm (inlet) of the packed bed. Average alkali concentrations of 4.6 mg K g<sup>-1</sup> sorbent and 1.1 mg Na g<sup>-1</sup> sorbent were measured in the 51-mm diameter reactor tests. Alkali concentrations in the top 5 cm of the 76-mm diameter reactor were lower because of the greater sorbent material volume.

Element balances around the getter reactor for K, Na, and Cl were generally poor because of the small analyte masses, compared to the total getter mass in the reactor. Element balances around the gasifier/ceramic filter/getter reactor system were generally acceptable. Carbon balances ranged from 93% to 103% of complete closure, with carbon conversion efficiencies on the order of 93%. Balances for K, which were present as ~1% of fuel mass, varied from 75% to 91% of closure. Balances for Cl (~0.6% of fuel mass) showed a wider range, from 63% to 93% of full closure. Sodium was present as ~0.1% of fuel mass, and elemental balances were in the range of 63% to 150%.

## TABLE OF CONTENTS

<b>1 . Introduction</b>	1
<b>2 . Review of Literature</b>	1
2.1 Alkali Removal Mechanisms	1
2.2 Experimental Methods	2
2.2.1 Thermogravimetric Studies	2
2.2.2 Packed Bed Studies	3
2.3 Materials	4
2.3.1 Emathlite and Fuller's Earth	5
2.3.1.1 Effects of Exposure Time	7
2.3.1.2 Effects of Water Vapor	10
2.3.1.3 Effects of Temperature	10
2.3.1.4 Effects of Gas Concentration	11
2.3.2 Bauxite	12
2.3.2.1 Effects of Gas-Phase Alkali Concentration	13
2.3.2.2 Effect of Sorbent Bed Temperature	15
2.3.2.3 Effect of Superficial Gas Velocity	15
2.3.2.4 Effect of Gas Hourly Space Velocity	15
2.3.2.5 Release of Alkali from Activated Bauxite	15
2.3.2.6 Regeneration of Activated Bauxite	16
2.3.3 Diatomaceous Earth	16
2.3.3.1 Alkali Capture Efficiency	16
2.3.3.2 Effect of Time Duration	17
2.3.4 Kaolinite	18
2.3.5 Low-Temperature Coal Char and Gasifier Ash	20
2.3.6 Attapulgius Clay	21
2.3.7 Burgess No. 10 Pigment	23
2.3.8 Silica Gel	23
2.3.9 Dolomite and Calcined Dolomite	23
2.4. Modeling	23
<b>3 . Materials and Methods</b>	24
3.1 Fuel	24
3.2 Getter Materials	24
3.3 Experimental Methods	24

<b>4. Results and Discussion</b>	33
4.1 Fuel Properties	33
4.2 Test Conditions	35
4.3 Gasifier Bed Material	38
4.4 Filter Char	38
4.5 Results from Baseline Test, 76G-B	41
4.6 Alkali Getter Tests	44
4.6.1 Alkali Getter Materials	44
4.6.2 Test Results	45
4.6.2.1 Test Conditions	45
4.6.2.2 Getter Visual Appearance	46
4.6.2.3 Getter Material Bulk Analyses	52
4.6.2.4 Getter Material Surface Analyses	56
4.6.2.5 Getter Reactor Exit Gas	56
4.6.2.6 Mass Balances	58
4.6.2.7 Comparison of Treatments	62
<b>5. Summary and Conclusions</b>	63
<b>6. References</b>	65
<b>Appendix A – TEST DATA</b>	68
Test 76G-B	
Test 76G-AB	
Test 51G-E	
Test 51G-AB	
Test 76G-E	
Test 51G-E-P	

## LIST OF FIGURES

Figure 1.	Sodium and K concentrations in pelleted emathlite (6.4 mm diameter, 6.4 mm length) as a function of duration of exposure to 10 ppmv NaCl and 4.6% H <sub>2</sub> O in N <sub>2</sub> carrier gas flow of 1 L min <sup>-1</sup> at 850°C, 1 bar.	8
Figure 2.	Sodium concentration in emathlite flake (0.5 mm thickness) as a function of duration of exposure to 150 ppmv NaCl in SFG (80% N <sub>2</sub> , 15% CO <sub>2</sub> , 3% O <sub>2</sub> , and 2% H <sub>2</sub> O) flow of 0.18 L min <sup>-1</sup> , 800°C, 1 bar.	9
Figure 3.	Percentage of initial K retained in emathlite pellets as a function of test temperature.	11
Figure 4.	Sample weight gain of emathlite flakes as a function of gas-phase NaCl concentration after 2-h exposure at 800°C, atmospheric pressure.	12
Figure 5.	Concentration of Na in bauxite as a function of time resulting from exposure to 185 ppmv NaCl in SFG (80% N <sub>2</sub> , 15% CO, 3% O <sub>2</sub> , and 2% H <sub>2</sub> O) at 800°C and atmospheric pressure.	14
Figure 6.	Weight gain of bauxite sample as a function of time resulting from exposure to 7.3 ppmv NaCl and 28.5 ppmv KCl in an Ar carrier gas at 800°C, atmospheric pressure.	14
Figure 7.	Weight gain of diatomaceous earth sample as a function of time.	17
Figure 8.	Sodium concentration of kaolin after 4-h exposure to 80 ppmv NaCl in various carrier gases at elevated temperature.	19
Figure 9.	Potassium concentration of kaolin after 4-h exposure to 80 ppmv NaCl in various carrier gases at elevated temperature.	19
Figure 10.	Weight gain of kaolinite sample as a function of time resulting from exposure to 230 ppmv NaCl SFG (80% N <sub>2</sub> , 15% CO, 3% O <sub>2</sub> , and 2% H <sub>2</sub> O) at 800°C and atmospheric pressure.	20
Figure 11.	Sodium concentration of coal char and gasifier ash-derived getter materials after 4-h exposure to 80 ppmv NaCl in various carrier gases at elevated temperature.	22
Figure 12.	Potassium concentration of coal char and gasifier ash-derived getter materials after 4-h exposure to 80 ppmv NaCl in various carrier gases at elevated temperature.	22
Figure 13.	Forced ambient air dryer containing chopped banagrass.	25

Figure 14. Schematic of bench-scale gasifier test facility.	26
Figure 15. Bench-scale fluidized bed reactor.	27
Figure 16. Heated ceramic filter assembly.	29
Figure 17. Fixed-bed, alkali getter reactor.	30
Figure 18. Fluidized-bed gasifier, ceramic filter, alkali getter reactor, and sample conditioning system	31
Figure 19. Major inorganic components of banagrass as percentage of fuel mass.	35
Figure 20. Elemental mass retained in the char as a percentage of elemental fuel input.	40
Figure 21. Element masses collected in various sections of the sample conditioning system with no getter material present in the alkali getter reactor (blank run).	43
Figure 22. Distribution of major element masses collected in the sample conditioning system as a percentage of total for blank run.	43
Figure 23. Samples of activated bauxite as-received from the manufacturer (fresh) and after exposure to 750°C/air environment for 4 h (heated).	48
Figure 24. Samples of emathlite as received from the manufacturer (fresh) and after exposure to 750°C/air environment for 4 h (heated).	48
Figure 25. Samples of activated bauxite recovered from the alkali getter reactor after test 76G-AB.	49
Figure 26. Samples of activated bauxite recovered from the alkali getter reactor after test 51G-AB.	49
Figure 27. Samples of emathlite recovered from the alkali getter reactor after test 51G-E.	50
Figure 28. Samples of emathlite recovered from the alkali getter reactor after test 76G-E.	50
Figure 29. Samples of emathlite recovered from the alkali getter reactor after test 51G-E-P.	51
Figure 30. Distribution of K, Na, and Cl in the activated bauxite from test 76G-AB as a function of cell location within the reactor.	53

Figure 31.	Distribution of K, Na, and Cl in the emathlite from test 51G-E as a function of cell location within the reactor.	54
Figure 32.	Distribution of K, Na, and Cl in the activated bauxite from test 51G-AB as a function of cell location within the reactor.	54
Figure 33.	Distribution of K, Na, and Cl in the emathlite from test 76G-E as a function of cell location within the reactor.	55
Figure 34.	Distribution of K, Na, and Cl in the emathlite from test 51G-E-P as a function of cell location within the reactor.	55
Figure 35.	Gas-phase concentration of K, Na, and Cl with an empty alkali getter reactor (blank) and with activated bauxite and emathlite used as getter materials in the 76-mm and 51-mm diameter getter reactors.	58
Figure 36.	Distribution of input stream gas-phase Cl between the getter material and the output gas stream.	59
Figure 37.	Distribution of input stream gas-phase K between the getter material and the output gas stream.	59
Figure 38.	Distribution of input stream gas-phase Na between the getter material and the output gas stream.	60
Figure 39.	Distribution of the Cl mass present in the input fuel among the outputs; gasifier bed, filter char, getter material, and gas phase.	61
Figure 40.	Distribution of the K mass present in the input fuel among the outputs; gasifier bed, filter char, getter material, and gas phase.	61
Figure 41.	Distribution of the Na mass present in the input fuel among the outputs; gasifier bed, filter char, getter material, and gas phase.	62

## LIST OF TABLES

Table 1.	Composition of alkali getter materials reported in the literature.	6
Table 2.	Thermodynamic equilibrium prediction of phase distribution in emathlite as a function of temperature.	7
Table 3.	Summary of analyses of banagrass samples taken from the gasifier fuel lot.	34
Table 4.	Summary of test conditions for the gasifier, hot ceramic filter, and alkali getter reactor.	37
Table 5.	Summary of elemental analyses of samples of bulk, pretest, gasifier bed material, and gasifier bed material recovered from the gasifier after each test.	39
Table 6.	Properties of ceramic filter char sample collected during the blank run test.	39
Table 7.	Element concentrations of Cl, K, and Na in the ceramic filter char for the test series.	40
Table 8.	Comparison of element concentrations (ppmw) in the dry product gas of the current study and previous measurements.	42
Table 9.	Vapor pressures of KCl and NaCl, and concentrations of K and Na as functions of temperature.	42
Table 10.	Compositions of as-received getter materials as provided by the manufacturer and as determined by independent analysis.	44
Table 11.	Comparison of getter material composition after 4 h at 750°C and moisture/volatile matter corrected data from Table 10.	45
Table 12.	Summary of test conditions and results for the alkali getter reactor.	46
Table 13.	Summary of semiquantitative elemental analyses of alkali getter material surfaces by SEM/XRF.	57

## 1. INTRODUCTION

Alkali metals, principally K and to a lesser extent Na, exist naturally in biomass.<sup>1,2</sup> Although present at minor levels, alkali and alkaline earth elements may be volatilized in thermal energy conversion facilities utilizing biomass fuels and react with other inorganic constituents, Si, S, and Cl, resulting in unwanted deposits and corrosion. In combustion systems,<sup>3-6</sup> alkali compounds foul heat transfer surfaces, participate in slag formation in grate-fired units, and contribute to the formation of fluidized bed agglomerates.<sup>7-9</sup> The result is reduced efficiency and availability of the energy conversion facility and increased operating costs. In the case of proposed biomass integrated gasifier combined-cycle systems, alkali vapor deposition onto combustion turbine working surfaces and subsequent hot corrosion are added concerns.<sup>10-13</sup>

One method of controlling alkali vapor in a hot gas stream is to remove it with alkali getters. In concept, getters would be employed as fixed beds of granular inorganic solid sorbents. In gasifier applications, getters would be located after hot gas filter equipment to remove alkali vapor before use in a gas turbine. An ideal getter material would possess characteristics of high temperature compatibility, rapid rates of adsorption, high loading capacity, transformation of alkali into a less corrosive form, and irreversible adsorption to prevent the release of adsorbed alkali during process fluctuations. Much of the past getter research<sup>14-22</sup> was concerned primarily with cleaning high-temperature (~800°-900°C) flue gases from pressurized, fluidized-bed combustors (PFBC) for use in gas turbine power generation applications. Getter beds were to be employed to simultaneously remove particulate and vapor-phase alkali. Gasifier combined cycle applications<sup>19,23</sup> were explored to a lesser extent and always in the context of using coal as the fuel source. In all the research, Na removal received greater emphasis than K removal. In the case of biomass fuels, K is often of greater concern as it occurs naturally in plant material.

Section 2 of this report contains a review of literature performed to identify materials of potential use for alkali removal from hot-filtered product gas. Based on this review, an experimental program was undertaken to investigate the effectiveness of alkali getter materials at cleaning a hot filtered product gas stream. Descriptions of the experimental methods are contained in Section 3, with experimental results following in Section 4. Section 5 presents the conclusion of the study.

## 2. REVIEW OF LITERATURE

### 2.1 Alkali Removal Mechanisms

Alkali is removed from the gas stream by adsorption onto the surface of the getter material. For this to occur, gas molecules must be transported across the boundary layer from the bulk flow to the solid surface. In cases of highly porous solids, pore structure and size distribution may critically influence the rate of transport. Upon reaching the solid surface, the gas molecule must arrive at, and attach to, a suitable site on the crystal lattice structure. The rate at which adsorption takes place is thus limited by the slower of the two phenomena, molecular transport or adsorption. Adsorption can be further classified into chemisorption or physical adsorption. The two differ by the strength of the attractive force between the gas molecule and the solid surface.

Physical adsorption is characterized by van der Waals or dispersion forces, which are weak intermolecular interactions arising from dipole-dipole or induced dipole attractions. Physical adsorption approaches equilibrium very rapidly and is generally reversible if the vapor pressure of the adsorbate is reduced. Hysteresis may result from the pore structure of the sorbent. The heat evolved during adsorption is comparable to a condensation process, being in the range of 4 to

40 kJ (g mole)<sup>-1</sup>, and as a result, is assumed to happen very quickly. The long-range nature of the attractive forces may cause physical adsorption to form several layers of adsorbed gas molecules on the solid surface. As the number of layers increases, the adsorption process approaches one of condensation.<sup>24,25</sup>

In contrast to physical adsorption, chemisorptive interaction between the solid surface and the adsorbed molecule is much stronger. Chemisorption is mainly responsible for gas-solid reactions and catalysis, and displays chemical specificity, i.e., is particular to the solid and gas species in terms of chemical forces and orientation. These requirements suggest that chemisorption can only occur as a monolayer. The forces involved between participants are of the same order as those in chemical reactions, with the heat of chemisorption being in the range of 40 to 600 kJ (g mole)<sup>-1</sup>. As a result, chemisorption may be slow and display rate behavior characteristic of processes possessing an activation energy. Gases that have been chemisorbed may be difficult to remove and may leave the surface altered, as in the case of oxygen adsorbed onto solid carbon, which is desorbed as CO or CO<sub>2</sub>.<sup>24,25</sup>

## 2.2 Experimental Methods

Studies reported in the literature used two basic experimental approaches: (1) thermogravimetric analysis (TGA) in which alkali capture by a single particle or a small collection of particles was monitored over the duration of the test; and (2) packed bed methods in which alkali capture was determined by monitoring the alkali content of the gas exiting the packed bed and/or by analyzing the getter material at the completion of the test. Thermogravimetric methods were used to study the effects of carrier gas flowrate,<sup>16</sup> alkali concentration in the carrier gas,<sup>16</sup> carrier gas species composition,<sup>19,20</sup> sorbent temperature,<sup>16,19,22</sup> sorbent particle size,<sup>16</sup> and elapsed time<sup>19-22</sup> on the capture of alkali species, and to obtain data suitable for modeling the rate kinetics of single particle alkali sorption.<sup>16,19-22</sup> Packed bed investigations were used to study the effects of sorbent temperature,<sup>14,23</sup> superficial gas velocity,<sup>14</sup> space velocity,<sup>14</sup> carrier gas moisture content,<sup>17</sup> partial pressure<sup>17</sup> of SO<sub>2</sub>, and carrier gas composition.<sup>23</sup> In most cases, pure alkali or an alkali compound was vaporized in a hot gas stream that was directed over a sample of the sorbent. The gas streams varied in origin and composition and included simulated flue gas (SFG) mixtures,<sup>14,17,21,22</sup> inert gases,<sup>16,19,23</sup> simulated producer gas,<sup>23</sup> methanol combustion products,<sup>19</sup> and air.<sup>18</sup> Packed beds were also used to study the release of alkali from as-received and regenerated getter materials, and the displacement of alkali inherent in the getter material by alkali from the gas stream.

### 2.2.1 Thermogravimetric Studies

Thermogravimetric equipment used to study the adsorption of alkali vapors on solid sorbents differed in design and capability. Quantities of getter used in the experimental apparatus varied from single flakes to a small collection of particles, with the total sample weighing a fraction of a gram in all cases. The apparatus of Luthra and Leblanc<sup>16</sup> was the simplest of those included in this review. The sample, in the form of 0.25- to 0.7-mm diameter particles contained in a crucible or a single pellet, was suspended from a microbalance. In a controlled 800° to 900°C environment, heated Ar flowed through a vaporizing NaCl or KCl bed, then over the sorbent material. Weight gain of the getter sample was monitored as a function of time. Alkali concentration in the gas stream was calculated from thermodynamic data and later verified by condensing and measuring the vapor downstream of the reactor. A similar equipment design was used by investigators at the University of Arizona<sup>20-22</sup> but included the capability of generating SFG (80% N<sub>2</sub>, 15% CO<sub>2</sub>, 3% O<sub>2</sub>, and 2% H<sub>2</sub>O) as a carrier for the alkali vapor. Workers at the Westinghouse Electric

Corporation Research and Development Center<sup>19,23</sup> (WECRDC) used two microbalances to simultaneously monitor the weight of a vaporizing alkali salt sample and that of the getter material, thus permitting the instantaneous gas-phase concentration of alkali and the rate of uptake of alkali by the sorbent to be determined. Nitrogen with ~5 vol% H<sub>2</sub>O was used as the carrier gas. All these thermogravimetric analyzer (TGA) systems allowed independent temperature control of the alkali source and the getter material. Getter materials were maintained at higher temperatures than the alkali source to prevent condensation of the alkali vapor and ensure that vapor adsorption was used to capture alkali. Control of the alkali source temperature was used in combination with carrier gas flowrate to obtain desired gas-phase concentrations. The advantage of the apparatus used by Bachovchin *et al.*<sup>19</sup> over the other two designs was that by monitoring the weight of the alkali sample, the gas-phase concentration could be calculated in real time. Alternative methods of determining alkali gas-phase concentration relied on computing a post-experiment average value based on the difference in alkali source weight over the course of the experiment or calculating a pre-experiment average value by running an experiment without sorbent present and collecting and measuring the alkali vapor as it exited the system.

### 2.2.2 Packed Bed Studies

Lee and coworkers<sup>14</sup> ran initial experiments at atmospheric pressure and temperatures of 800° to 875°C. In a manner similar to the TGA work described earlier, a NaCl source suspended from a microbalance was vaporized into a heated carrier gas stream producing an SFG (3% O<sub>2</sub>, 16% CO<sub>2</sub>, ~180 ppm H<sub>2</sub>O, ~300 ppm SO<sub>2</sub>, and ~80 ppm NaCl or KCl, balance N<sub>2</sub>) that was directed through a bed of sorbent material housed in a 2.5-cm diameter tube. The stream was quenched after the getter bed and the condensate analyzed for alkali. Capture efficiencies were computed for each test by comparing the weight of alkali vaporized ahead of the getter bed and the amount collected in the condensate after the sorbent bed. Post-test analyses of the sorbent material were not reported, which represents a serious limitation to the data set. Tests were conducted using NaCl, KCl, and K<sub>2</sub>SO<sub>4</sub>. Later work<sup>17</sup> was carried out with similar experimental equipment designed to withstand 10 bar pressure and 900°C to simulate PFBC conditions.

A similar experimental apparatus was employed by Punjak and Shadman.<sup>20</sup> Sodium or KCl sources suspended from a microbalance were vaporized into a carrier stream of air or N<sub>2</sub> at 850°C, atmospheric pressure, then passed through a getter bed volume of 0.6 cm<sup>3</sup>. Alkali released from the source was monitored over the duration of the experiment, and getter material was analyzed after the experiment by acid solubilization and atomic absorption (K) or atomic emission spectroscopy (Na).

Jain and Young<sup>18</sup> screened a number of alkali getter materials using slightly different methods. Alkali vapor was generated by atomizing a NaCl and water solution into an air stream that was subsequently heated to vaporize the droplets. The alkali-laden stream was directed through a bed (5 cm deep) of getter particles (~1 mm diameter) housed in a tube with 6-cm inner diameter. The superficial gas velocity was calculated as 51 cm s<sup>-1</sup> with a corresponding bed residence time of 0.1 s. Experiments were conducted at atmospheric pressure and 790°C for a maximum duration of 3 h, with alkali loading in the gas stream at ~40 ppmw. Getter activity was determined by dissolving material samples in acid and analyzing the resulting solution using atomic absorption spectroscopy. Several candidate getter materials would not completely dissolve in acid, and an alternative hot water leaching technique was employed for alkali recovery with analysis by ion selective electrode. The latter technique does not guarantee complete solubilization of adsorbed alkali, and the reported results should be considered with this in mind.

Jain and Young<sup>18</sup> advanced five candidate getter materials for further testing in an apparatus that could be operated in either fixed- or spouting-bed mode using particles of ~1 mm diameter. An adequate physical description and dimensions of this piece of equipment were not provided; this omission detracts from the interpretation of the experimental results. A NaCl aerosol was introduced into a heated air stream to produce a nominal alkali concentration of 20 ppmw. Dual measurements of the sodium and chlorine concentrations in the gas stream before and after the getter bed were determined by using (1) a condensation train and ion selective electrode, and (2) a flame photometer system. Experience with the flame photometer showed that it was difficult to maintain the instrument's stability over the duration of an experiment and its use was discontinued early in the test series. Limited analysis of the bed material was performed except in pursuit of additional data to improve chlorine balances. Chlorine content of the used getter material was determined by hot water leaching and analyzing the leachate with a colorimeter.

Preliminary packed bed work at WECRDC<sup>23</sup> used a 25-mm diameter heated tube containing the alkali source material in one end and a platinum gauze basket that held 10 to 15 getter pellets in the opposite end. Carrier gas passing through the tube transported volatilized alkali salt from the source to the getter bed. Tests were conducted at 11 atm pressure and a temperature range from 800° to 900°C. Later work<sup>19</sup> used similar apparatus, but at atmospheric pressure with a single pellet impaled on a thermocouple rather than a packed bed. A common problem cited with these experiments was that the gas-phase concentrations of alkali predicted by thermodynamic data did not agree well with measured values. Unlike the work of Lee *et al.*,<sup>14,17</sup> pelleted getter samples were subjected to extensive post-test analysis.

Bench-scale tests were performed by investigators at WECRDC<sup>19</sup> with packed beds (314 cm<sup>2</sup> area, 40 cm depth) of pelleted getter material weighing about 10 kg. Experiments were conducted at a nominal pressure and temperature of 11 atm and 860°C, respectively. Methanol containing a small amount of water and dissolved NaCl was fired in a combustor to produce a hot gas stream with a nominal alkali concentration of 10 ppmv, which was directed through the getter bed. Test durations were about 100 h and average alkali content in the exit stream from the bed was determined periodically using an extraction probe and condensation train that provided a time-integrated sample. Sodium levels in the resulting liquid samples were measured using an ion-selective electrode, and gas-phase concentrations were calculated based on the cumulative flow through the sampling system. Pressure drop across the getter bed was monitored over the test duration to detect any changes in bed structure caused by loss of pellet integrity, settling, or pellet fusing caused by high alkali loading. Pellet samples were removed from 12 layers or depths within the bed. Scanning electron microscopy (SEM), x-ray diffraction, and x-ray fluorescence characterizations of pellet surfaces and cross-sections were performed. Bulk samples were analyzed by H<sub>2</sub>O-, HCl-, and hydrogen fluoride/perchloric acid-soluble alkali fractions using atomic absorption techniques. Analytical results were related to the location (depth) of the pellet in the bed.

### 2.3 Materials

Scandrett and Cliff<sup>15</sup> studied the thermodynamics of alkali removal from model coal combustor flue gas on Si, AlSi, and alumina solids using chemical equilibrium analyses. Experimental getter tests reported in the literature have focused on inorganic solid sorbents. Lee and Johnson<sup>14</sup> screened alundum, diatomaceous earth, silica gel, Burgess No. 10 pigment, Attapulugus clay, and activated bauxite for their abilities to remove NaCl, KCl, and K<sub>2</sub>SO<sub>4</sub> from an SFG stream. Punjak *et al.*

studied the adsorption of NaCl on kaolinite<sup>20</sup> and later expanded the scope of their work to include bauxite and emathlite.<sup>21</sup> Luthra and Leblanc<sup>16</sup> examined the sequestration of NaCl and KCl on activated bauxite and activated alumina. Jain and Young<sup>18</sup> experimented with 13 sorbents for use in a dry-plate scrubber designed to simultaneously remove particulate and alkali vapor from flue gases generated by a PFBC. The materials tested included three types of diatomaceous earth, two types of activated bauxite, Attapulugus clay, fuller's earth, silica gel, dolomite, calcined dolomite, alumina, and two types of Norton catalyst containing primarily alumina and silica.<sup>18</sup> Mulik *et al.*<sup>23</sup> examined the gettering potential of kaolinite, ash from low-temperature coal char, and ash from a high-temperature coal gasifier.

Compositions of each material reported in the literature are given in Table 1. As shown, the two main constituents of the getters are SiO<sub>2</sub> and Al<sub>2</sub>O<sub>3</sub> and the fraction of each varies across a range from silica gel (pure SiO<sub>2</sub>) to alumina (pure Al<sub>2</sub>O<sub>3</sub>). The exceptions to this are the two dolomite getters tested by Jain and Young,<sup>18</sup> which contained primarily Mg and Ca oxides or carbonates. The unit cell of silica consists of four oxygen atoms located at the vertices of a tetrahedron with the silicon atom located at the geometric center. Adjoining unit cells in the lattice structure share a common oxygen atom.<sup>26</sup> In the  $\alpha$ -alumina unit cell, the oxygen atoms form a hexagonally close-packed array and the aluminum atoms are distributed symmetrically among the octahedral interstices.<sup>27</sup> Broken bonds, imperfections, and substitution of ions of lower valence within the solid lattice structure all produce unsatisfied charges that have the potential to attract and adsorb gas molecules. Reducing particle size or increasing the porosity of the solid and thus the number of free edges is one method to improving sorbent capacity. Lee and Johnson<sup>14</sup> noticed that sorbent effectiveness was generally related to internal surface area, which is primarily contributed by small pores.

### 2.3.1 Emathlite and Fuller's Earth

As shown in Table 1, emathlite<sup>16,21,22</sup> and the fuller's earth<sup>18</sup> sample are the same type of material in that each contains, in oxide form, roughly 70% SiO<sub>2</sub> and 10% Al<sub>2</sub>O<sub>3</sub>, with the remainder composed of smaller amounts (<5%) of MgO, Fe<sub>2</sub>O<sub>3</sub>, TiO<sub>2</sub>, CaO, K<sub>2</sub>O, and Na<sub>2</sub>O. One of the emathlite samples<sup>21,22</sup> contained CaO at a level of 5%, substantially higher than the other samples.<sup>18,19</sup> With this exception, the three independent reports were in relatively close agreement. Analyses<sup>19</sup> of the H<sub>2</sub>O-soluble, HCl-soluble, and HCl-insoluble fractions of emathlite revealed that Na, K, Si, Al, Mg, Fe, and Ti were HCl insoluble and Ca was HCl soluble; none of the species were water soluble. Solubility fractionation was used as an indicator of how tightly bound the species are in the solid matrix. Water-soluble material is volatile; acid-soluble species are typically carbonates, and insoluble materials are likely to be oxides or silicates.

Bachovchin *et al.*<sup>19</sup> identified emathlite as a fuller's earth, a name that originated in the use of clays for removing oils from wool, an activity called fulling. The clays selected, calcium montmorillonites, possess a large surface area, high cation exchange, and high adsorptive capacities.<sup>26,27</sup> Emathlite is a colloidal clay mineral sponge consisting of hydrated calcium magnesium aluminum silicate.<sup>19</sup> Using x-ray diffraction analysis, Punjak *et al.*<sup>21</sup> determined that the major phases present in emathlite were alpha quartz, cristobalite, and Al<sub>2</sub>SiO<sub>5</sub>. Similar analysis was provided by the Mid-Florida Mining Company for the emathlite supplied for studies at WECRDC,<sup>19</sup> 80% cristobalite, 10% quartz, 5% feldspar, and 4% clay minerals. Thermodynamic equilibrium analysis of the oxide composition by Bachovchin *et al.* generally supported the experimental findings, although a phase change was reported as a function of temperature as shown in Table 2. Sodium and K are predicted to be present as stable feldspars (NaAlSi<sub>3</sub>O<sub>8</sub> and KAlSi<sub>3</sub>O<sub>8</sub>) over the temperature range from 400° to 900°C.

Table 1. Composition of alkali getter materials reported in the literature.

Getter Material	Ref.	weight %											Und.*	Getter Geometry	Dimensions (mm)
		Al <sub>2</sub> O <sub>3</sub>	SiO <sub>2</sub>	MgO	Fe <sub>2</sub> O <sub>3</sub>	TiO <sub>2</sub>	CaO	K <sub>2</sub> O	Na <sub>2</sub> O	CaCO <sub>3</sub>	MgCO <sub>3</sub>				
Diatomaceous Earth	1	5	92										3	particles	0.84<d<2.4
Diatomaceous Earth	5	5	92										3	particles	1<d<1.2
Kaolinite	7	44.9	52.1		0.8	2.2							0.0	disks	thick.=0.4
Kaolinite	8	44.9	52.1		0.8	2.2							0.0	disks/flakes	thick.=0.5
Kaolinite	9	44.9	52.1		0.8	2.2							0.0	flakes	thick.=0.5
Kaolin	10							0.08	0.07				99.85	cylinders	d=3.1, L=3.1
Emahlite	9	13.9	73.4	2.6	0.4	0.4	5	1.2	0.1				3.0	flakes	thick.=0.5
Emahlite	8	13.9	73.4	2.6	3.4	0.4	5	1.2	0.1				0.0	disks/flakes	thick.=0.5
Emahlite	6	9.85	70.1	1.38	3.58	0.44	1.94	0.93	0.059				11.72	pellets	d=6.4, L=6.4
Fuller's Earth	5	12	66		4								18	particles	1<d<1.2
Activated Bauxite	1	81.5	10										8.5	particles	0.84<d<2.4
Activated Bauxite	4	81.5	10		3	3.5							2.0		0.84<d<2.4
Activated Bauxite	3	88	7		1.2	3							0.8	particles	0.25<d<0.7
Bauxite	8	84.2	11		4.8								0.0	disks/flakes	thick.=0.5
Activated Bauxite	5	81	10										9	particles	1<d<1.2
Activated Bauxite	5	88	7										5	particles	1<d<1.2
Bauxite	7	88.3	7.0		1.2	3.5							0.0	flakes	thick.=0.3
Bauxite	9	84.2	11		4.8								0.0	flakes	thick.=0.5
Activated Alumina	3				no analysis reported							100	cylinders	d=3, L=20	
Alumina	5	100											0	particles	1<d<1.2
Norton Catalyst SA 5201	5	80-90	5-10										0-15	particles	1<d<1.2
Alundum	1	99.5											0.5	particles	0.84<d<2.4
Attapulugus Clay	1	12	68	10.5									9.5	particles	0.84<d<2.4
Attapulugus Clay	5	12	68	10									10	particles	1<d<1.2
Low Temperature Coal Char	10							2.88	0.41				96.71	cylinders	d=3.1, L=3.1
Silica Gel	1		100										0	particles	0.84<d<2.4
Burgess No. 10 Pigment	1	38.6	45										16.4	particles	0.84<d<2.4
Silica Gel	5		100										0	particles	1<d<1.2
Dolomite	5									56	42		2	particles	1<d<1.2
Calcined Dolomite	5			39			61						0	particles	1<d<1.2
Coal Ash from Gasifier	10							1.82	0.07				98.11	cylinders	d=3.1, L=3.1

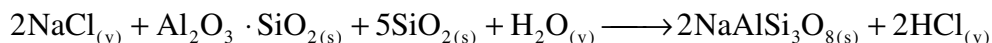
\* Amount unidentified in reported analysis.

Table 2. Thermodynamic equilibrium prediction of phase distribution in emathlite as a function of temperature (Bachovchin *et al.*<sup>6</sup>).

Emathlite Species (% weight)	Temperature (°C)	
	400	500 - 900
NaAlSi <sub>3</sub> O <sub>8</sub>	0.6	0.6
KAlSi <sub>3</sub> O <sub>8</sub>	6.2	6.2
CaO·Al <sub>2</sub> O <sub>3</sub> ·2 SiO <sub>2</sub>	0.1	10.9
CaO·MgO·2 SiO <sub>2</sub>	8.4	
Al <sub>2</sub> SiO <sub>5</sub>	14.7	2.1
Al <sub>2</sub> O <sub>3</sub> ·TiO <sub>2</sub>	1.1	1.1
Fe <sub>2</sub> O <sub>3</sub>	4.1	4.1
SiO <sub>2</sub>	64.9	69.5
Mg Al <sub>2</sub> O <sub>4</sub>		5.5

Equilibrium analysis<sup>19</sup> of gaseous alkali species expected to volatilize from emathlite at atmospheric pressure indicated that total gas-phase alkali would be less than 1 ppb at 700°C, 13 ppb at 900°C, and 128 ppb at 1,000°C, with sodium and potassium hydroxides as the dominant forms. Increasing pressure to 10 bar decreased the gas-phase concentrations at 900° and 1,000°C to 4 and 40 ppb, respectively.

Further equilibrium analysis<sup>19</sup> of emathlite in a producer gas environment (44% CO, 20% CO<sub>2</sub>, 0.6% N<sub>2</sub>, 13% H<sub>2</sub>O, and 10 ppm NaCl) predicted that ~50% of the alkali would be removed from the gas and sequestered as NaAlSi<sub>3</sub>O<sub>8</sub> at atmospheric pressure at 700° to 875°C. At 700°C, the saturation capacity of the emathlite matrix was projected to be 11.3% NaAlSi<sub>3</sub>O<sub>8</sub> or ~10 mg Na g<sup>-1</sup> of sorbent material. Chlorine (from the NaCl gas) would be released primarily as volatile HCl, but also as chlorides of K, Fe, and Mg, which were initially present in the emathlite solid matrix. Liberation of K from the solid increases the alkali concentration of the gas. Thermodynamic analysis reported by Scandrett and Clift<sup>15</sup> concluded that alumino-silicate with an Al<sub>2</sub>O<sub>3</sub> to SiO<sub>2</sub> ratio of 1 to 3.6 would remove 99% of alkali chlorides in the presence of water vapor at 730°C according to the reaction:



Reductions in alkali capture were predicted at higher reaction temperatures.

### 2.3.1.1 Effects of Exposure Time

A series of TGA tests<sup>19</sup> exposing pelleted emathlite to ~10 ppm NaCl in a gas stream of N<sub>2</sub> and 4.6% water vapor was conducted for 25, 50, 75, 100, and 150 h. Final concentrations of the total and acid-insoluble Na and K in the getter material from each test are presented in Figure 1 as functions of test duration. Tests were conducted at 850°C and 1 bar pressure. Sodium concentration of the getter material increased as a function of time, from less than 0.5 mg Na g<sup>-1</sup> sorbent initially to slightly greater than 33 mg Na g<sup>-1</sup> sorbent after 150 h, a nominally linear loading rate of 0.2 mg Na g<sup>-1</sup> sorbent h<sup>-1</sup>. It is not apparent from these data that the pellet is approaching a Na saturation value. Nearly all of the Na is present in the getter matrix in acid-insoluble form. The presence of Cl was reported in the H<sub>2</sub>O-soluble fraction, but always at a Na to Cl molar ratio greater than unity indicating the dissociation of NaCl. Total Cl content was less than 0.1 mg Cl g<sup>-1</sup>

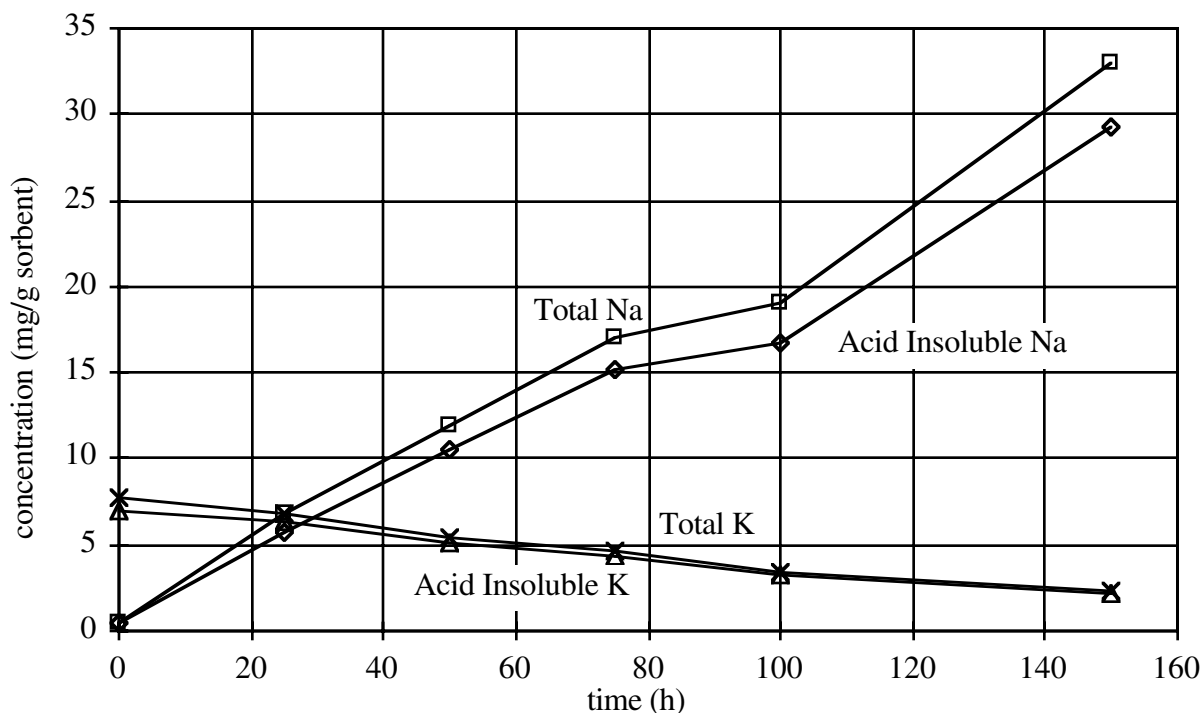


Figure 1. Sodium and K concentrations in pelleted emathlite (6.4 mm diameter, 6.4 mm length) as a function of duration of exposure to 10 ppmv NaCl and 4.6% H<sub>2</sub>O in N<sub>2</sub> carrier gas flow of 1 L min<sup>-1</sup> at 850°C, 1 bar. (Data from reference 6.)

sorbent from which a molar ratio of Na to Cl of 214 can be calculated, evidence that Cl is released into the gas phase. Pellet K concentration decreased linearly over time at a rate of approximately -0.04 mg K g<sup>-1</sup> sorbent h<sup>-1</sup> reaching a final value equal to roughly one-third its initial concentration. The K released was primarily from the acid-insoluble fraction. The net rate of alkali (Na plus K) adsorption by emathlite under these conditions was approximately 0.16 mg alkali g<sup>-1</sup> sorbent h<sup>-1</sup>. In addition to changes in the alkali content of emathlite, Si concentration was found to change over the course of the gettering experiment. Acid-insoluble Si decreased and acid-soluble Si increased, although not in equal amounts. Volatilization of Si as SiO gas was proposed to account for the shortfall.

From an initial light-colored appearance, pellets were observed to be darkened and cracked after 25 h, cracked with a slightly glassy surface at 50 h, covered by a readily apparent glassy surface with cracks visible beneath (75 h), and covered by a thick glass that obscured any surface cracks below at 100 and 150 h. Although volume reduction of 8% to 10% was measured for the pellets in all tests, the glassy surface encasing the pellet accounted for 12% of the total volume in the 100 h specimen. The glassy surface was determined to be sodium silicate, Na<sub>2</sub>SiO<sub>5</sub>, complexed with increasing amounts of SiO<sub>2</sub> at greater distance from the surface. Feldspar was present in the region below the glassy layer in the partially reacted pellet.

Independent results of TGA experiments to determine the gettering qualities of emathlite reported by Punjak *et al.*<sup>21</sup> and Uberoi *et al.*<sup>22</sup> are shown in Figure 2. Unlike the results<sup>19</sup> of Figure 1, the sample appears to be approaching an adsorptive capacity of about 150 mg Na g<sup>-1</sup> sorbent after only 40 h of exposure. This is the likely result of differences in experimental conditions. The data in Figure 2 were obtained with a 0.5-mm flake exposed to 150 ppmv NaCl gas stream compared to a

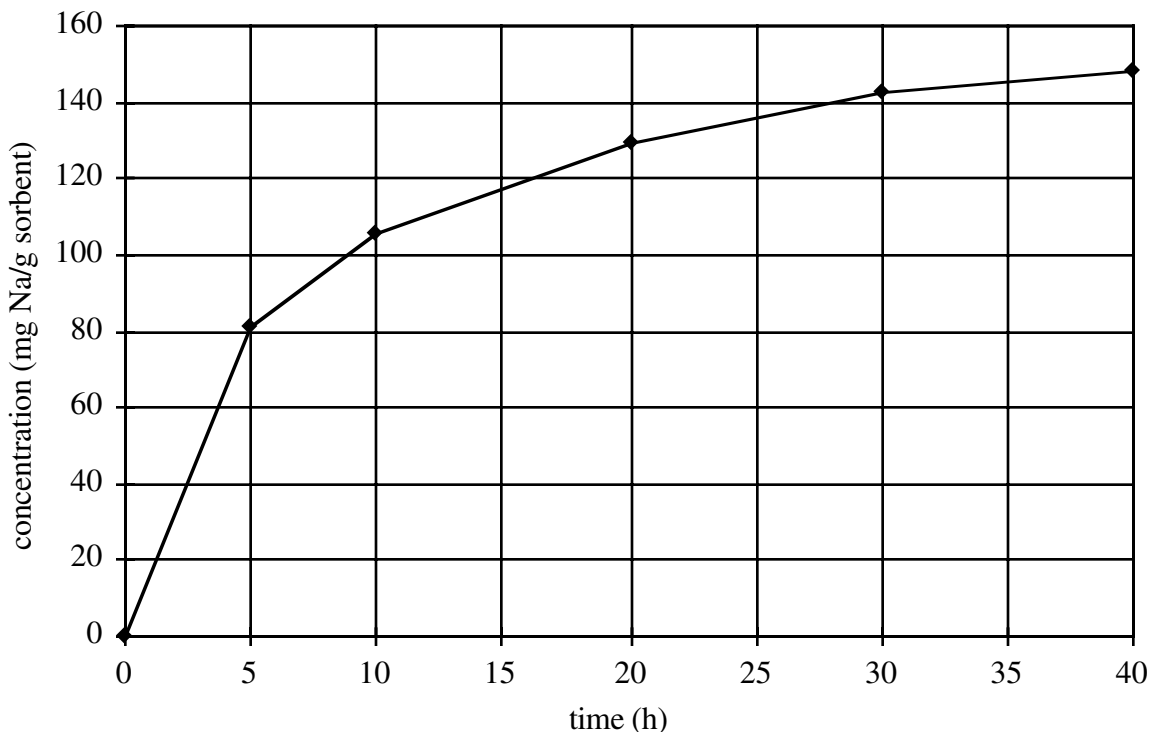
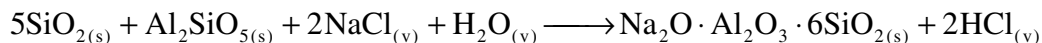


Figure 2. Sodium concentration in emathlite flake (0.5 mm thickness) as a function of duration of exposure to 150 ppmv NaCl in SFG (80% N<sub>2</sub>, 15% CO<sub>2</sub>, 3% O<sub>2</sub>, and 2% H<sub>2</sub>O) flow of 0.18 L min<sup>-1</sup>, 800°C, 1 bar. (Data from reference 8.)

6.4-mm diameter pellet and a 10 ppmv NaCl gas stream in Figure 1. The larger dimensions of the pelleted sample and lower vapor concentrations of NaCl would limit mass transport to the interior of the pellet. Formation of a glassy deposit on the surface may also affect mass transport and limit complete saturation of the pellet.

X-ray diffraction analysis of the saturated samples<sup>21,22</sup> indicated that Na had reacted with the emathlite matrix to form albite, Na<sub>2</sub>O·Al<sub>2</sub>O<sub>3</sub>·6SiO<sub>2</sub>. Albite has the same atom ratios as feldspar, NaAlSi<sub>3</sub>O<sub>8</sub>, reported by Bachovchin *et al.*<sup>19</sup> The presence of Cl was not detected in the saturated material, and Punjak *et al.* proposed the following reaction to describe the sorption process:



Within the limits of the experimental conditions, the irreversibility of this reaction was determined by extending several TGA tests to subject samples of alkali-saturated emathlite to a clean (alkali-free), high-temperature gas flow. In all cases, the alkali was retained in the solid matrix. The release of Cl as HCl in the gettering process is troublesome in that it may induce corrosion in downstream equipment.<sup>29-31</sup> In addition, K present in the as-received emathlite (8.9 mg K g<sup>-1</sup> sorbent) was almost completely volatilized with the final concentration in the getter material measured at 0.7 mg K g<sup>-1</sup> sorbent. Viewed from the perspective of net alkali exchange, however, the amount of K released is small compared to the Na sequestered. It is not evident from these studies whether the alkali present in as-received emathlite would be released if KCl rather than NaCl were present in the gas phase.

Jain and Young<sup>18</sup> included fuller's earth in initial screening experiments of candidate getter materials, but it was not selected for additional testing because the amount of alkali retained was found to be negligible. This was likely due to the analytical methods employed. Alkali content of the sorbent was determined by water leaching the sample and analyzing the leachate. The work of Bachovchin *et al.*<sup>19</sup> indicates that nearly all the alkali captured by emathlite is retained in H<sub>2</sub>O- and acid-insoluble forms, implying that the methods used by Jain and Young did not yield accurate results.

Bachovchin *et al.*<sup>19</sup> ran a series of tests using packed beds of pelleted emathlite with a total sorbent mass on the order of 10 kg. Combustion products of methanol containing ~10 ppmv NaCl were passed through the bed at ~850°C and 10 bar pressure. Tests lasted about 100 h and measured Na concentrations in the gas exiting the 40-cm deep bed ranged from 0.2 ppmv in the first hours of the test, to ~1.5 ppmv at the conclusion. Various-sized pellets were used in the bed for individual tests and variation in outlet gas NaCl concentration was deemed consistent with a dependency on available sorptive surface area. The bed was unloaded and pellets from various depths within the bed were analyzed for Na content. Values ranged from 43 mg Na g<sup>-1</sup> sorbent at the bed inlet to 3.0 mg Na g<sup>-1</sup> sorbent near the bed outlet. The more completely reacted pellets at the inlet were light green with pellet discoloration gradually transitioning to that of unreacted emathlite at the bed outlet.

### **2.3.1.2 Effects of Water Vapor**

The effects of the gas stream water vapor content on alkali adsorption were investigated by Bachovchin *et al.*<sup>19</sup> because water vapor was perceived to play a role in the solubilization of Si in the emathlite matrix, a necessary step in forming the glassy Na<sub>2</sub>SiO<sub>5</sub> surface layer associated with enhanced Na capture. Three, 75-h TGA experiments were conducted with emathlite pellets at 850°C, atmospheric pressure, approximately 10 ppmv NaCl, and 2.5%, 4.6%, and 6.2% H<sub>2</sub>O in N<sub>2</sub>. To correct for experimental variation in the NaCl gas concentration, test results were compared in terms of weight gain per ppmv NaCl<sub>(v)</sub>. On this basis, tests using 2.5%, 4.6%, and 6.2% H<sub>2</sub>O vapor, adsorbed 1.8, 2.1, and 2.1 mg Na g<sup>-1</sup> sorbent ppmv<sup>-1</sup> NaCl, respectively. This was interpreted as indicating that Na was more readily adsorbed at higher water vapor (2.5% versus 4.6%) concentrations, but with diminishing returns beyond some critical value (4.6% versus 6.2%). Given the experimental variation associated with the experiments, the lack of replication, and the small differences in adsorption values, an equally justifiable interpretation could have been that the tests demonstrated no dependence on water-vapor concentration.

A second series of four TGA tests was performed to further study the dependence of alkali adsorption on water vapor. These included periods of exposure to: (1) alkali in N<sub>2</sub>, (2) water vapor in N<sub>2</sub>, and (3) water vapor and alkali in N<sub>2</sub>. Only during periods when both alkali and water vapor were present did the sample exhibit weight gain, clearly demonstrating that water vapor is a necessary participant in alkali capture by emathlite. This behavior was true regardless of the order in which the gas streams were applied.

### **2.3.1.3 Effects of Temperature**

TGA tests were conducted with commercially fabricated emathlite pellets<sup>19</sup> at 755°, 850°, and 900°C, atmospheric pressure, in a N flow containing 10 ppmv NaCl and 4.6% H<sub>2</sub>O. Over this

temperature range, emathlite adsorption of Na was not significantly affected. Similar results were reported by Uberoi *et al.*<sup>22</sup> in an SFG environment. Potassium concentration of the pellets<sup>19</sup> decreased at higher test temperatures (shown in Figure 3), indicating that K release by the getter bed may be controlled without significantly affecting Na uptake by operating at lower temperatures. In addition, temperature insensitivity of Na adsorption can greatly reduce getter bed control requirements for industrial applications.

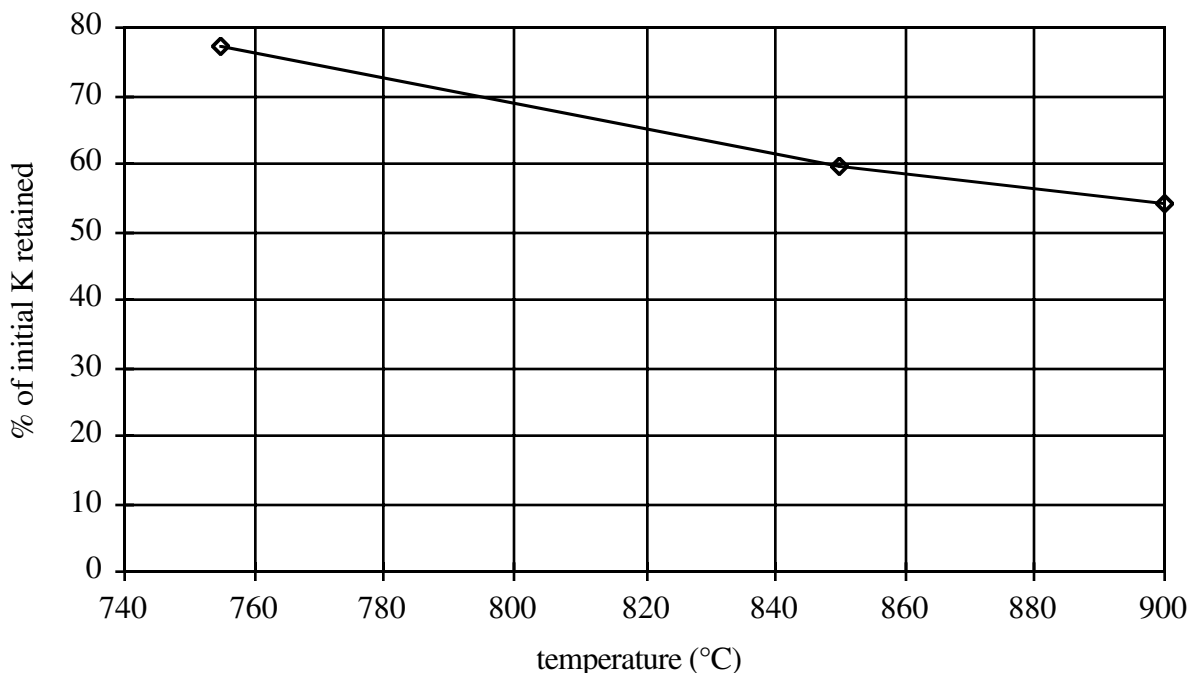


Figure 3. Percentage of initial K retained in emathlite pellets as a function of test temperature. Test conditions: 10 ppmv NaCl, 4.6% H<sub>2</sub>O in N<sub>2</sub> carrier gas, atmospheric pressure. (Data from reference 6.)

#### 2.3.1.4 Effects of Gas Concentration

Punjak *et al.*<sup>21</sup> and Uberoi *et al.*<sup>22</sup> reported results of short duration TGA tests in a range of 2 to 4 h, with NaCl gas concentrations of 65, 80, and 125 ppmv, a temperature of 800°C and atmospheric pressure. As shown in Figure 4, higher rates of getter flake weight gain were evident in the higher-concentration NaCl environment, exhibiting a nearly linear dependence on gas concentration in these short-duration tests. Unfortunately, none of the tests lasted long enough for the sample to achieve a saturated weight. From the available data, it is impossible to predict whether all the samples will attain a common final loading.

Bachovchin *et al.*<sup>19</sup> conducted tests at NaCl gas concentrations of 0.02 ppmv at 850°C, 1 atm pressure to determine whether gettering would occur at low gas-phase concentrations, conditions of particular interest in getter bed design for industrial applications. The initial Na content of the single pellet sample (0.9 mg Na g<sup>-1</sup> emathlite) doubled over the 4,368 h of exposure, capturing roughly 40% of the Na present in the total gas volume. A final test at high gas concentration (>50 ppmv) and extended duration (1,464 h) was performed to determine the ultimate Na loading of emathlite. At the conclusion of the test, the pellet was almost completely converted to a green translucent glass except for a small unreacted core at the center. Glass blobs were found directly

under the pellet indicating it had been molten and flowed, a potential mechanism for bed plugging in long-term industrial applications. The glass was found to contain 188 mg Na g<sup>-1</sup> by weight, higher than the value of 142 mg Na g<sup>-1</sup> reported elsewhere<sup>21,22</sup> (see Figure 2).

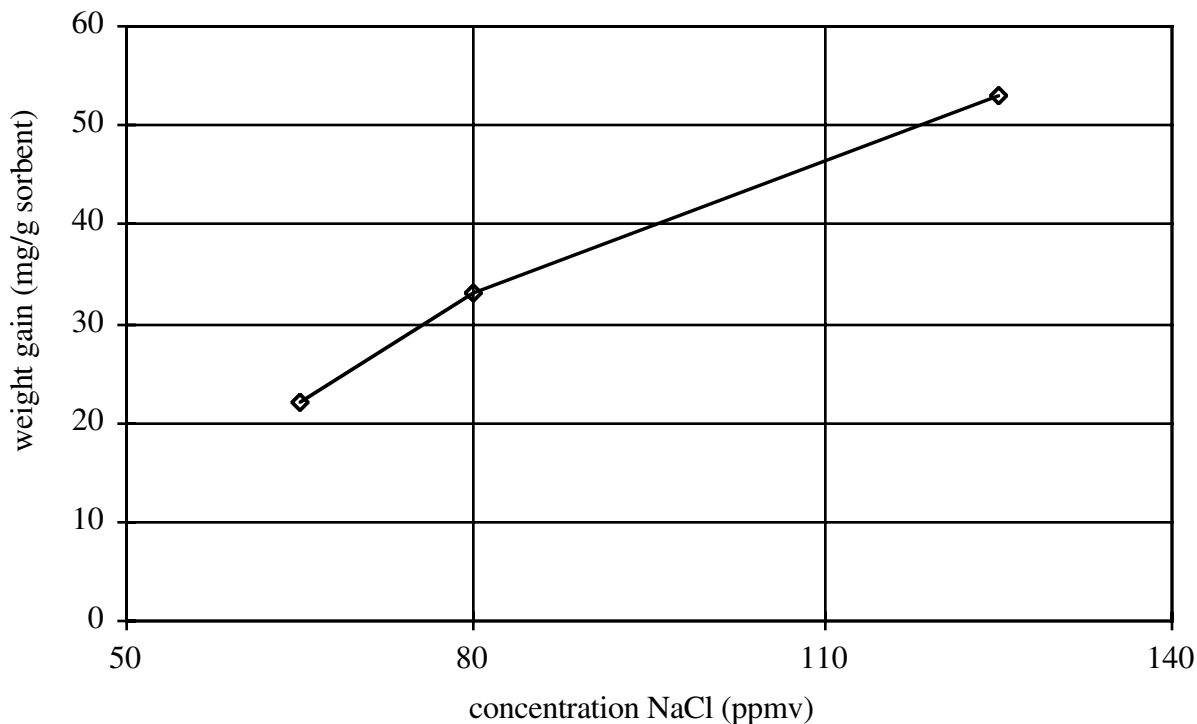


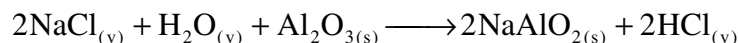
Figure 4. Sample weight gain of emathlite flakes as a function of gas-phase NaCl concentration after 2-h exposure at 800°C, atmospheric pressure. (Data from references 8 and 9.)

### 2.3.2 Bauxite

Several studies have been performed to determine the gettering characteristics of bauxite and activated bauxite.<sup>14,16-18,20-22,32,33</sup> In one instance,<sup>32</sup> a slip stream from a 71-MW<sub>e</sub> demonstration PFBC unit was passed through an activated bauxite getter bed as a method of measuring time-averaged gas-phase alkali content of the flue gas.

As shown in Table 1, bauxite samples were very similar in composition, containing 81% to 88% alumina, 7% to 11% silica, and smaller amounts of TiO<sub>2</sub>, Fe<sub>2</sub>O<sub>3</sub>, and other impurities. Samples from the same manufacturer<sup>1,3,4,7</sup> exhibit variation in composition. Surface area,<sup>16</sup> pore volume,<sup>14</sup> and average pore radii<sup>16</sup> of activated bauxite were determined to be 87.3 m<sup>2</sup> g<sup>-1</sup>, 0.325 cm<sup>3</sup> g<sup>-1</sup>, and 3.5 nm, respectively.

Thermodynamic calculations<sup>15</sup> of equilibrium constants for the reaction of NaCl with alumina according to the reaction:



indicate that sodium and K chlorides are not favored to react with a pure alumina getter material at temperatures higher than 530°C. Experimental work supports this conclusion. Luthra and Leblanc<sup>16</sup> compared TGA test weight gains against the masses of Na and Cl recovered from water leaching the samples after the experiment's completion and found them to agree within 20%. Work by Lee *et al.*<sup>33</sup> concluded that 50% of the alkali chloride captured by freshly activated bauxite and 80% retained by water regenerated (leached) material was water soluble. This evidence, viewed in consideration with experimental results presented below, was taken to indicate that alkali gettering by activated bauxite was predominantly a physical adsorption process rather than one involving chemisorption. Some chemisorption, however, may be expected to occur between the NaCl and silica or mineral impurities present in the bauxite ore.

### 2.3.2.1 Effects of Gas-Phase Alkali Concentration

Figure 5 shows the weight gain profile of bauxite exposed to 185 ppmv NaCl in an SFG environment (80% N<sub>2</sub>, 15% CO, 3% O<sub>2</sub>, and 2% H<sub>2</sub>O) at 800°C and atmospheric pressure.<sup>21,22</sup> The upper curve exhibits weight gain for the first 6 h of exposure with constant weight thereafter, about 58 mg Na g<sup>-1</sup> bauxite. The lower curve is indicative of sorptive behavior when NaCl is removed from the gas stream after 6 h of exposure. As a result, approximately 10% of the adsorbed material is released into the gas stream, a potential problem in an industrial setting where such conditions might occur during a process upset. Similar results are shown in Figure 6 for bauxite weight gain simultaneously exposed to 7.3 ppmv NaCl and 28.5 ppmv KCl in an Ar carrier gas at 800°C, atmospheric pressure.<sup>16</sup> Unlike the curve in Figure 5, which attained a constant weight in ~6 h, the curve in Figure 6 approaches a steady value after 200 h. Three major differences are apparent between the two experiments: (1) the carrier gas composition, in particular the presence of water vapor in the results from Punjak *et al.*;<sup>21</sup> (2) the total gas-phase alkali concentrations (185 ppmv versus 36 ppmv); and (3) the presence of KCl as the predominant alkali salt in the latter figure. Other studies concluded there was no difference between the adsorption of NaCl and KCl on bauxite.<sup>20,33</sup> Lee and Johnson<sup>14</sup> experimentally showed that NaCl, KCl, and K<sub>2</sub>SO<sub>4</sub> were adsorbed by bauxite with equal efficiency. Luthra and Leblanc<sup>16</sup> presented data that showed equilibrium was approached much more quickly at higher gas-phase alkali concentrations, the likely root of the differences between the figures.

Luthra and Leblanc<sup>16</sup> conducted experiments that featured several step changes in the gas-phase concentration of alkali chloride over the duration of a single TGA test. This demonstrated that the final alkali loading of bauxite was dependent on the gas-phase concentration. From the results, it was concluded that the bauxite getter sample attained the same weight gain whether the step change in gas-phase alkali occurred as a reduction in concentration from a higher value (i.e., 200 ppmv to 100 ppmv, or 110 ppmv to 100 ppmv) or as an increase from a lower value (50 ppmv to 100 ppmv). The results from Punjak *et al.*<sup>21</sup> in Figure 5 would appear to contradict this since the final weight gain of the sample subjected to a step change from 185 ppmv to 0 ppmv (Figure 5 desorption curve) would probably not be identical to one exhibited by a step decrease from 35 ppmv to 0 ppmv.

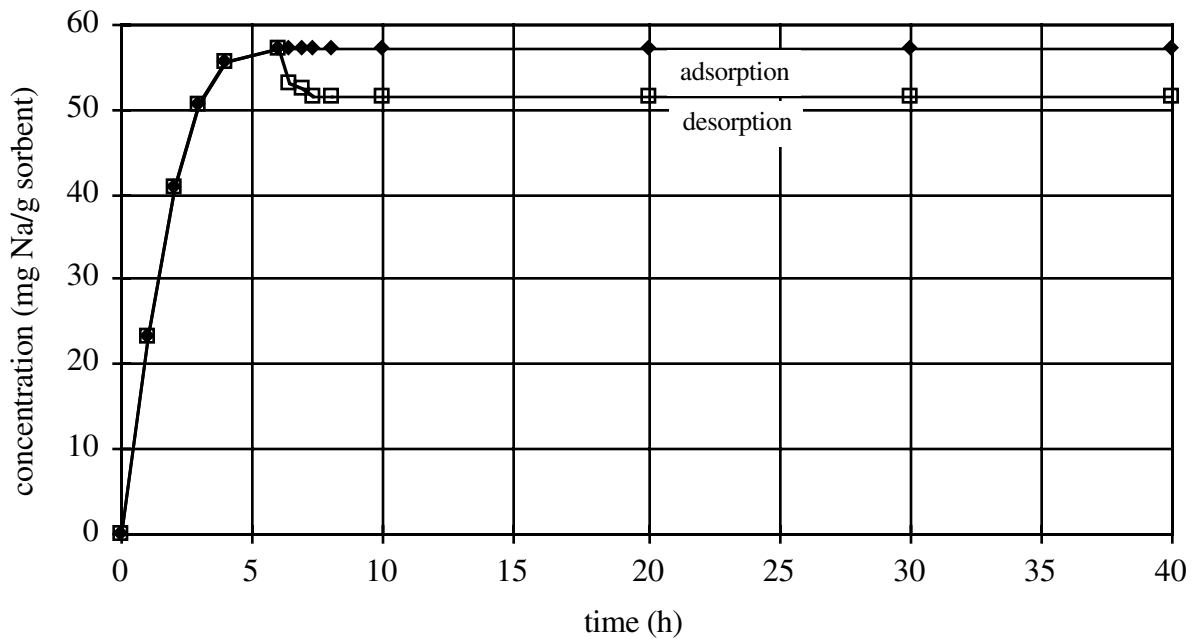


Figure 5. Concentration of Na in bauxite as a function of time resulting from exposure to 185 ppmv NaCl in SFG (80% N<sub>2</sub>, 15% CO, 3% O<sub>2</sub>, and 2% H<sub>2</sub>O) at 800°C and atmospheric pressure. NaCl removed from gas stream after 6 h in the desorption curve. (Data taken from references 8 and 9.)

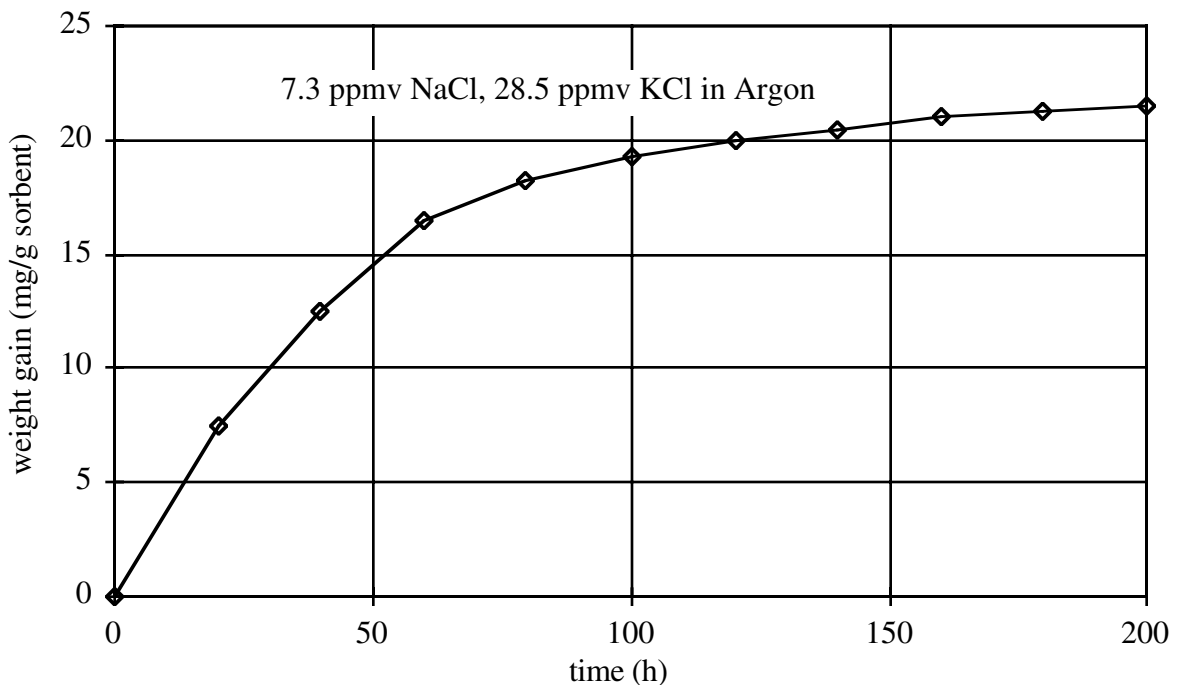


Figure 6. Weight gain of bauxite sample as a function of time resulting from exposure to 7.3 ppmv NaCl and 28.5 ppmv KCl in an Ar carrier gas at 800°C, atmospheric pressure. (Data taken from reference 3.)

### 2.3.2.2 Effect of Sorbent Bed Temperature

Lee and Johnson<sup>14</sup> performed tests of bauxite gettering at 800° and 880°C in a dry SFG containing 80 ppmv NaCl. After 4.5 h of exposure, the higher temperature sample had adsorbed 16 mg NaCl g<sup>-1</sup> of bauxite, whereas the sample at 800°C was determined to contain 21 mg NaCl g<sup>-1</sup>, about a 25% difference. Similar results were obtained by Luthra and Leblanc<sup>16</sup> from tests conducted with 225 ppmv NaCl in argon at 800° and 900°C. After 68 h, the samples had adsorbed 43 and 26 mg NaCl g<sup>-1</sup> bauxite, a 40% higher value at the lower temperature. Although neither experiment had clearly attained saturated loading, the curves suggested that the final steady loading value would be temperature dependent. This directly contradicts the conclusions drawn from a modeling study by Uberoi *et al.*, which stated that temperature affected the rate of alkali adsorption but not the final limit.<sup>22</sup>

### 2.3.2.3 Effect of Superficial Gas Velocity

The effect of superficial gas velocity in packed beds was investigated<sup>14</sup> at 800°C and atmospheric pressure over a range of 25 to 155 cm s<sup>-1</sup>, while maintaining a constant gas hourly space velocity (GHSV) of 67,000 h<sup>-1</sup>. No significant difference in alkali capture rate by bauxite was found over this range of values. Additional tests performed at 870°C, superficial velocity of 8 cm s<sup>-1</sup>, and a lower GHSV showed an 85% reduction in alkali capture compared to these results. Although there were differences in the experimental conditions, it was apparent that lower superficial gas velocities result in reduced rates of alkali capture, possibly because of mass transfer limitations from the bulk fluid to the external getter surface. Luthra and Leblanc<sup>16</sup> reported no effect of carrier gas flow rate (300 to 1200 cm<sup>3</sup> min<sup>-1</sup>) on the results of their TGA tests using a collection of bauxite particles in a platinum mesh crucible.

### 2.3.2.4 Effect of Gas Hourly Space Velocity

As noted earlier, gas hourly space velocity (GHSV) is defined as the volumetric gas flow rate divided by the sorbent volume. Packed bed tests performed with bauxite particles in the size range of 0.8 to 2.4 mm using 80 ppmv NaCl in flue gas at 800°C, atmospheric pressure, and superficial gas velocity of 66 cm s<sup>-1</sup> determined alkali capture efficiencies of 81%, 93%, and 99% for GHSV values of 18.6, 9.3, and 5.2 s<sup>-1</sup>, respectively. In decreasing order of GHSV, these correspond to gas-getter contact times of 0.05, 0.1, and 0.2 s. For the stated experimental conditions, decreased GHSV clearly improves the alkali capture efficiency of bauxite over the range of values tested, but increasing contact time beyond 0.2 s must obviously meet with diminishing returns.

### 2.3.2.5 Release of Alkali from Activated Bauxite

Lee *et al.*<sup>17</sup> determined that Na and K were present as impurities in activated bauxite at levels of 0.034% and 0.002% (mass basis), respectively. Under getter reactor conditions associated with PFBC applications, 850°C, 10 bar pressure, and gas composition of 3% O<sub>2</sub>, 16% CO<sub>2</sub>, 5% H<sub>2</sub>O, 250 ppmv SO<sub>2</sub>, and the balance N<sub>2</sub>, the release of the two alkali elements present in bauxite was monitored as a function of time. Over the first 5 h of exposure, 1.3% of the Na and 1.15% of the K contained in the getter material were released to the gas phase. No volatile emission of either element was measured for the remaining 15 h of the test.

### 2.3.2.6 Regeneration of Activated Bauxite

Lee and coworkers conducted tests to determine the extent to which bauxite loaded with adsorbed alkali could be regenerated and reused as part of process development planning for industrial application.<sup>17,33</sup> A series of tests was performed that cyclically exposed bauxite to an alkali-laden gas stream (as previously described) and a bath of boiling distilled water. The water leachate from the regeneration process was analyzed for Na, K, and Cl. Bauxite samples were characterized for color, porosity, and attrition. The original color of bauxite was a light pink, and after sorption, the surface was a milky white, the color of condensed NaCl. The pink color was restored after water leaching and forced-air oven drying at 200° to 400°C. Porosity in the range of pore sizes <0.2 μm increased with each successive loading/unloading cycle. This was attributed to the solubilization of compounds formed between Na and Si or other impurities present in the bauxite.<sup>17,33</sup> Attrition of the getter material was monitored for each successive regeneration cycle, measuring 5.5% in the first cycle but stabilizing at about 2% thereafter in experiments including as many as 10 cycles.

A 10-cycle regeneration experiment<sup>33</sup> was performed with attrited bauxite replaced with fresh material to keep a constant getter weight for each cycle. The sorption tests were conducted using SFG containing 35 ppmv NaCl at 800°C, atmospheric pressure. Alkali capture efficiency was consistently 98% or better for each of the sorption cycles. In the initial cycle, 54% of the captured NaCl was recovered via leaching. This increased to an average of >80% in subsequent cycles. Analysis of the leachate determined that the ratio of Na to Cl was consistently of the order unity indicating that, unlike emathlite, both elements were retained. Cold-water leaching was investigated and found to remove about 70% of the NaCl recovered by the boiling water method. A similar study involving five sorption/regeneration cycles was completed using KCl as the alkali source with similar results to those described here for NaCl.

### 2.3.3 Diatomaceous Earth

Diatomaceous earth was tested for sorbent qualities by Lee and Johnson<sup>14</sup> and Jain and Young.<sup>18</sup> Diatomaceous earth samples used by the former<sup>14</sup> were identified as sedimentary rock originating from marine or lacustrine deposition. Both studies reported identical compositions (Table 1) of 92% SiO<sub>2</sub> and 5% Al<sub>2</sub>O<sub>3</sub>, which appear to be supplied by the manufacturer. Clay, carbonaceous matter, iron oxide, and sand were thought to be present as impurities<sup>14</sup> but were not reported in the quantitative analyses. Jain and Young screened three types of diatomaceous earth (MP94, MP91, and MP99) for gettering activity. Compositions of all three were reported to be identical and any characteristics that made the materials different were not identified. The pore volume<sup>14,18</sup> and surface area<sup>18</sup> of diatomaceous earth were determined to be about 1 cm<sup>3</sup> g<sup>-1</sup> and 9.25 m<sup>2</sup> g<sup>-1</sup>, respectively. Approximately 70% of the pore volume was contained in pores ranging in size from 0.2 to 1.0 μm in diameter.

#### 2.3.3.1 Alkali Capture Efficiency

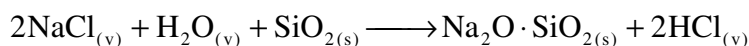
Lee and Johnson conducted tests to assess the efficiency of removing NaCl from air, and NaCl, KCl, and K<sub>2</sub>SO<sub>4</sub> from simulated PFBC flue gas. NaCl removal efficiency in air and dry flue gas were reported to be 75% and 96%, respectively, with the disparity attributed to differences in experiment duration, NaCl vapor concentration, and superficial gas velocity. Diatomaceous earth displayed similar capture capabilities for KCl, removing 98% of the alkali present in the gas stream. Experiments conducted using K<sub>2</sub>SO<sub>4</sub> resulted in a capture efficiency of 74%. This lower value was attributed to a high superficial gas velocity (reduced contact time) for the tests. In

general, these tests provide ample evidence that NaCl, KCl, and K<sub>2</sub>SO<sub>4</sub> can be captured by diatomaceous earth, but stronger conclusions are not possible because of the varied test conditions employed for the different alkali forms.

### 2.3.3.2 Effect of Time Duration

Results of tests by Jain and Young<sup>18</sup> and Lee and Johnson<sup>14</sup> shown in Figure 7 are not in agreement over the range of common data. Jain and Young's test results are consistently lower than comparable experiments cited in the literature. The upper curve appears to be approaching an asymptotic value of ~18 mg Na g<sup>-1</sup> diatomaceous earth. This is approximately 30% more than was retained by bauxite under directly comparable experimental conditions.<sup>14</sup>

Diatomaceous earth was not sensitive to variation in temperatures of 800° to 880°C. Sensitivity to superficial gas velocity and GHSV was similar to that of activated bauxite. No effect on the rate of NaCl capture was apparent at 25 to 160 cm s<sup>-1</sup>, but at about 8 cm s<sup>-1</sup>, the rate was roughly 10% of the value at the higher superficial velocities. Cutting the GHSV by a factor of two (doubling the contact time), improved the capture efficiency of diatomaceous earth from 86% to 97%. Water leaching tests determined that some Na and Cl were removable by water leaching; however, the mole ratio of Na to Cl was about eight, indicating that NaCl was not adsorbed as a molecule. This supports the mechanism proposed by Lee and Johnson<sup>14</sup> for adsorption of alkali on diatomaceous earth:



The resulting sodium silicate compound is not water soluble.

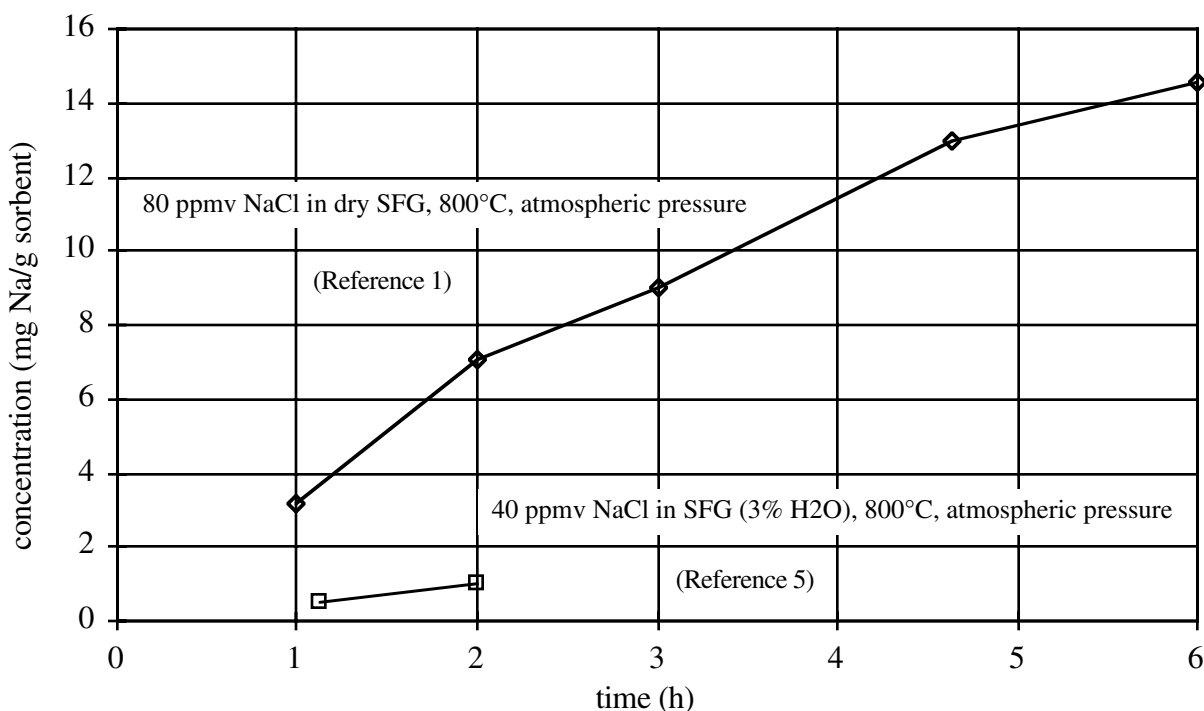


Figure 7. Weight gain of diatomaceous earth sample as a function of time.

### 2.3.4 Kaolinite

Kaolin is a group of clay minerals that includes nacrite, dickite, kaolinite, and halloysite, each composed of silica sheets linked to modified gibbsite sheets. The kaolin group<sup>16</sup> has a common composite unit formula of  $\text{Al}_2\text{Si}_2\text{O}_5(\text{OH})_4$ . The composition of kaolinite (Table 1) used in alkali sorbent research<sup>20-22</sup> was reported to contain primarily 45%  $\text{Al}_2\text{O}_3$  and 52%  $\text{SiO}_2$  with small amounts of  $\text{Fe}_2\text{O}_3$  and  $\text{TiO}_2$ . Mulik *et al.*<sup>23</sup> reported that kaolinite contained 0.08%  $\text{K}_2\text{O}$  and 0.07%  $\text{Na}_2\text{O}$ . Sodium was found to be equally distributed between water-soluble and -insoluble forms, whereas K was predominantly insoluble. Kaolinite getter material used by Mulik *et al.*<sup>23</sup> was pulverized until the lattice structure was completely destroyed, producing an amorphous Al-Si material in an effort to maximize ion exchange capacity. Material used in experiments at the University of Arizona<sup>20-22</sup> was formed into particles by making slurry from kaolinite powder, allowing it to dry, then crushing the resulting slabs to obtain a desired size distribution.

Heat treating kaolinite from 660° to 880°C in an inert environment at 11 bar resulted in a shift of water-insoluble Na and K to water-soluble forms with no volatilization of either alkali.<sup>23</sup> The mass concentration of total alkali increased slightly because small amounts of volatile compounds were lost.

Tests were performed exposing kaolin samples to 80 ppmv NaCl in various carrier gases at 850° and 900°C, 11 bar pressure for 4 h.<sup>23</sup> The study included three carrier gases: (1) argon, (2) 10%  $\text{H}_2$  with balance  $\text{N}_2$ , and (3) a synthetic fuel gas composed of 7.5%  $\text{CO}_2$ , 23%  $\text{CO}$ , 14%  $\text{H}_2$ , 55%  $\text{N}_2$ , and the balance composed of  $\text{H}_2\text{S}$  and  $\text{HCl}$ . Surprisingly, the synthetic fuel gas contained no water vapor. The effects of these treatments on the Na and K concentration of kaolin are shown in Figures 8 and 9. Sodium was adsorbed in all cases, but only slightly above the as-received (25°C) level in the inert environment.

Greater adsorption at higher temperature was evident only in the  $\text{H}_2/\text{N}_2$  environment. In the synthetic fuel gas environment, Na adsorption was consistently 8 mg Na  $\text{g}^{-1}$  kaolin higher than the as-received material. Potassium loss was in the range of 0.1 to 0.3 mg K  $\text{g}^{-1}$  kaolin for all experiments. The as-received material contained 5 mg Na  $\text{g}^{-1}$  kaolin but only 0.7 mg K  $\text{g}^{-1}$  kaolin and K was lost in the NaCl environment. Equilibrium calculations indicate that the reaction of KCl with aluminosilicate is thermodynamically favored,<sup>15</sup> but the fate of Na and K initially bound in the kaolin matrix is undetermined under the conditions of a gas stream containing KCl, information potentially more useful to biomass gasifier process stream applications depending on the chosen fuel.

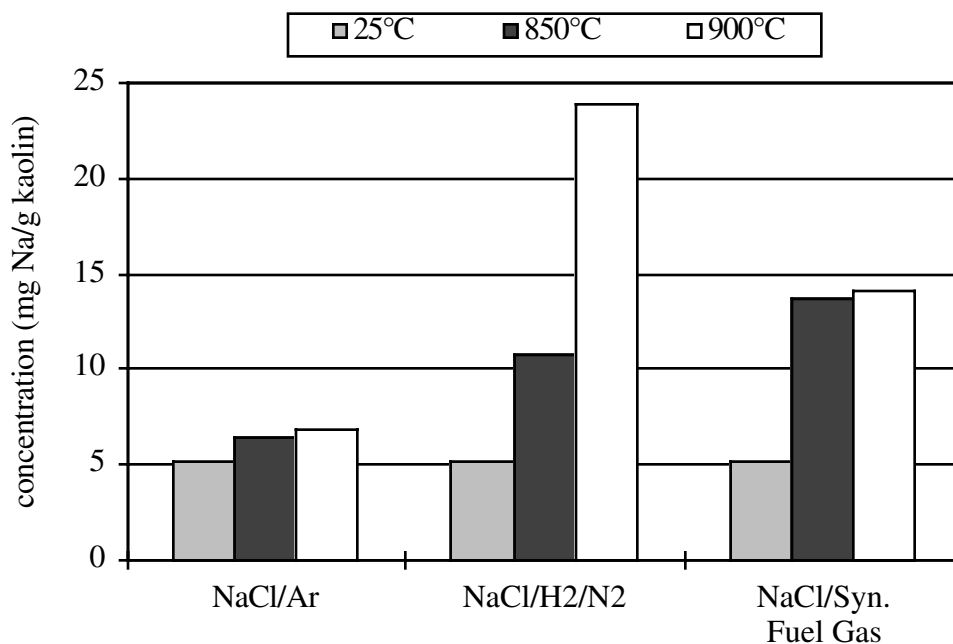


Figure 8. Sodium concentration of kaolin after 4-h exposure to 80 ppmv NaCl in various carrier gases at elevated temperature. The 25°C data points are all identical and represent the as-received material. Carrier gases are argon, 10% H<sub>2</sub> in N<sub>2</sub>, and synthetic fuel gas containing 7.5% CO<sub>2</sub>, 23% CO, 14% H<sub>2</sub>, 55% N<sub>2</sub>, and the balance composed of H<sub>2</sub>S and HCl. (Data from reference 10.)

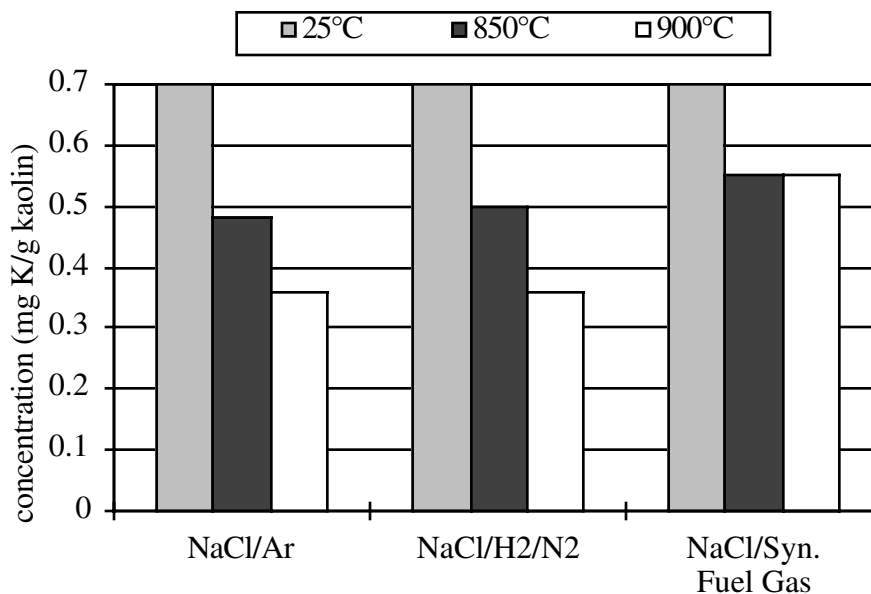
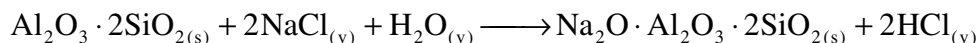


Figure 9. Potassium concentration of kaolin after 4-h exposure to 80 ppmv NaCl in various carrier gases at elevated temperature. The 25°C data points are all identical and represent the as-received material. Carrier gases are argon, 10% H<sub>2</sub> in N<sub>2</sub>, and synthetic fuel gas containing 7.5% CO<sub>2</sub>, 23% CO, 14% H<sub>2</sub>, 55% N<sub>2</sub>, and the balance composed of H<sub>2</sub>S and HCl. (Data from reference 10.)

Tests by Punjak and coworkers<sup>20-22</sup> determined that kaolinite effectively removed more than 90% of alkali (NaCl or KCl) in a carrier gas of N<sub>2</sub> or air.<sup>20</sup> The adsorption occurred irreversibly and the rate of adsorption was determined to increase with greater gas-phase concentration of the alkali. Adsorption capacity was found to depend on the presence of water vapor, in a similar manner to the behavior demonstrated by emathlite. In an SFG (15% CO<sub>2</sub>, 3% O<sub>2</sub>, 80% N<sub>2</sub>, and 2% H<sub>2</sub>O) environment, kaolinite gained 266 mg for every gram of sample mass, but only 52 mg for every gram in a N<sub>2</sub> carrier gas. Although not explicitly stated, the weight gain is presumably Na rather than NaCl, since sample spectra indicate the presence of Na and the absence of Cl. A proposed mechanism for the adsorption of NaCl on metakaolin (dehydrated kaolin) to form nephelite was given as:



The stoichiometry of the reaction suggests a fully reacted capacity of 279 mg Na g<sup>-1</sup> kaolinite, in good agreement with the experimental value of 266 mg Na g<sup>-1</sup> kaolinite. Weight gain as a function of time for kaolinite exposed to 230 ppmv NaCl vapor in SFG is shown in Figure 10.

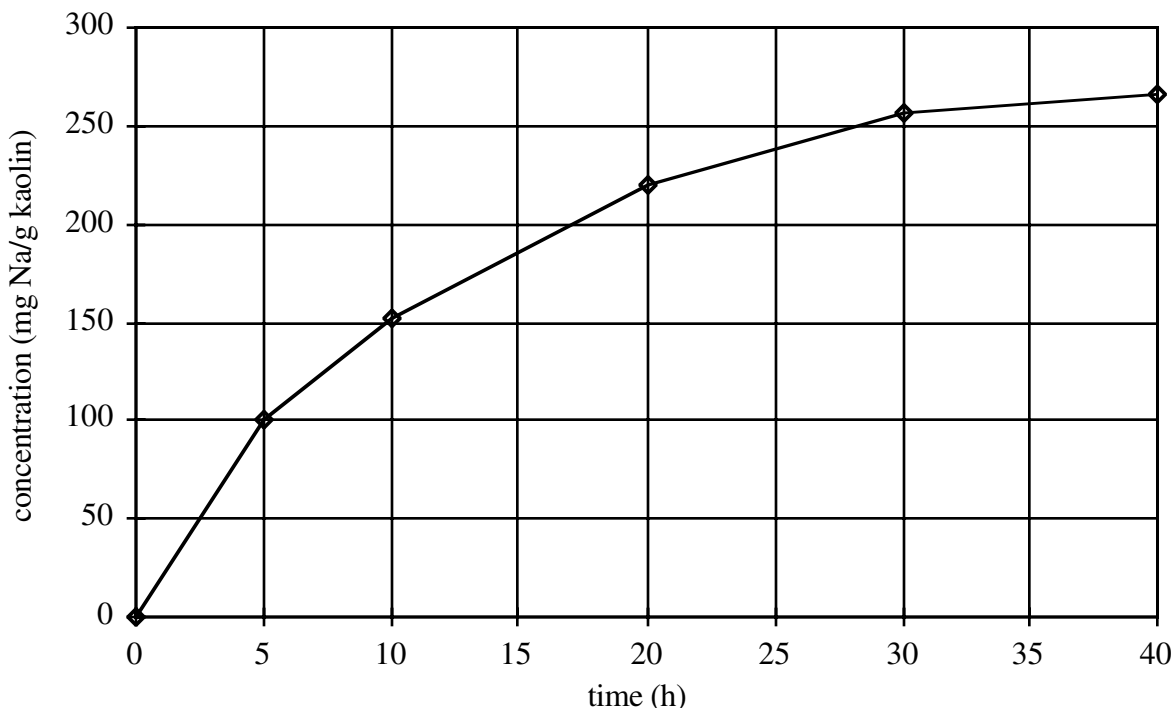


Figure 10. Weight gain of kaolinite sample as a function of time resulting from exposure to 230 ppmv NaCl in SFG (80% N<sub>2</sub>, 15% CO, 3% O<sub>2</sub>, and 2% H<sub>2</sub>O) at 800°C and atmospheric pressure. (Data taken from references 8 and 9.)

### 2.3.5 Low-Temperature Coal Char and Gasifier Ash

Mulik *et al.*<sup>23</sup> investigated the use of low-temperature coal char and coal gasifier ash as alkali getters. The materials were derived from Minnehaha or Renton feed char from the Westinghouse PDU devolatilization unit and high-temperature Pittsburgh ash formed in an agglomerating coal gasifier. Both were ashed at 600°C to remove remaining carbon, producing samples with carbon

contents of ~1.2% by weight. Each was formed into pellets for gettering tests. Potassium content (as K<sub>2</sub>O) of the Minnehaha char and Pittsburgh gasifier ash was 2.87% and 1.82%, respectively. Sodium content (as Na<sub>2</sub>O) of the Minnehaha char was 0.4% and Pittsburgh gasifier ash contained 0.07% Na<sub>2</sub>O as shown in Table 1. Elemental analyses for the balance of the samples were not reported. Back scatter electron and scanning x-ray microprobe techniques applied to the samples detected the presence of Al, Si, K, Na, Cl, S, Ti, and Fe. X-ray diffraction analysis found a wide variety of heavy metal compounds in trace amounts.

Samples of both materials were heated to 675°, 800°, and 900°C in an inert environment. Total Na concentrations in the two materials remained unchanged, as did the distribution of Na between water-soluble and -insoluble forms. The same was true for K in the gasifier coal ash and for the low-temperature coal char at 675°C. At the two remaining temperatures, 800° and 900°C, the water-soluble K transitioned into water-insoluble forms in both materials, with a greater degree of conversion at higher temperature. The total K concentration was reduced by about 10%, indicating that some volatilization may have occurred.

Performance of the getter materials after 4-h exposures to two carrier gases (Ar, and 10% H<sub>2</sub> with the balance N<sub>2</sub>) containing 80 ppmv NaCl is shown in Figures 11 and 12. Sodium adsorption at 850°C is relatively insensitive to carrier gas type; all yielding results are 23 to 37 mg Na g<sup>-1</sup> sorbent. Adsorption in the Ar carrier gas at 900°C is approximately 100 mg Na g<sup>-1</sup> sorbent for both materials, a better than threefold improvement over performance at 850°C. The presence of H<sub>2</sub> appears to limit Na adsorption at high temperatures, possibly by competing for active sites on the sorbent surface. Of the two materials, low-temperature coal char is the more effective getter material in terms of Na adsorption under directly comparable conditions. Potassium retention by both sorbents decreases with higher reactor temperature. The Ar carrier gas tests proved to volatilize larger amounts of K than the H<sub>2</sub>/N<sub>2</sub> mixture. Under conditions more representative of gasification (10% H<sub>2</sub> in N<sub>2</sub>), net alkali removal ranged from 25 to 33 mg alkali g<sup>-1</sup> sorbent, with the low-temperature coal char performing better than the gasifier ash at both temperatures.

### 2.3.6 Attapulugus Clay

Attapulugus clay is a member of the palygorskite group of clay minerals, so named because of their origins in Attapulugus County, Georgia.<sup>26,27</sup> Palygorskites have an idealized formula of (OH)<sub>2</sub>Mg<sub>5</sub>Si<sub>8</sub>O<sub>20</sub>·8H<sub>2</sub>O. The lattice structure of attapulugites exhibits substitution of Al for Mg at an Al:Mg ratio of about 1:1; this is easily confirmed for the composition reported in Table 1, 12% Al<sub>2</sub>O<sub>3</sub>, 68% SiO<sub>2</sub>, and 10.5% MgO. Attapulugus clay was tested by Lee and Johnson<sup>14</sup> for use as a getter material and found to remove 64% of the NaCl vapor during a 3-h test. At the conclusion of the test, the sample was found to be friable and was rejected from further consideration. Testing was also performed by Jain and Young.<sup>18</sup> Over a 3-h duration at 790°C in an air flow containing 40 ppmw NaCl vapor and 3% H<sub>2</sub>O vapor, Attapulugus clay adsorbed 0.35 mg Na g<sup>-1</sup> material. These results were not competitive with those of other materials in the screening series, and Attapulugus clay was not advanced for further testing.<sup>18</sup>

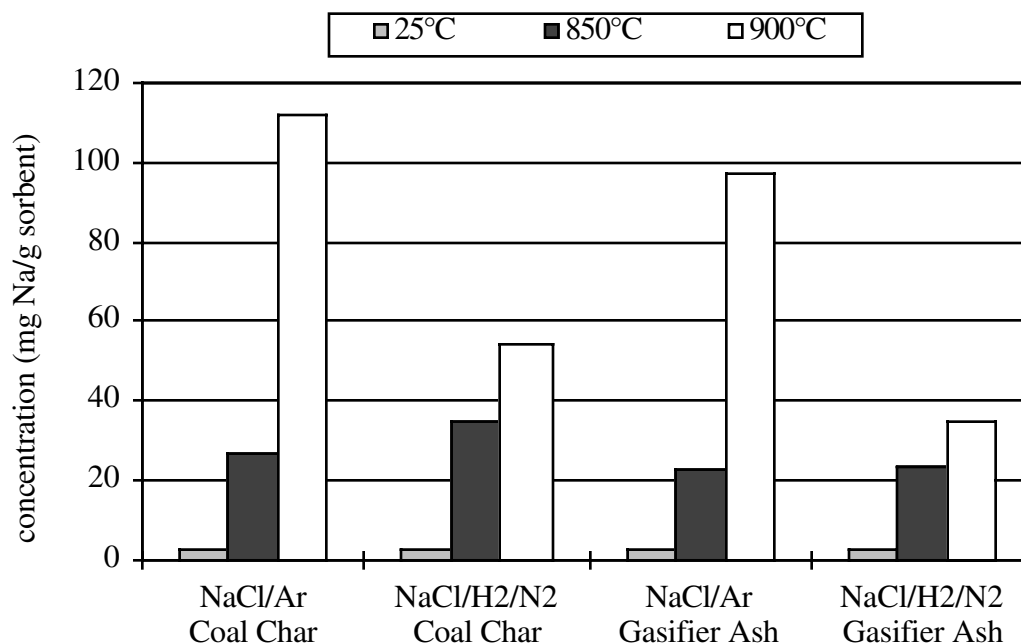


Figure 11. Sodium concentration of coal char- and gasifier ash-derived getter materials after 4-h exposure to 80 ppmv NaCl in various carrier gases at elevated temperature. The 25°C data points are all identical and represent the as-received material. Carrier gases are Ar, and 10% H<sub>2</sub> in N<sub>2</sub>. (Data from reference 10.)

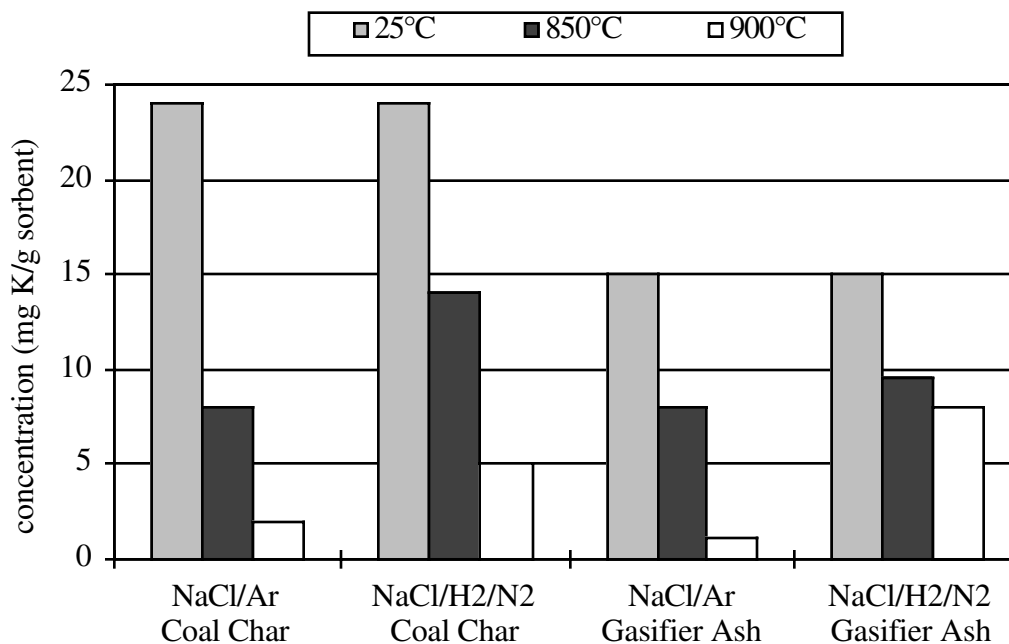


Figure 12. Potassium concentration of coal char- and gasifier ash-derived getter materials after 4-h exposure to 80 ppmv NaCl in various carrier gases at elevated temperature. The 25°C data points are all identical and represent the as-received material. Carrier gases are Ar, and 10% H<sub>2</sub> in N<sub>2</sub>. (Data from reference 10.)

### 2.3.7 Burgess No. 10 Pigment

Lee and Johnson<sup>14</sup> included Burgess No. 10 pigment with a composition of 38.6% Al<sub>2</sub>O<sub>3</sub> and 45% SiO<sub>2</sub> in alkali getter screening tests. Using NaCl in air, and NaCl and KCl in dry SFG, experiments determined that Burgess No. 10 pigment removed 78%, 85%, and 74% of the alkali, respectively. Activated bauxite and diatomaceous earth were included in the program and found to possess superior gettering qualities. As a result, Burgess No. 10 pigment was not included in further tests.

### 2.3.8 Silica Gel

Silica gel was included in the test programs of Lee and Johnson<sup>14</sup> and Jain and Young.<sup>18</sup> Lee and Johnson found that it collected only 40% of the NaCl present in the air flow. Inspection of the material showed that preheating the silica gel sample had severely diminished its pore structure; this was cited as the cause of reduced gettering efficiency. This conclusion appears to be supported by the results of Jain and Young, which showed that 0.26 mg Na g<sup>-1</sup> silica gel were adsorbed in a 2-h test, but that no incremental amount of alkali was adsorbed during a 3-h experiment. This type of behavior is consistent with a severe reduction of pore structure in the early stages of the test, possibly because of high-temperature exposure.

### 2.3.9 Dolomite and Calcined Dolomite

Dolomite and calcined dolomite were included in the test battery performed by Jain and Young.<sup>18</sup> The compositions in Table 1 reflect the decomposition of the magnesium and calcium carbonates to oxide forms in the calcination process. Testing of the two materials was limited. In 2-h exposures to 40 ppmv NaCl, 3% H<sub>2</sub>O in air at 790°C, both dolomite and calcined dolomite collected about 0.1 mg Na g<sup>-1</sup> sorbent. In similar experiments, diatomaceous earth retained about 1 mg Na g<sup>-1</sup> sorbent.

## 2.4. Modeling

Modeling of the gettering process was approached differently, depending on whether it was perceived as physical adsorption or chemisorption. Luthra and Leblanc<sup>16</sup> determined that data from their study of NaCl gettering by bauxite and alumina could be described using physical adsorption isotherms. By plotting the data, they determined that an extension of the Brunauer Emmet Teller (BET) isotherm best described their results. The BET isotherm overestimated the amount of adsorption, whereas the Langmuir isotherm underestimated it. Values of monolayer coverage of NaCl and KCl on alumina rods were estimated at 31 and 40 mg adsorbate g<sup>-1</sup> sorbent, respectively. They concluded that kinetics of adsorption would be fast enough and the binding constant (ratio of the vapor pressure of the adsorbate at process conditions to the partial pressure of the adsorbate at process conditions) sufficiently large for alumina-based sorbents to be effective. The limitation of applying this method of gas cleaning was perceived to be one of mass transport given that microporous sorbents were to be employed.

Several investigators<sup>20-22</sup> employed simple geometries (slab or sphere) to describe porous sorbent particles in modeling the processes involved in alkali gettering. The models were used to extract kinetic parameters from the experimental data and varied in sophistication. A simple reaction-diffusion model was employed that used effective diffusivities and reaction rates to describe the physical processes within the porous particle. An initial model<sup>20</sup> defined a critical time

at which a saturated layer formed on the surface of the particle with different mathematical descriptions for saturated and unsaturated regions. A simpler approach<sup>21,22</sup> incorporated the maximum loading rates obtained from the experiment into the model, in effect guaranteeing that the two should agree in the final state. Kinetic parameters and diffusivities were chosen to fit the weight gain profile from initial exposure to final loading. Application of the model to independent data sets and an investigation of the effect of particle size on alkali uptake provided good results.

A model was developed for cylindrical particle geometry<sup>19</sup> with three parameters that determined the global kinetics of the Na adsorption reaction, the film mass transfer coefficient, the final alkali loading of the sorbent, and the lumped diffusivity for alkali in the solid phase. Comparison of model predictions of pellet final Na weight percentage with experimental results from tests varying gas-phase alkali concentration and duration of exposure differed by 10% to 85%. Differences were partly attributed to difficulties in measuring and maintaining constant gas-phase NaCl concentrations during experiments. This single pellet model was used as the basis for a simple fixed-bed reactor model adapted from Kunii and Levenspiel.<sup>34</sup> Model results were consistent, to within an order of magnitude, with experimental results in predicting pellet Na concentrations as a function of bed depth and alkali concentration of the outlet gas.

### **3. MATERIALS AND METHODS**

An experimental investigation of alkali gettering was performed. Banagrass, a fuel used in previous tests,<sup>12</sup> was gasified to produce a high-alkali gas stream, then passed through a ceramic filter and an alkali sorbent bed. Measurements were made to determine the amounts of alkali and Cl retained on the gasifier bed material, contained in the char filtered from the product gas stream, captured by sorbent material, and residual remaining in the product gas.

#### **3.1 Fuel**

Approximately 1.5 tonnes of banagrass were hand-harvested from fields at the Waiialua Sugar Company, Inc., on Oahu, Hawaii. Fresh stalks were passed through a chipper for initial particle size reduction, then dried to equilibrium moisture content in a 1.22 m x 1.22 m x 4.88 m bed using forced, ambient air (Figure 13). The dried fuel lot was subsequently hammermilled to pass through a 3.2-mm screen, thoroughly mixed, and finally sampled for analysis.

#### **3.2 Getter Materials**

Emathlite and activated bauxite were selected as candidate getter materials for the test series and quantities of each were obtained from Mid-Florida Mining Company (Lowell, Florida) and Porocel Adsorbents and Catalysts (Houston, Texas), respectively. Each lot was screened to obtain particles of 2.36 to 3.35 mm class in sufficient quantities for testing. Emathlite was also screened to obtain a quantity of material in the size range 4.0 to 4.75 mm.

#### **3.3 Experimental Methods**

Tests were conducted in a bench-scale fluidized-bed gasification system. The system is shown schematically in Figure 14 and a detailed drawing of the gasifier is presented in Figure 15. The gasifier is constructed of 310 stainless steel pipe, with a dense bed diameter of 89 mm and a freeboard diameter of 152 mm. The dense bed section is externally heated by four, 4-kW heaters (Model 274A, Thermcraft, Inc., Winston-Salem, North Carolina) and the disengagement zone is



Figure 13. Forced ambient air dryer containing chopped banagrass.

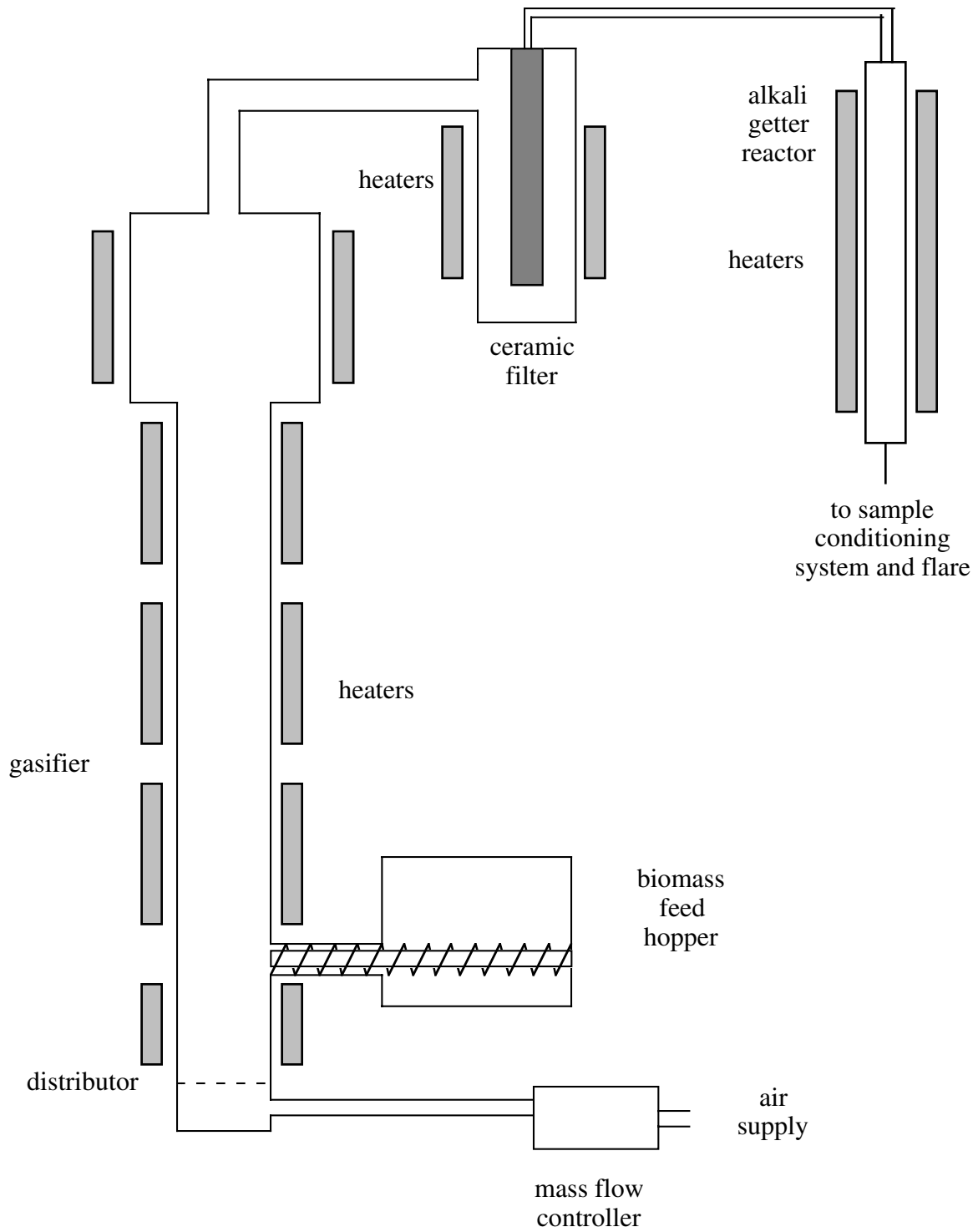


Figure 14. Schematic of bench-scale gasifier test facility.

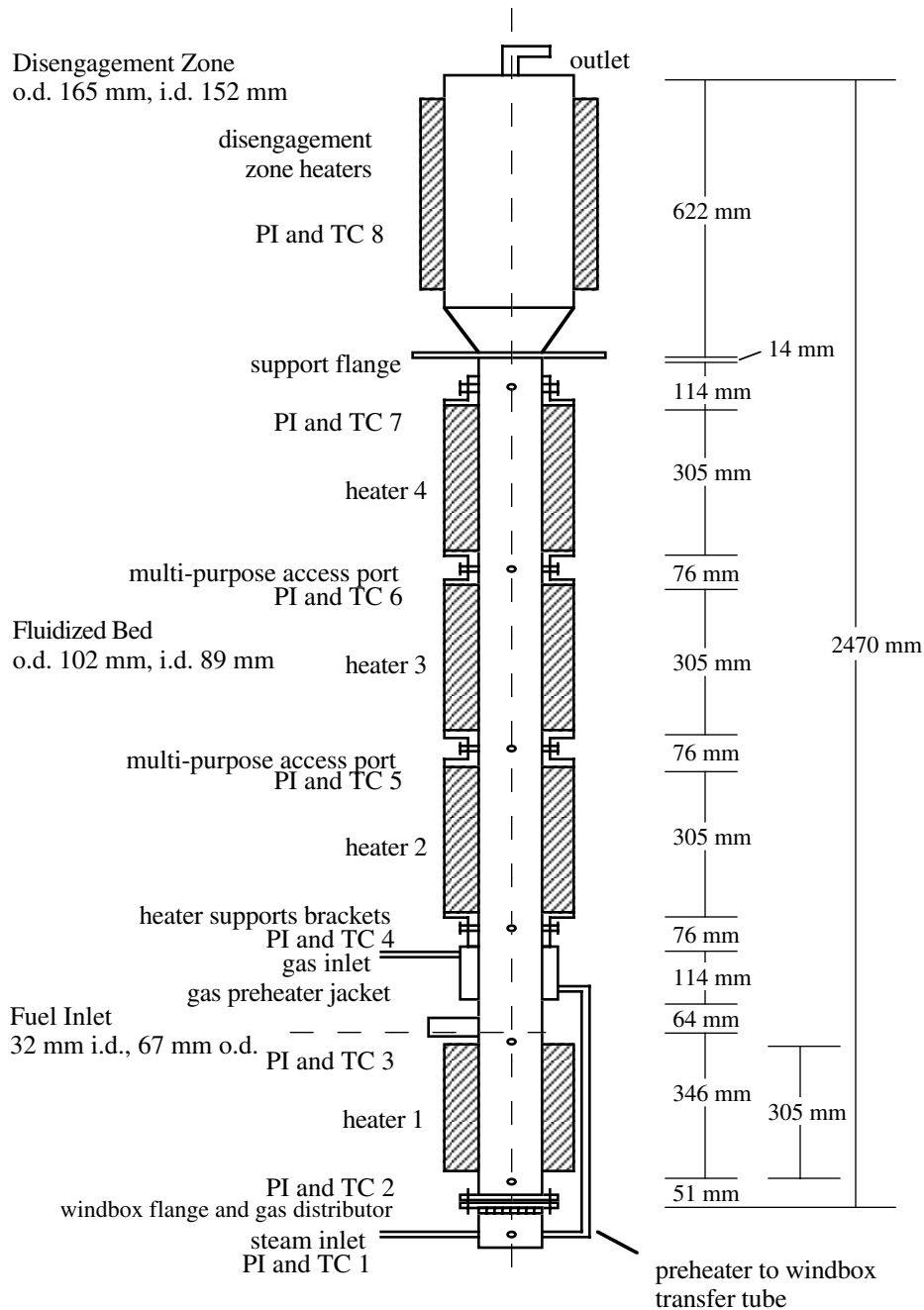


Figure 15. Bench-scale fluidized bed reactor.

equipped with an 8.7-kW heater (Mellen Co., Inc., Webster, New Hampshire). Pressure taps, thermocouples, and probe access ports are located along the height of the reactor. All electronic signals are processed using two, 32-channel multiplexer amplifiers (Model SCXI-1100, National Instruments, Austin, Texas) and a 12-bit, analog-to-digital converter board (Model AT-MIO-16E-2, National Instruments, Austin, Texas) in an IBM PC-750 personal computer.

Fuel is fed to the reactor from a sealed fuel hopper via a variable-speed metering screw. Air, used as the fluidizing agent for the tests, is metered into the windbox below the distributor by a mass-flow controller (Model 5851E, Brooks Instruments, Hatfield, Pennsylvania). The bed material consists of beads with diameters 0.21 to 0.42 mm (+40–70M) (Norton-Alcoa, Fort Smith, Arkansas).

Flow exits the reactor and passes through a heated silicon carbide filter with 40-mm internal diameter, 60-mm external diameter, 559-mm length, and pore size of 5  $\mu\text{m}$  (Model A-901346-0, Industrial Filter and Pump Mfg. Co., Cicero, Illinois) contained in a stainless steel housing (Figure 16). The filter vessel is heated in a 10-kW, split-hinged, tube furnace (Model SC12-5X30V, Mellen Co., Inc., Webster, New Hampshire) to maintain product stream temperature.

Flow exiting the filter vessel is directed to a fixed-bed alkali getter reactor housed in a 12-kW split-hinged tube furnace (Model SC12-7X24V, Mellen Co. Inc., Webster, New Hampshire) as shown in Figure 17. Two interchangeable stainless steel alkali getter reactor bodies of different internal diameters (51 and 76 mm) were fabricated to permit testing with different gas residence times. The getter material was separated into 15 distinct volumes, or cells, along the length of the reactor using stainless steel screens to permit the bed to be analyzed in increments. Flow exiting the alkali getter reactor was directed to a sample conditioning system, shown in Figure 18. The sample conditioning system consists of two parallel trains, one that diverts the flow around the alkali getter reactor, allowing it to be bypassed, and a second located downstream of the getter reactor. The bypass train, consisting of a cooling coil mounted in an ice bath and a condensate collection trap, is used during system start-up and shut-down and serves to cool the gas stream and remove condensable species from the filtered product flow. The bypass line is not used for quantification but permits the gasifier to reach a steady condition before flow is directed to the getter reactor. The second conditioning train cools the product gas exiting the alkali getter reactor, removes and collects condensable species, permits gas grab sampling for off-line analysis, and records the total volume of dry gas flow through the system. A cooling coil and condensate collection trap identical to the bypass line described earlier was connected to the exit of the alkali getter reactor. Flow exiting the condensate collection trap was directed through two additional traps, connected in series, which contained stainless steel wool packing to remove entrained condensate. The traps were followed by coalescing filters (Hepa-Cap 36, Whatman Inc., Haverhill, Massachusetts) to remove fine aerosol. The clean dry gas stream passed through a dry test meter to measure the total gas volume. Grab samples were collected in glass sample bombs and analyzed off-line for the permanent gases  $\text{H}_2$ ,  $\text{N}_2$ ,  $\text{CO}$ ,  $\text{CH}_4$ ,  $\text{CO}_2$ , and  $\text{C}_2\text{H}_m$  using a gas chromatograph (GC) (AutoSystem, Perkin-Elmer, Norwalk, Connecticut) equipped with a 1.5 m x 3 mm packed column (Carboxen 1000, Supelco, Bellefonte, Pennsylvania) and thermal conductivity detector. A three-point GC calibration was performed using a certified standard gas before each test. A slip stream of clean dry gas exiting either sample conditioning systems is directed to an on-line non-dispersive infrared radiation gas analyzer (Model URAS 10E, Applied Automation/Hartmann & Braun, Bartlesville, Oklahoma) to measure  $\text{CO}$ ,  $\text{CO}_2$ , and  $\text{CH}_4$ . The on-line analyzer was calibrated before each test using certified zero and span gases. Calibration was reconfirmed after each test using the same calibration gases. Finally, the product gas was combusted in a propane-piloted flare for disposal.

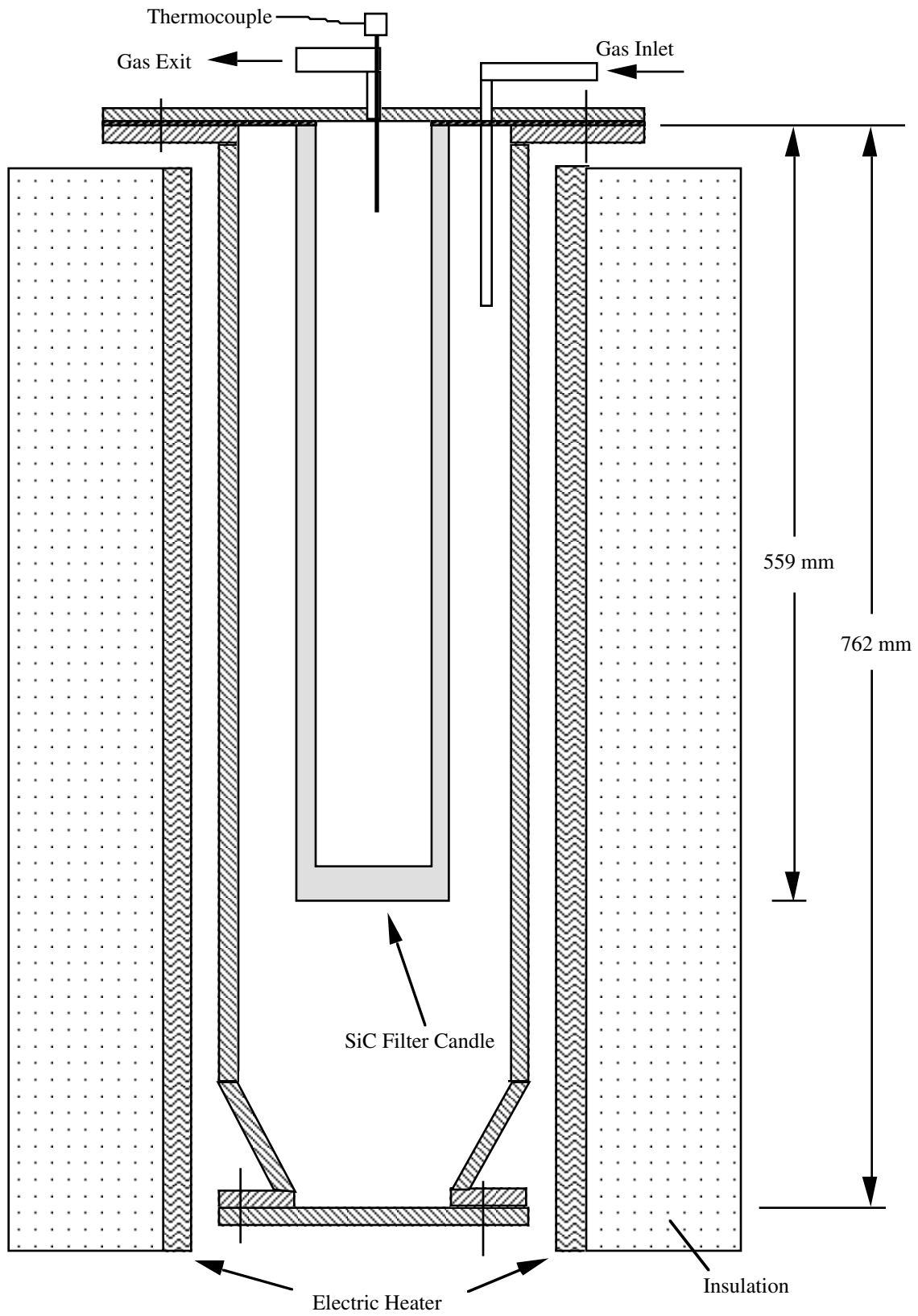


Figure 16. Heated ceramic filter assembly.

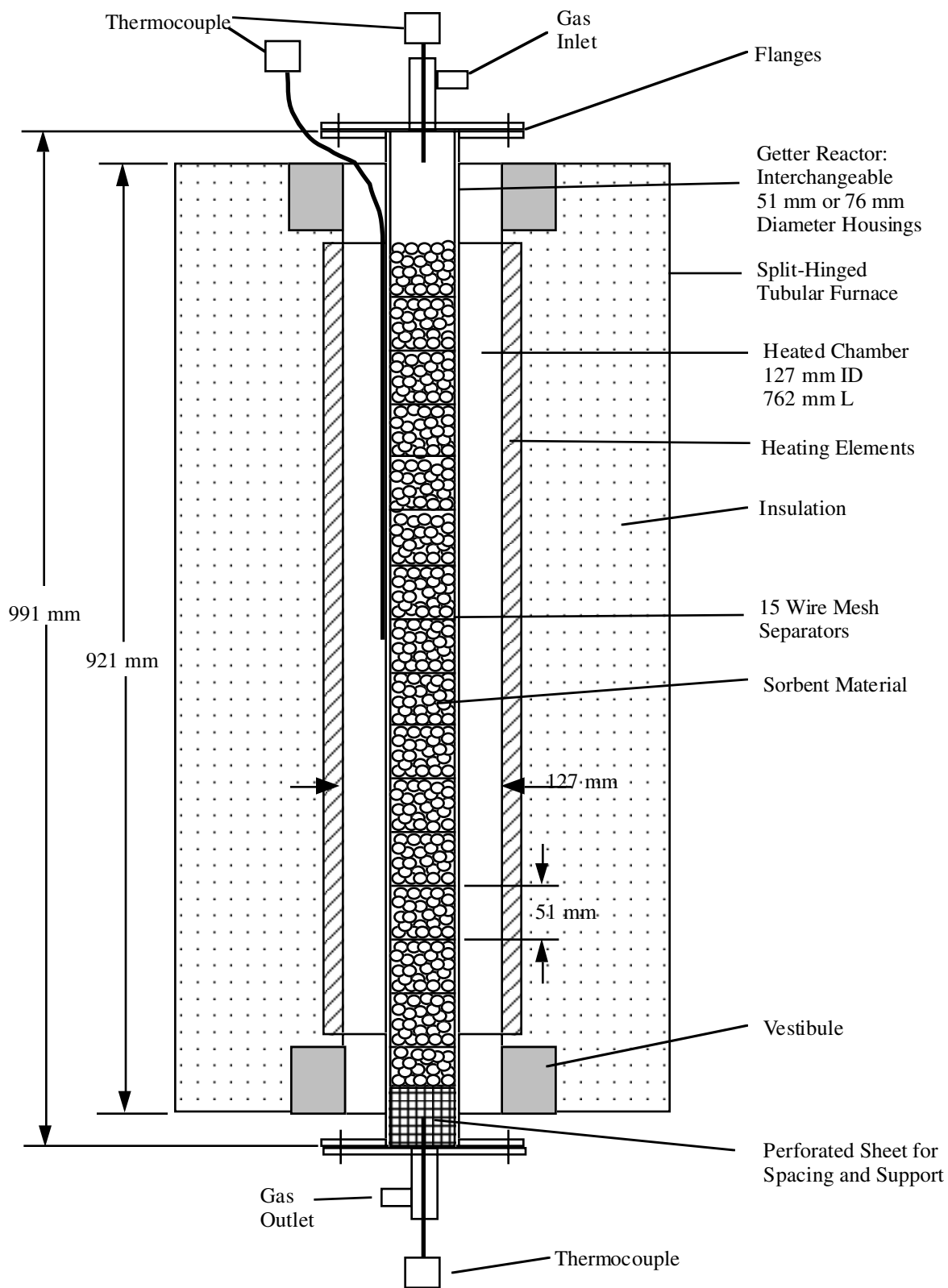


Figure 17. Fixed-bed, alkali getter reactor.

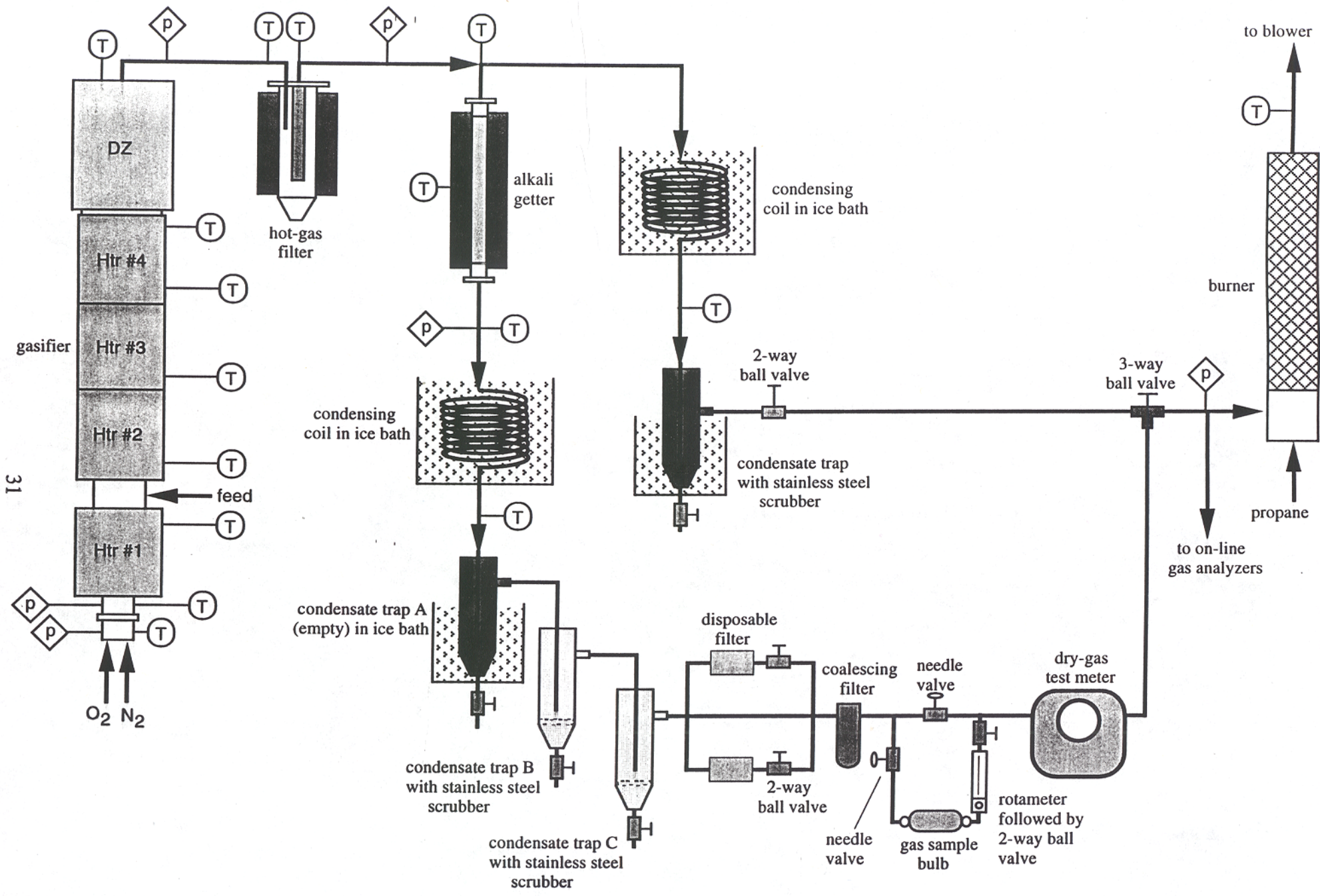


Figure 18. Fluidized bed gasifier, ceramic filter, alkali getter reactor, and sample conditioning system.

All alkali getter tests were conducted over a 4-week period. In preparation for each test, fresh bed material and fuel were weighed and placed in the reactor and the fuel hopper, respectively. Quantities of getter material were weighed in equal increments and placed in each individual volume defined by the stainless steel screen dividers. All tests were performed at 820°C and the bed was preheated using the external heaters with air flowing through the reactor until a stable temperature profile was obtained. The filter vessel and getter reactors were also preheated to ~725° and ~660°C, respectively, using external heaters.

To begin the test, the feeder was turned on and air flow to the reactor adjusted to produce the desired equivalence ratio. These conditions were maintained throughout the duration of each test, and identical feeder and air control settings were used for all tests. During the start-up period, the product gas stream exiting the filter vessel was diverted through the bypass sample conditioning system. Quantitative sampling, as described later, was begun when the system had attained a steady temperature distribution and relatively constant gas composition as determined by on-line gas analyzers. Steady conditions were normally achieved about 1 h after fuel feeding started; the flow was then directed through the alkali getter reactor and quantitative sampling system. Sampling periods generally lasted 3 h. At the conclusion of the sampling period, product gas flow was redirected to the bypass sample conditioning system and shortly thereafter, the test was terminated by simultaneously shutting down fuel and air flow to the reactor and all system heaters.

Immediately after each test, the sample conditioning system following the alkali getter reactor was dismantled. The weight of condensate drained from the cooling coil during the course of the test and collected in the trap located directly beneath was measured and recorded. The coil and downstream traps were cleaned with acetone and the weights of the resulting solutions were measured and recorded. After the system cooled, remaining fuel was removed from the feed hopper, char was recovered from the ceramic filter, and bed material was removed from the gasifier. Each was sampled and weighed. The alkali getter reactor was dismantled and the getter material in each volume increment was recovered, weighed, and sampled. The surfaces of the alkali getter reactor exposed to the gas flow were rinsed with distilled water and the resulting solution was weighed and recorded.

An initial test was performed with an empty getter reactor in the process stream, hereafter referred to as the "blank run" in this report. Samples of fuel and gasifier bed material were obtained before this test, and analyses generated from these samples were considered to be representative for all subsequent tests. Fuel samples were subjected to ultimate (C, H, O, N, S, and Cl), proximate (volatile, fixed carbon, and ash), heating value, and elemental ash (Si, Al, Ti, Fe, Ca, Mg, Na, K, P, S, Cl, and CO<sub>2</sub>) analyses (Hazen Research, Inc., Golden, Colorado). The fresh, pretest, gasifier bed material was analyzed for Ca, C, Cl, Mg, Na, K, P, and S. At the conclusion of the blank run, bed material recovered from the gasifier was subjected to identical analyses. Char collected in the ceramic filter was subjected to ultimate, proximate, heating value, and ash analyses, identical to those described earlier for the fuel samples. Condensate from the cooling coil, acetone solutions from cleaning the traps, and the distilled water rinse from the inside of the alkali getter reactor were collected and stored in individual sealed Nalgene containers. Each was analyzed for Na, K, Cl, Ca, Mg, Si, Al, P, Fe, and S.

Samples collected from subsequent tests of various alkali getter materials were subjected to a reduced battery of analyses. Given that the conditions in the gasifier and filter were kept constant for all tests, the post-test bed material and the filter char from each of the tests were analyzed for K, Na, and Cl to compare against the results of the blank run as a check of reproducibility of

conditions within the gasifier. Samples collected downstream of the alkali getter reactor, cooling coil condensate, acetone cleaning solutions, and the distilled water rinse from inside the alkali getter reactor were analyzed for K, Na, Cl, Ca, and P.

Alkali getter materials as received from the manufacturers were subjected to analyses for Ca, C, Cl, Mg, Na, K, P, and S. Samples of both alkali getter materials were heated to 750°C in a muffle furnace for 4 h, then subjected to the same analytical tests as the as-received material. Alkali getter material recovered after each test from the partitioned volumes within the reactor was subsampled using the cone and quarter method and analyzed for K, Na, and Cl. Samples were also examined using an SEM (Zeiss 962) equipped with an energy-dispersive x-ray fluorescence analysis system (Oxford Instruments) operated by the Analytical Electron Microscope Laboratory at the University of Hawaii. This technique was used to obtain semiquantitative elemental analyses of the surface of individual getter particles for 11 inorganic ash elements (Ca, Cl, Mg, P, K, Na, S, Al, Fe, Si, and Ti) and oxygen. Each spectrum was collected from the full screen at an SEM magnification of 1,000X at a rate of ~3,000 counts per second over a period of 150 s. Ten particles, randomly chosen from each test, were examined and a mean concentration and standard deviation were computed for each element. Element maps of Ca, Cl, Mg, P, K, Na, S, Al, Fe, Si, and Ti were collected.

## 4. RESULTS AND DISCUSSION

### 4.1 Fuel Properties

Three samples were removed from the fuel lot and analyzed. Results of these analyses and average fuel properties are presented in Table 3. The results of the three individual analyses are generally consistent, showing little variation. The exceptions are the concentration of  $\text{Al}_2\text{O}_3$  and  $\text{Fe}_2\text{O}_3$  in the ash of sample 1 and the CaO concentration in the ash of sample 3. The  $\text{Al}_2\text{O}_3$  and  $\text{Fe}_2\text{O}_3$  concentrations in sample 1 (0.58% and 0.51%, respectively) are both higher than those found in samples 2 (0.15% and 0.32%, respectively) and 3 (0.08% and 0.27%, respectively). This may be a result of contamination of sample 1 with soil, since both are soil elements. The lower CaO concentration in sample 3 (1.01%) compared to samples 1 (5.20%) and 2 (5.11%), though notable, does not have a clear explanation.

The average concentrations of inorganic elements as a percentage of dry fuel mass are graphed in Figure 19. Silicon, K, Cl, and N are all present at concentrations higher than 0.2%, with the remaining elements present at lower levels. Sodium, the other alkali element present in plants, was found at a concentration of ~0.1%. The high concentrations of K and Cl in the fuel indicate the high likelihood for fouling and slagging. On a unit energy basis (Table 3), total alkali and Cl are present at average concentrations of 0.82 and 0.34  $\text{kg GJ}^{-1}$ , respectively. By comparison, bagasse, a fuel that has historically been used in thermochemical energy conversion facilities without ash-handling problems<sup>35</sup> has significantly lower values for total alkali and Cl of 0.12 and 0.03  $\text{kg GJ}^{-1}$ , respectively.<sup>12</sup> A total alkali content of 0.3  $\text{kg GJ}^{-1}$  is a general limit above which ash deposition is likely to occur. In the literature, fuels with Cl concentrations of about 0.3  $\text{kg GJ}^{-1}$  were associated with slagging, deposition, and corrosion problems.<sup>6</sup>

Table 3. Summary of analyses of banagrass samples taken from the gasifier fuel lot.

	Sample 1	Sample 2	Sample 3	Average
<u>Proximate Analysis (weight %, dry basis)</u>				
Fixed Carbon	17.69	18.26	16.59	17.51
Volatiles	76.58	75.83	77.68	76.70
Ash	5.73	5.91	5.73	5.79
HHV* (MJ/kg, dry basis)	17.9	17.9	17.8	17.9
<u>Ultimate Analysis (weight %, dry basis)</u>				
C	43.14	43.69	43.50	43.44
H	5.44	5.59	5.62	5.55
O	44.62	43.85	44.19	44.22
N	0.38	0.30	0.28	0.32
S	0.08	0.07	0.06	0.07
Cl	0.61	0.59	0.62	0.61
Ash	5.73	5.91	5.73	5.79
<u>Ash Analysis (weight %, dry basis)</u>				
SiO <sub>2</sub>	51.55	52.71	53.27	52.51
Al <sub>2</sub> O <sub>3</sub>	0.58	0.15	0.08	0.27
TiO <sub>2</sub>	<0.01	<0.01	0.02	0.01
Fe <sub>2</sub> O <sub>3</sub>	0.51	0.32	0.27	0.37
CaO	5.20	5.11	1.01	3.77
MgO	3.89	3.69	4.10	3.89
Na <sub>2</sub> O	2.59	2.98	2.80	2.79
K <sub>2</sub> O	21.2	22.9	22.8	22.30
P <sub>2</sub> O <sub>5</sub>	3.26	3.21	2.96	3.14
SO <sub>3</sub>	2.28	2.26	2.08	2.21
Cl	7.00	8.07	7.96	7.68
CO <sub>2</sub>	0.13	0.09	0.13	0.12
Other	1.81	-1.49	2.52	0.94
<u>Concentration per Unit Energy Basis (kg/GJ)</u>				
K <sub>2</sub> O+Na <sub>2</sub> O	0.78	0.86	0.83	0.82
Cl	0.34	0.33	0.35	0.34
SO <sub>3</sub>	0.11	0.10	0.08	0.10

\* HHV = higher heating value

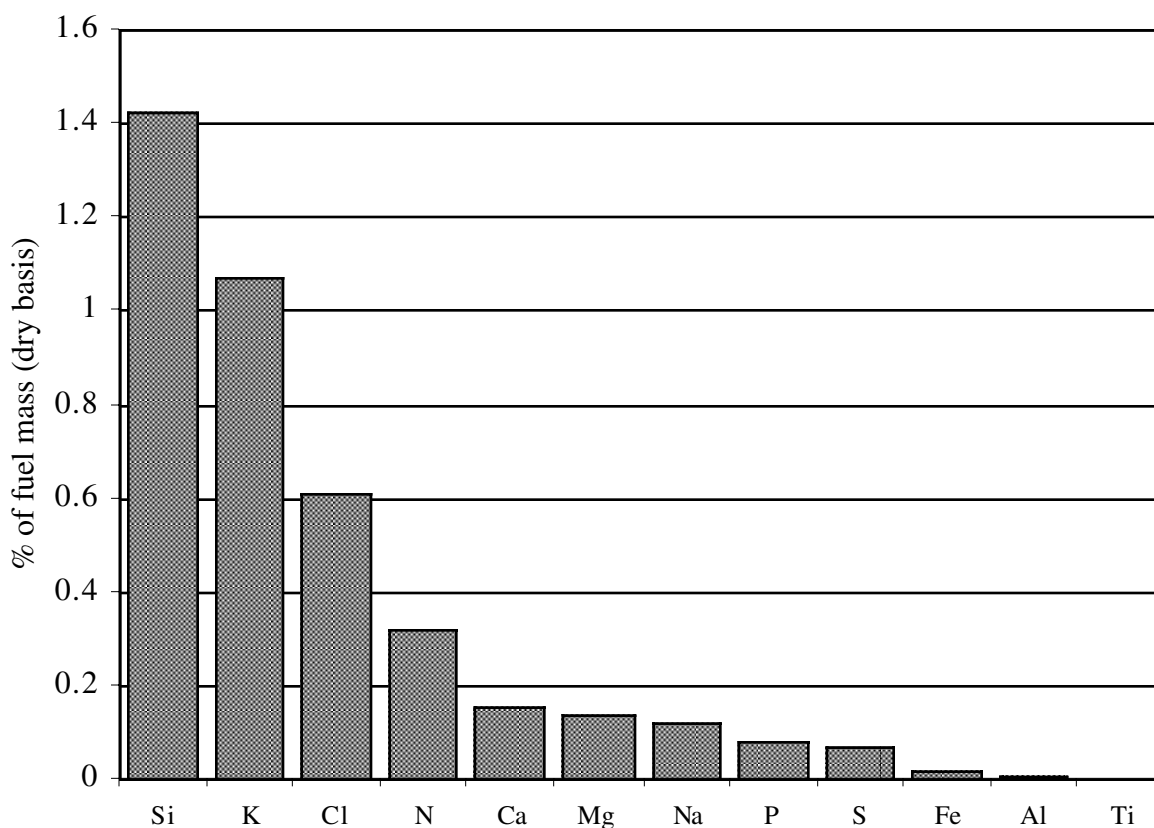


Figure 19. Major inorganic components of banagrass as percentage of fuel mass.

## 4.2 Test Conditions

Six tests were performed: an initial test with no material present in the alkali getter reactor, four subsequent tests defining a matrix of two getter materials and two getter reactor diameters (space time), and a final test that used a different getter particle size. The test conditions are summarized in the upper section of Table 4. Each test is labeled according to the getter reactor diameter used (76 mm versus 51 mm), the type of getter material used (AB = activated bauxite and E = emathlite). As an example, test 76G-AB used the 76-mm diameter reactor with activated bauxite. The first test presented in Table 4, 76G-B was the blank (B) test conducted with no getter material in the reactor. The last test presented in Table 4, 51G-E-P, used larger particles of getter material than the other tests, thus the designation (-P) added to the name. Great effort was made to duplicate conditions in the gasifier and heated ceramic filter to generate a product gas stream of constant composition, both permanent gas species and vapor phase alkali. A dry fuel feed rate of  $\sim 1 \text{ kg h}^{-1}$ , equivalence ratio of  $\sim 0.3$ , and dense bed gasifier temperature of  $\sim 820^\circ\text{C}$  were maintained for each 4-h test. Fuel moisture ranged from 7% to 8%, wet basis.

Product gas compositions for each test in Table 4 are averages of GC analyses of six samples taken at 30-min intervals over the sampling duration. The average product gas over all tests consisted of 11%  $\text{H}_2$ , 55%  $\text{N}_2$ , 11%  $\text{CO}$ , 4%  $\text{CH}_4$ , and 18%  $\text{CO}_2$ ; the balance was composed of higher hydrocarbons. Consistency of gas composition between tests was generally good, with the largest

absolute difference for any component equal to ~4%. Relative differences (the difference between largest and smallest test values relative to the smallest test value times 100%) were largest for H<sub>2</sub> (30%) and CH<sub>4</sub> (20%). The remaining major gas species, CO, N<sub>2</sub>, and CO<sub>2</sub> exhibited values of less than 7%. Dry gas yield was calculated using two methods: (1) from the measurement of dry gas volume and fuel feed rate; and (2) based on the measured flow rate of N<sub>2</sub> into the reactor, the product gas N<sub>2</sub> concentration, and the fuel feed rate. The first method consistently produced values ~15% higher than the second method. The measurements of dry gas volume, inlet N<sub>2</sub> flow rate, and N<sub>2</sub> concentration in the product gas are the possible sources of disagreement. Fuel-bound N<sub>2</sub> and air intrusion into gas samples during sampling are also possible sources of error, but are thought to be of smaller magnitude. Consistency across tests ranged from 2.1 to 2.4 nm<sup>3</sup> kg<sup>-1</sup> for the first calculation method and from 1.8 to 2.1 nm<sup>3</sup> kg<sup>-1</sup> for the second. Wet product gas yield (Table 4) based on the measured dry gas volume, the weight of condensate removed from the product stream, and the fuel feed rate ranged from 2.5 to 2.7 nm<sup>3</sup> kg<sup>-1</sup> over the test series, a difference of about 8%.

Thermocouple measurements of gas stream temperature were made at the ceramic filter vessel inlet and outlet. Average values are shown in Table 4. Average inlet temperatures ranged from 635° to 655°C, and after passing through the heated ceramic filter unit the average outlet temperatures were in a range from 710° to 740°C. Variation of filter inlet and outlet temperatures between tests was largely the result of differences in the manner insulation was installed in preparing each test, and consequently, differences in heat loss from the filter vessel and piping. Carbon conversion, as determined by the percentage of fuel carbon recovered in the filter char, was consistent across tests, ranging from 93% to 94%. Total carbon balances over the duration of the sampling period using prorated fuel and carbon masses and gas volumes determined using the dry test meter ranged from 93% to 103% and are deemed to be acceptable.

Appendix A contains plots of the measurements made during each test experiment. Figures are organized by test and each set of test graphs contains plots of (1) thermocouple measurements along the height of the gasifier reactor as indicated in Figure 15 (TC1 through TC8); (2) thermocouple measurements of gas stream temperature at the inlet and outlet of the heated ceramic filter unit (Figure 16); (3) getter reactor thermocouple measurements of the inlet gas temperature, temperature at the upper surface of the first cell in the packed bed, and temperature of the outlet gas stream (Figure 17); and (4) CO, CO<sub>2</sub>, and CH<sub>4</sub> concentrations in the gas exiting the alkali getter reactor.

Table 4. Summary of test conditions for the gasifier, hot ceramic filter, and alkali getter reactor.

Test Identification	76G-B	76G-AB	51G-E	51G-AB	76G-E	51G-E-P
Getter Material	none <sup>a</sup>	activ. <sup>b</sup> baux.	emath. <sup>c</sup>	activ. <sup>b</sup> baux.	emath. <sup>c</sup>	emath. <sup>c</sup>
Getter Reactor Diameter (mm)	76	76	51	51	76	51
Getter Particle Size Range (mm)		2.4-3.4	2.4-3.4	2.4-3.4	2.4-3.4	4.0-4.8
Fuel Weight, Wet (kg)	4.524	4.349	4.712	4.305	4.685	4.503
Fuel Moisture (% wet basis)	8.0	8.1	7.5	7.3	7.0	7.5
Test/Fuel Feeding Duration (h)	4.24	4.07	4.06	4.02	4.03	4.03
Dry Feedrate (kg h <sup>-1</sup> )	0.98	0.98	1.07	0.99	1.08	1.03
Oxygen Flowrate (L min <sup>-1</sup> @ stp)	4.8	4.8	4.8	4.8	4.8	4.8
Nitrogen Flowrate (L min <sup>-1</sup> @ stp)	18.1	18.1	18.1	18.1	18.1	18.1
Equivalence Ratio	0.33	0.33	0.30	0.33	0.30	0.32
Average Gasifier Bed Temp. (°C)	817	819	820	819	821	820
Dry Product Gas Analysis (% vol)						
H <sub>2</sub>	9.0	12.5	10.2	12.9	9.5	10.8
N <sub>2</sub>	55.3	54.4	55.3	52.9	56.6	54.4
CO	11.9	11.0	11.4	11.4	11.4	11.8
CH <sub>4</sub>	3.5	4.0	3.8	4.4	3.9	3.6
CO <sub>2</sub>	18.0	17.7	18.0	17.6	17.5	18.3
C <sub>2</sub> H <sub>2</sub>	1.0	0.0	0.0	0.1	0.0	0.0
C <sub>2</sub> H <sub>4</sub>	1.3	0.3	1.3	0.7	1.2	1.1
C <sub>2</sub> H <sub>6</sub>	0.0	0.0	0.1	0.0	0.0	0.0
Molecular Wt (kg kmol <sup>-1</sup> )	28.1	27.1	27.8	27.0	27.9	27.7
Sampled Dry Gas Volume (nm <sup>3</sup> )	6.684	7.015	6.854	7.104	7.005	6.928
Product Stream Condensate (kg)	0.585	0.592	0.753	0.643	0.746	0.671
Sampling Duration (h)	3.00	3.00	3.00	3.00	3.00	3.00
Dry Gas Yield 1 <sup>d</sup> (nm <sup>3</sup> kg <sup>-1</sup> )	2.27	2.38	2.13	2.38	2.16	2.24
Dry Gas Yield 2 <sup>e</sup> (nm <sup>3</sup> kg <sup>-1</sup> )	2.00	2.03	1.83	2.06	1.78	1.93
Wet Gas Yield <sup>f</sup> (nm <sup>3</sup> kg <sup>-1</sup> )	2.54	2.65	2.45	2.67	2.47	2.53
Average Filter Inlet Temp. (°C)	645	645	655	645	635	643
Average Filter Outlet Temp. (°C)	724	731	715	733	708	743
Filter Char Yield (kg)	0.249	0.262	0.282	0.268	0.293	0.275
Char Carbon as % of Fuel Carbon	6.0	6.6	6.5	6.7	6.7	6.6
Carbon Balance (%)	103	96	93	101	93	97

<sup>a</sup> no material in the alkali getter reactor

<sup>b</sup> activated bauxite

<sup>c</sup> emathlite

<sup>d</sup> calculated from measured gas volume

<sup>e</sup> calculated from N<sub>2</sub> input and GC analysis

<sup>f</sup> calculated from measured gas volume and condensate

### 4.3 Gasifier Bed Material

Samples were obtained from the bulk lot of gasifier bed material before testing began and from the bed material recovered from the gasifier after each test. The pretest bed material and post-test bed material from the blank run were subjected to analyses for Ca, C, Cl, Mg, P, K, Na, and S. Analysis of samples from subsequent tests was limited to the major elements of interest, K, Cl, and Na, to indicate the degree to which gasifier reactor conditions were repeated over the test series. The mass of bed material and analytical results for each test are presented in Table 5. To compare test results on a common basis, the element mass retained in the bed material as a percentage of fuel mass was calculated for each test and is also presented in Table 5. The results show that >40% of the P, K, and Na present in the fuel was retained in the bed material. Potassium retention varied from 58% to 78% over the six tests. Between 42% and 59% of fuel Na mass was retained in the bed material during the first five tests. The sixth test was an exception with a calculated value of 140%. This discrepancy may be the result of contamination of the bed material sample or analytical error. Ca, C, and S were retained at levels of less than 0.1%. Chlorine retention, which was tracked in the bed material for each test, varied from 0.4% to 3.6%. For the single test sample analyzed, less Mg was recovered in the post-test bed material than from the pretest beads. It is not apparent whether this is a result of experimental error or a volatile loss. Results from previous work showed a net retention of Mg mass, although the fuel ash chemistry and bed material composition were not directly comparable to the present study. Based on the results of a single test, 61% of P was retained in the bed. This also contradicts earlier work, which exhibited a net loss of P from post-test bed samples, although differences in fuel chemistry and bed composition may be responsible, as discussed earlier. Consistency of results for the three elements (Cl, K, and Na), which were tracked in the bed material over all the tests, was deemed acceptable.

### 4.4 Filter Char

Char collected in the ceramic filter unit during the blank run was subjected to proximate, ultimate, heating value, and ash analyses. Results are presented in Table 6. Char is composed primarily of carbon and ash with a small amount of volatile matter. The fixed carbon content (proximate analysis) of the sample was reported to be ~3% (absolute) greater than the total carbon determined by the ultimate analysis. This discrepancy is most likely the result of error associated with the analytical methods. Compared to the ash analysis of the fuel samples, the char ash is enriched in Si, Al, Ti, Fe, Ca, and Mg, and depleted in Na, K, P, S, and Cl, indicating that the latter species are preferentially volatilized.

Char from tests conducted subsequent to the blank run were subjected to analyses for Cl, K, and Na to provide, in the same manner as the bed material, an indication of the repeatability of gasifier operations over the battery of tests. Results of the analyses and comparison of fuel elemental input recovered in the char for each test are presented in Table 7 and Figure 20, respectively. As shown in Figure 20, the elemental mass present in the char as a percentage of the elemental fuel input for Cl, K, and Na was constant over the test series. Retention of element was 10% to 15% in all but two tests. Previous work using similar fuel<sup>12</sup> produced comparable values for char element retention of Cl (18%), K (8%), and Na (12%).

Table 5. Summary of elemental analyses of samples of bulk, pretest, gasifier bed material, and gasifier bed material recovered from the gasifier after each test.

Test Identification	76G-B	76G-AB	51G-E	51G-AB	76G-E	51G-E-P	
Gasifier Bed Mass (g)	10,007	10,000	10,002	9,999	10,000	10,000	
<u>Concentration (% wt)</u>	Pretest <sup>a</sup>	Post-Test Analyses					
Ca	0.371	0.371					
C	0.04	0.060					
Cl	0.004	0.005	0.007	0.006	0.009	0.011	
Mg	0.046	0.021					
P as P2O5	0.152	0.198					
K	0.48	0.813	0.770	0.826	0.773	0.754	
Na	0.089	0.113	0.114	0.120	0.111	0.111	
S	0.01	0.010					
<u>Element Mass Retained in Gasifier Bed Material as % of Fuel Element Mass</u>							
Ca	0.0						
C	0.1						
Cl	0.4	1.2	0.8	2.1	2.6	3.6	
Mg	-44.2						
P	60.8						
K	74.7	67.7	74.0	68.5	58.7	77.9	
Na	48.2	52.2	59.3	46.0	42.2	140.2	
S	0.0						

<sup>a</sup> Pretest bed material also contained 30.2% Al, 4.3% Fe, 5.2% Si, and 1.7% Ti.

Table 6. Properties of ceramic filter char sample collected during blank run test.

<u>Proximate Analysis (wt %, dry basis)</u>		<u>Ash Analysis (wt %, dry basis)</u>	
Fixed Carbon	46.61	SiO <sub>2</sub>	61.93
Volatiles	3.10	Al <sub>2</sub> O <sub>3</sub>	1.31
Ash	50.29	TiO <sub>2</sub>	0.09
HHV (MJ/kg, dry basis)	16.39	Fe <sub>2</sub> O <sub>3</sub>	4.73
		CaO	6.27
<u>Ultimate Analysis (wt %, dry basis)</u>		MgO	4.50
C	43.36	Na <sub>2</sub> O	0.81
H	0.68	K <sub>2</sub> O	6.85
O	3.44	P <sub>2</sub> O <sub>5</sub>	2.70
N	0.62	SO <sub>3</sub>	0.64
S	0.19	Cl	2.49
Cl	1.42	CO <sub>2</sub>	0.12
Ash	50.29		

Table 7. Element concentrations of Cl, K, and Na in the ceramic filter char for the test series.

Test Identification	76G-B	76G-AB	51G-E	51G-AB	76G-E	51G-E-P
Getter Material	none	activ. baux.	emath.	activ. baux.	emath.	emath.
<b>Element concentration (%)</b>						
Cl	1.42	0.94	0.85	1.04	0.86	0.53
K	2.86	2.16	1.91	2.24	2.16	2.06
Na	0.30	0.28	0.20	0.25	0.36	0.24

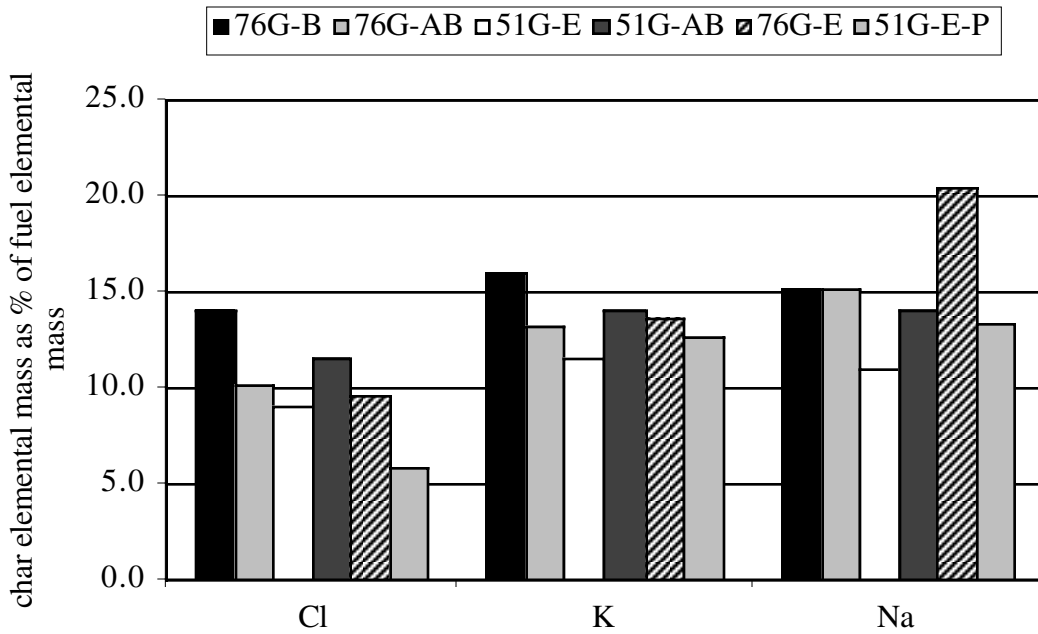


Figure 20. Elemental mass retained in the char as a percentage of elemental fuel input.

#### 4.5 Results from Baseline Test, 76G-B

The initial test, with no material present in the alkali getter reactor, was performed to obtain baseline inorganic gas-phase concentrations for the heated product stream exiting the ceramic filter. The test, 76G-B, was conducted with the 76-mm diameter getter reactor in place, followed by the sample conditioning system (see Figure 18). Condensate from the cooling coil, acetone solutions from cleaning the sample conditioning system, and distilled water solution from rinsing the inner surfaces of the getter reactor were analyzed for Al, Ca, Cl, Fe, Mg, P, K, Si, Na, and S. Element masses collected in the sample conditioning system are shown in Figure 21. Chlorine and K were present in the greatest quantities: Fe and Na were present in smaller amounts. The origin of the Fe likely was from the stainless steel material present in the sample conditioning system. The remaining elements were present at reduced levels, totaling less than 0.01 g each. The distribution of the element masses among the components of the sampling system (Figure 22) shows that most of the captured amount was retained in the condensate collected from the product stream. For Cl, K, and Na, the condensate contained 90%, 70%, and 60% of the total collected, respectively. The coil and first trap rinse and the second and third trap rinses contained <7% and 3%, respectively. Chlorine recovery from the getter reactor accounted for less than 1% of the Cl total. For K and Na, the rinse from the getter reactor represented approximately 25% of the total mass of each.

Table 8 contains the results of calculations of dry gas element concentrations from the element masses presented in Figure 21 and the dry gas volumes in Table 4. Previous work<sup>12</sup> reported gas-phase concentration under similar gasifier operating conditions. These are included in the table for comparison. Chlorine and K concentrations measured in the current work are 62% and 53%, respectively, of the earlier experimental results. Sodium concentrations are similar, at about 10 ppmw in both studies. Table 9 contains vapor pressures<sup>36</sup> for KCl and NaCl in ppmw and corresponding concentrations of K and Na, for comparison to the experimental measurements. Potassium concentrations of 30 and 62 ppmw are predicted at 650° and 675°C, respectively, bracketing both measurements cited in Table 8. Similarly, Na concentrations at the same temperatures are predicted to be 9 and 19 ppmw, respectively; this range includes the measurements of Table 8. Average filter inlet and outlet temperatures were 645° and 731°C, respectively, for the results reported here, whereas the filter temperature of the previous work<sup>12</sup> was reported as 730°C. Considering the potential differences between the tests, the vapor pressure data and the experimental data agree remarkably well. The current work provides a more integrated measurement over the duration of the test; 6,600 L of dry gas were measured at the exit of the sample conditioning system, compared to 500 L via the slip stream sampling system employed for the earlier measurement.<sup>12</sup> Both sets of data indicate that Cl is present in a molecular form (probably HCl)<sup>11</sup> other than alkali chloride, as both have alkali to Cl molar ratios of about 0.03.

Table 8. Comparison of element concentrations (ppmw) in the dry product gas of the current study and previous measurements.

	Dry Gas Concentration (ppmw)	
	Current Work, Test 76G-B	Turn <i>et al.</i> , 1998 <sup>12</sup>
K	28	53
Na	11	8
Cl	1309	2119

Table 9. Vapor pressures of KCl and NaCl, and concentrations of K and Na as a function of temperature.<sup>36</sup>

T (°C)	ppmw			
	KCl	NaCl	K <sup>a</sup>	Na <sup>a</sup>
550	2	0.7	1	0.3
575	5	2	3	0.7
600	12	4	6	2
625	26	10	14	4
650	57	23	30	9
675	118	49	62	19
700	236	99	123	39
725	453	194	237	76
750	842	368	441	145
775	1518	676	796	266
800	2661	1205	1395	474
825	4540	2092	2380	823
850	7557	3540	3961	1392
875	12291	5848	6442	2299
900	19561	9447	10253	3714

<sup>a</sup> concentrations based on KCl and NaCl vapor pressures

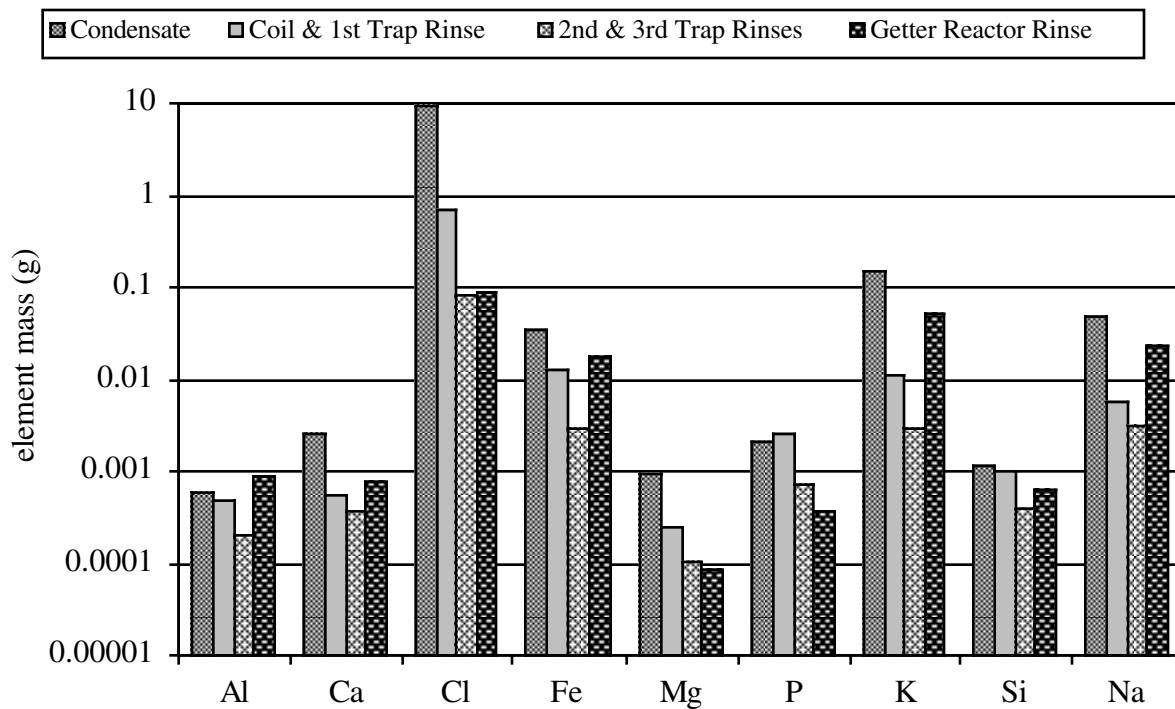


Figure 21. Element masses collected in various sections of the sample conditioning system with no getter material present in the alkali getter reactor (blank run).

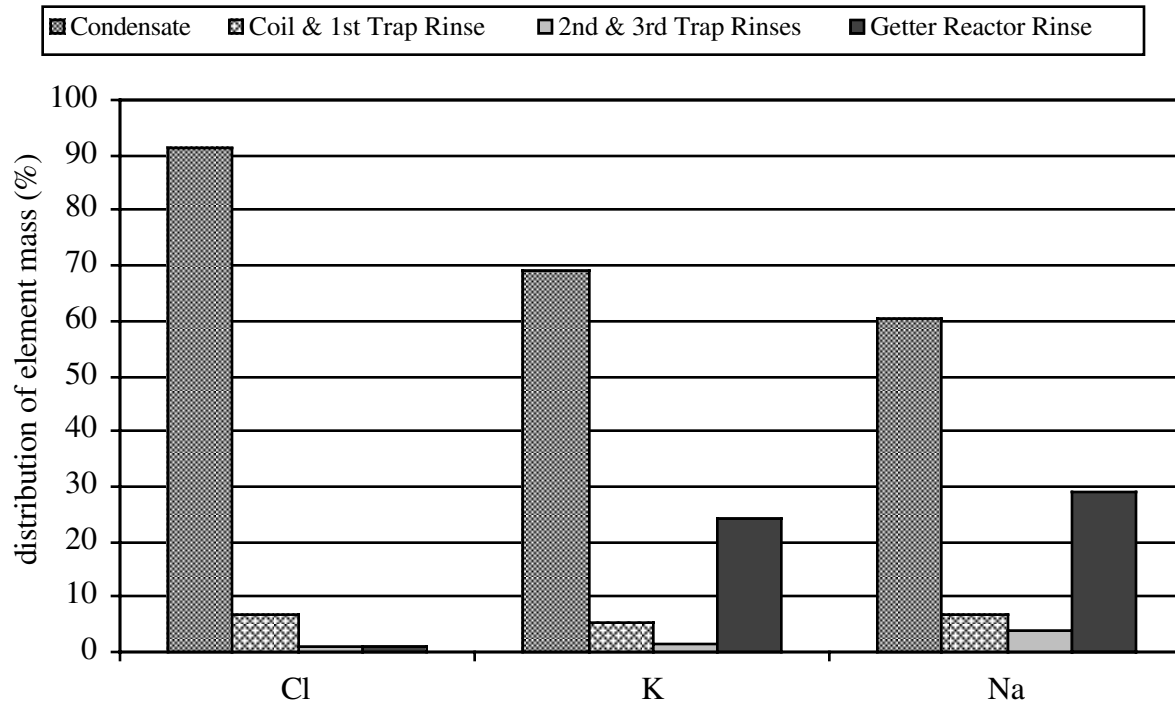


Figure 22. Distribution of major element masses collected in the sample conditioning system as a percentage of total for blank run.

## 4.6 Alkali Getter Tests

### 4.6.1 Alkali Getter Materials

The remaining five tests were conducted with fixed beds of either activated bauxite or emathlite in the alkali getter reactor as shown in Table 4. Typical chemical analyses of each material, as provided by the manufacturer and as determined as part of the current study, are presented in Table 10. A range of typical values of emathlite composition, included in Table 10 as well, was provided by the supplier. Analysis performed as part of the current study was concerned primarily with the minor elements, particularly K, Na, and Cl, to determine pre-existing levels of elements targeted for adsorption. Moisture contents of emathlite and activated bauxite were determined to be 8.6% and 1.8% (wet basis), respectively, which agrees well with the moisture content data provided with the material. Loss on ignition data shows both materials contain 6% to 9% volatile matter. Per the data provided by the manufacturers, emathlite and activated bauxite are composed primarily of SiO<sub>2</sub> (64% and 6%, respectively) and Al<sub>2</sub>O<sub>3</sub> (10% and 89%, respectively). Both materials contain about 2% to 3% Fe<sub>2</sub>O<sub>3</sub>; TiO<sub>2</sub> is present in similar quantity in activated bauxite but in reduced quantities (<0.5%) in emathlite.

Analysis of activated bauxite for Cl, MgO, and K<sub>2</sub>O found them to be present at levels <0.005%, with K<sub>2</sub>O measured at 0.0012%. P<sub>2</sub>O<sub>5</sub> and Na<sub>2</sub>O content in activated bauxite were found to be slightly higher at 0.046% and 0.015%, respectively. CaO, C, and S were found at higher levels, all present in the range from 0.1% to 0.2%.

Table 10. Compositions of as-received getter materials as provided by the manufacturer and as determined by independent analysis.

	Emathlite <sup>a</sup>	Activated <sup>a</sup> Bauxite	-----Emathlite <sup>b</sup> -----  Typical	Range	Activated <sup>c</sup> Bauxite
<u>Composition of as-received material (% wet basis)</u>					
CaO	5.26	0.16	7.41	1.4-10.7	
C	0.92	0.13			
Cl	0.015	0.005			
MgO	5.31	0.005	3.34		
P <sub>2</sub> O <sub>5</sub>	1.49	0.046			
K <sub>2</sub> O	0.75	0.0012	0.33	0.33-1.7	
Na <sub>2</sub> O	0.16	0.015			
S	0.03	0.21			
SiO <sub>2</sub>			63.85	47-64	6.0
Al <sub>2</sub> O <sub>3</sub>			10.07	9-11	89.0
Fe <sub>2</sub> O <sub>3</sub>			2.83	2.8-3.5	2.0
TiO <sub>2</sub>			0.44	0.34-0.44	3.0
Moisture	8.6	1.8	5.44		
Loss on Ignition <sup>d</sup>	8.92	5.86	6.24		6.0

<sup>a</sup> analysis from current study

<sup>b</sup> "typical analysis" and possible range of values provided by Mid-Florida Mining Industries

<sup>c</sup> "typical analysis" provided by Porocel

<sup>d</sup> determined for current work by heating at 750°C for 4 h

Calcium and MgO each accounted for ~5% of as-received emathlite. Carbon, P<sub>2</sub>O<sub>5</sub>, and K<sub>2</sub>O were all present at roughly 1% of getter mass; Na<sub>2</sub>O was measured at 0.16%. Chlorine and S were found in the range of 0.015% to 0.03%.

Samples from each getter material lot were heated to 750°C for 4 h, then subjected to an identical battery of analyses as the as-received material, results of which are presented in Table 11. Also presented in Table 11 are the analyses of as-received samples (Table 10) that have been renormalized after subtracting the moisture and volatile components. Concentrations of C in both materials and Cl in emathlite were reduced by more than 65% (relative) in the heated samples compared to the renormalized as-received samples, evidence that they were partially volatile. The concentration of K<sub>2</sub>O in the heated emathlite sample was lowered by about 10% (relative), indicating that it was also volatile, but to a lesser degree. Concentrations of the remaining compounds were essentially constant or increased in the heated samples, but this does not permit firm conclusions to be drawn regarding volatility. Lee *et al.*<sup>14</sup> observed approximate 1% losses of K and Na after heating activated bauxite to 850°C in a 10 bar SFG environment. The data from the current study generally agree. Experimental results of Bachovchin *et al.*<sup>6</sup> showed similar behavior for K and Na in samples heated to 850°C in TGA experiments. Potassium and Na concentrations in the heated samples increased compared to as-received samples, but when the as-received samples were corrected for volatile loss, the concentrations of the two analyses were comparable.

Table 11. Comparison of getter material composition after 4 h at 750°C and moisture/volatile matter corrected data from Table 10.

	Emathlite <sup>a</sup>	Activated <sup>a</sup> Bauxite	Emathlite <sup>b</sup>	Activated <sup>b</sup> Bauxite
<u>Composition of material (% , volatile and moisture free basis)</u>				
CaO	7.71	0.22	6.38	0.18
C	0.11	0.03	1.12	0.14
Cl	0.006	0.005	0.018	0.005
MgO	7.01	0.005	6.43	0.005
P <sub>2</sub> O <sub>5</sub>	1.77	0.084	1.81	0.05
K <sub>2</sub> O	0.80	0.004	0.91	0.001
Na <sub>2</sub> O	0.18	0.015	0.19	0.016
S	0.02	0.23	0.04	0.23

<sup>a</sup> analysis from current study, composition of material after 4 h at 750°C

<sup>b</sup> analysis of as-received material from Table 10, renormalized after subtracting moisture and loss-on-ignition components

## 4.6.2 Test Results

### 4.6.2.1 Test Conditions

Table 12 contains a summary of conditions in the getter reactor for each test; the table columns follow the order in which the tests were conducted. Bed depths for the 51-mm and 76-mm reactors were 81.3 cm and 72.2 cm, respectively. Activated bauxite was approximately 50% denser than emathlite, resulting in greater getter mass per cell within the reactor. The first four tests were conducted with getter material particles of 2.4 to 3.4 mm, and the final test was conducted with larger particles of emathlite (4.0-4.8 mm). Average getter reactor temperatures varied from 600° to 700°C with the first three tests (76G-AB, 51G-E, 51G-AB) grouped in the

upper part of the range from 670° to 700°C. In all tests, filtered product gas passed through the reactor for 3 h with accrued gas volumes of 7.8 to 8 nm<sup>3</sup>, resulting in contact times between the gas and the getter material, i.e., space time, of ~1.4 s and 0.7 s for the 76- and 51-mm reactors, respectively.

Table 12. Summary of test conditions and results for the alkali getter reactor.

Test Identification	76G-AB	51G-E	51G-AB	76G-E	51G-E-P
Getter Material	activ. baux.	emath.	activ. baux.	emath.	emath.
Getter Reactor Diameter (mm)	76	51	51	76	51
Getter Bed Depth (cm)	72.24	81.28	81.28	72.24	81.28
Number of Getter Cells	14	15	15	14	15
Average Getter Mass per Cell (g)	217	65	93	143	66
Getter Material Particle Size Range (mm)	2.4-3.4	2.4-3.4	2.4-3.4	2.4-3.4	4.0-4.8
Average Getter Reactor Temperature (C)	669	684	702	605	645
Duration of Getter Exposure (h)	3.0	3.0	3.0	3.0	3.0
Wet Gas Volume through Getter Reactor (nm <sup>3</sup> )	7.82	7.88	7.98	8.02	7.84
Superficial Gas Velocity (m s <sup>-1</sup> )	0.5	1.2	1.2	0.5	1.1
Getter Space Time (s)	1.44	0.70	0.68	1.51	0.74
<u>Element Loading (mg g<sup>-1</sup> sorbent)</u>					
Cell 1					
K	1.3	4.6	4.4	1.8	4.9
Na	0.4	1.0	0.9	0.3	1.4
Cl	1.5	6.6	2.3	10.7	13.2
Cell 2					
K	0.07	0.7	0.2	0.2	0.6
Na	0.001	0.1	0.1	0.01	0.2
Cl	0.8	4.2	0.6	8.2	8.6
<u>Molar Ratio of Total Alkali to Chlorine (moles (K+Na): moles Cl)</u>					
Cell 1	1.20	0.87	2.31	0.20	0.50
Cell 2	0.084	0.20	0.55	0.021	0.099

#### 4.6.2.2 Getter Visual Appearance

Photographs of the as-received and heated getter materials and those removed from the reactor after testing are shown in Figures 23 through 29. Activated bauxite is grayish pink in its as-received (fresh) state and becomes a lighter pink after heating (Figure 23). Emathlite also exhibits slight color change (Figure 24) from its original light gray to tan after heating.

Figures 25 and 26 contain photos of the activated bauxite removed from the getter reactors after tests 76G-AB and 51G-AB, respectively. Each figure contains material from several cells located at various depths within the reactor, from cell 1 at the inlet, to cell 14 or 15 at the outlet. In both figures, the appearance of the getter particles transitions from a darkened state at the reactor inlet to that of the heated samples shown in Figure 23. This darkening appears to be the result of carbon deposited on the surface of the particles. Deposits are not attached tenaciously and can be removed in part by simple handling. The material from cells 1 and 4 in the 51-mm reactor are both darkened, whereas cell 4 in the 76-mm reactor shows less discoloration than cell 1, indicating that the C deposition process is dependent on contact time of the gas with the getter particles.

Figures 27 through 29 contain photos of the emathlite removed from the getter reactors after tests 51G-E, 76G-E, and 51G-E-P. Again, each figure contains samples from several cells located at various depths within the reactor. Carbon deposition is also evident in the emathlite samples, but the trend of heavy deposition at the reactor inlet tapering off to no deposition with greater depth, evident in the activated bauxite samples, is not apparent. Deposition appears to be heaviest in the mid-depth cells (cells 7 and 10) with varied degrees of lighter deposition near the inlet. An explanation for this pattern is not obvious.

Small variation in color among individual particles from the same reactor depth is evident in the photographs (Figures 25 to 29). This may be the result of the gas flow channeling as it passes through the fixed getter bed. Although no experimental work was performed to determine the velocity profile in the fixed-bed reactor, relatively high superficial gas velocities (0.5 to 1.2 m s<sup>-1</sup>; Table 7) and small getter particle sizes (2.4 to 3.4 mm) would be expected to facilitate flow uniformity.

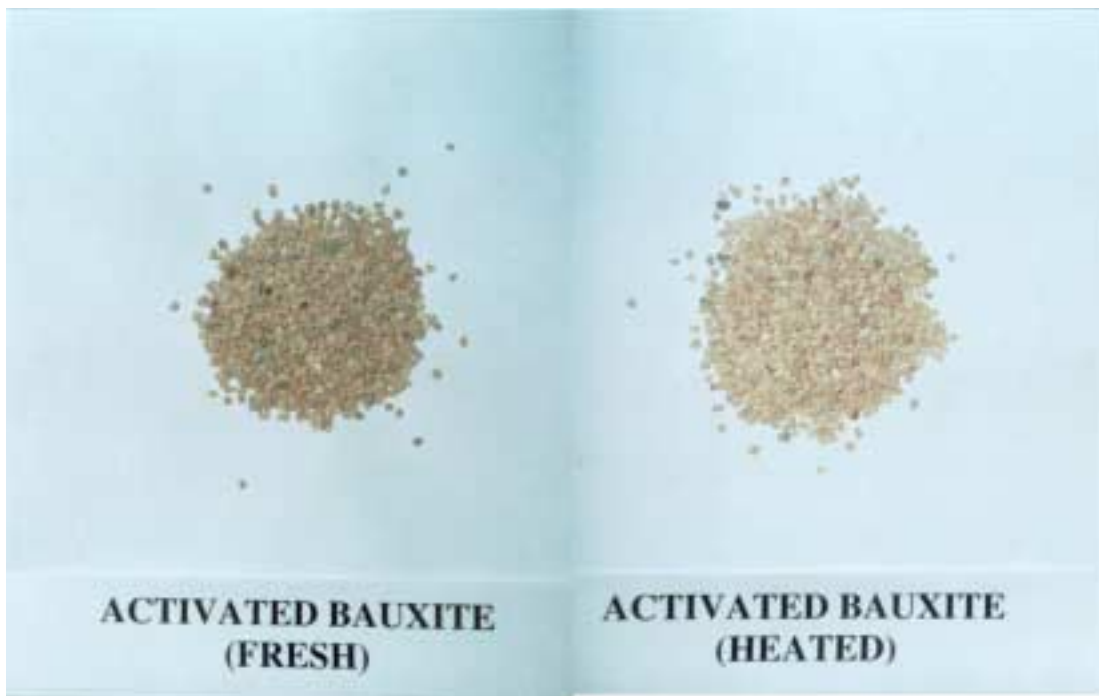


Figure 23. Samples of activated bauxite as received from the manufacturer (fresh) and after exposure to 750°C/air environment for 4 h (heated).

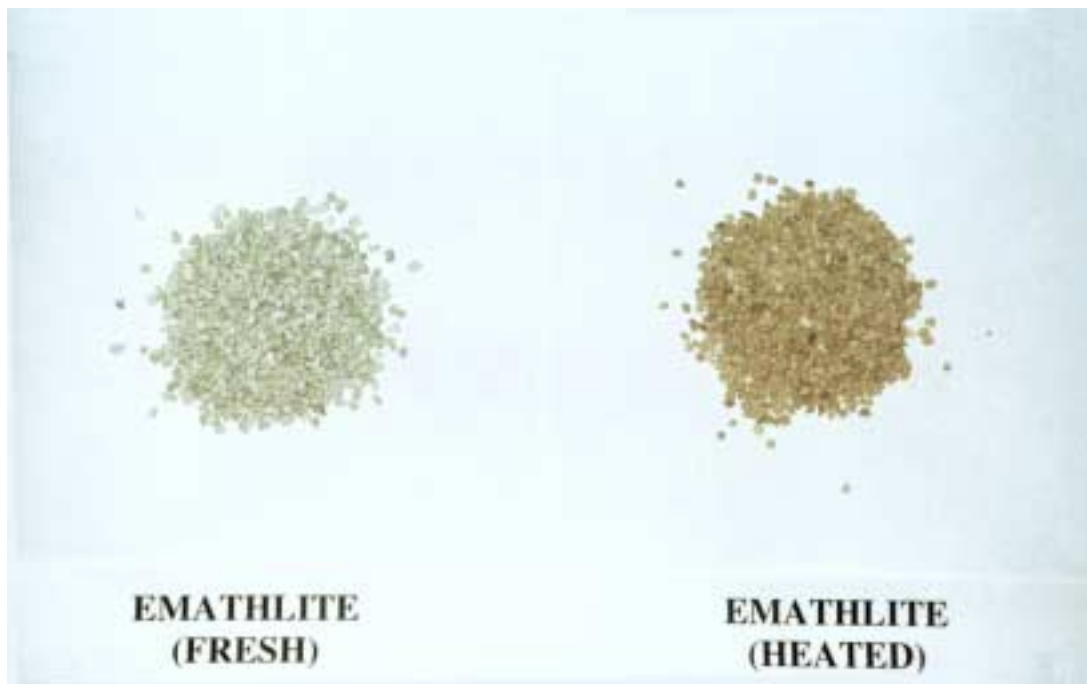


Figure 24. Samples of emathlite as received from the manufacturer (fresh) and after exposure to 750°C/air environment for 4 h (heated).

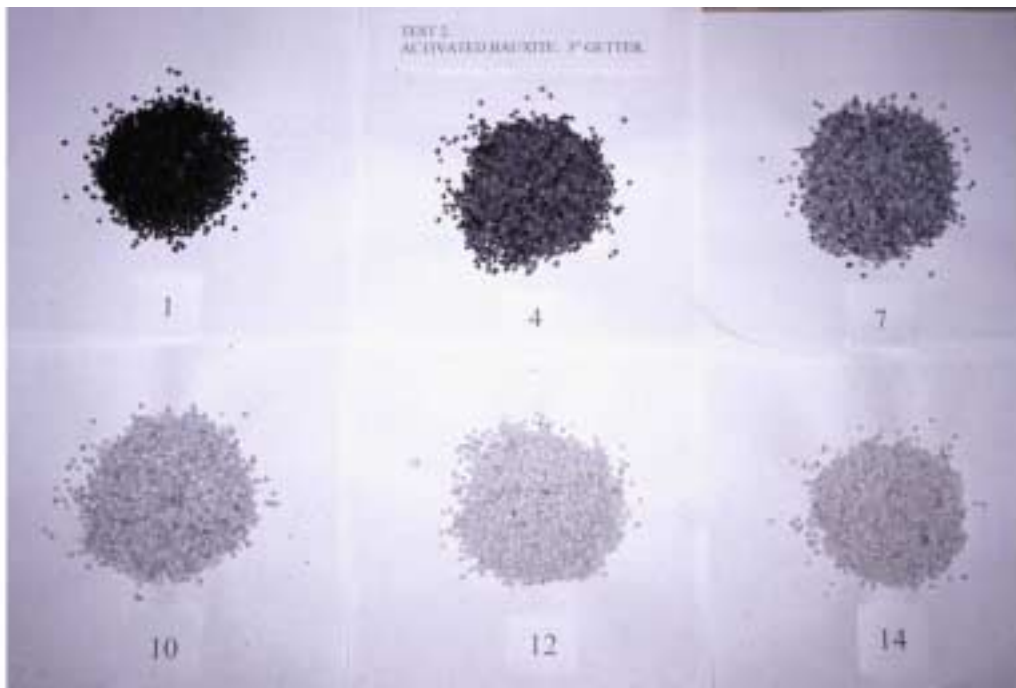


Figure 25. Samples of activated bauxite recovered from the alkali getter reactor after test 76G-AB. Numbers designate cell number within the reactor, with cell 1 at the inlet and cell 14 at the outlet.

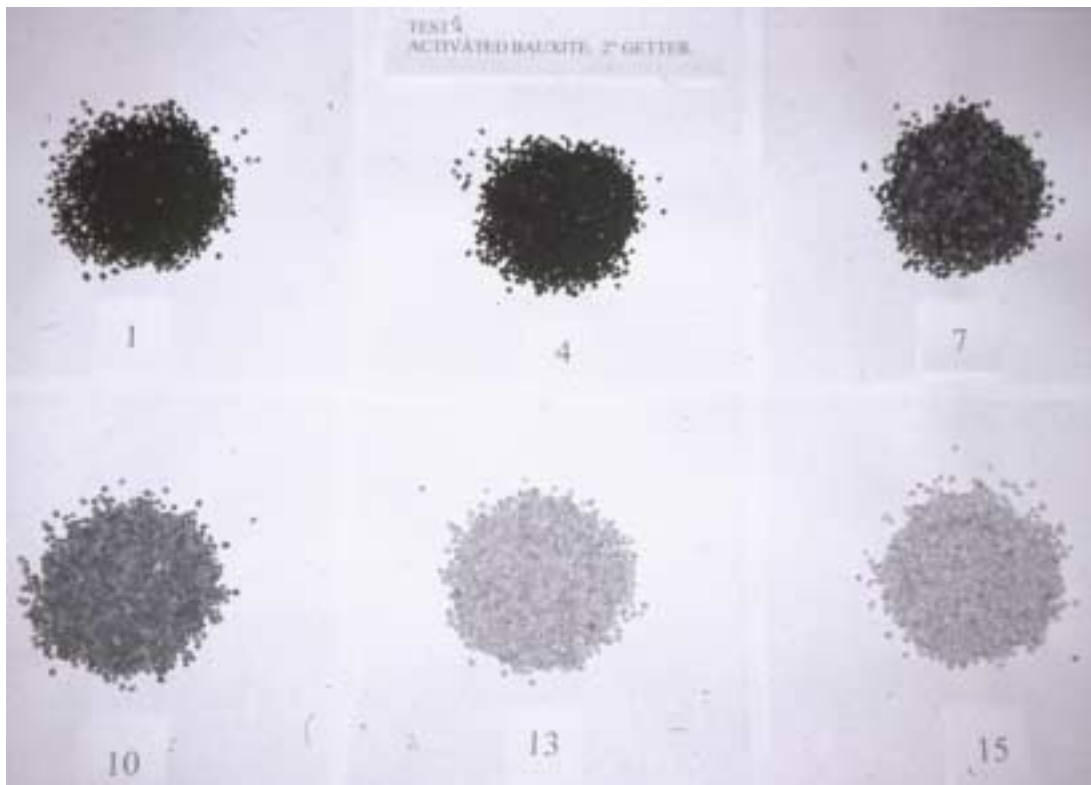


Figure 26. Samples of activated bauxite recovered from the alkali getter reactor after test 51G-AB. Numbers designate cell number within the reactor, with cell 1 at the inlet and cell 15 at the outlet.

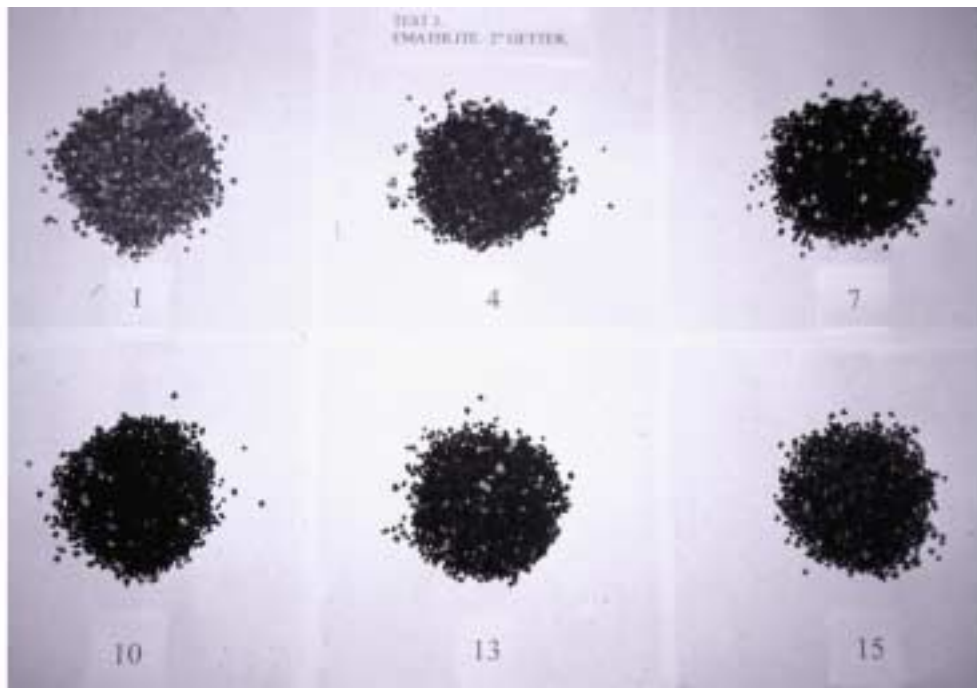


Figure 27. Samples of emathlite recovered from the alkali getter reactor after test 51G-E. Numbers designate cell number within the reactor, with cell 1 at the inlet and cell 15 at the outlet.

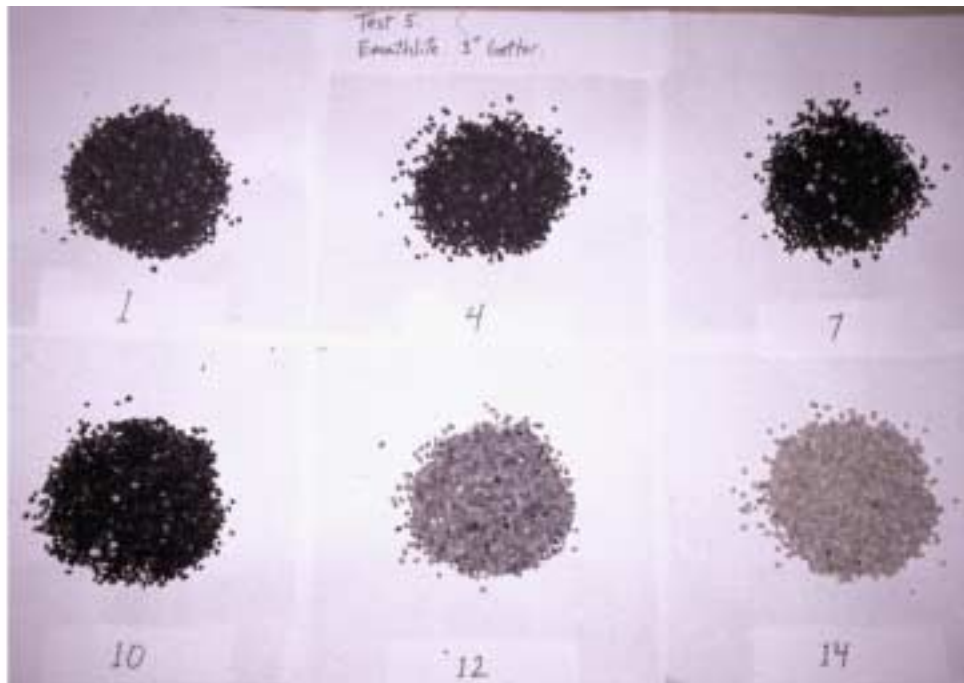


Figure 28. Samples of emathlite recovered from the alkali getter reactor after test 76G-E. Numbers designate cell number within the reactor, with cell 1 at the inlet and cell 14 at the outlet.

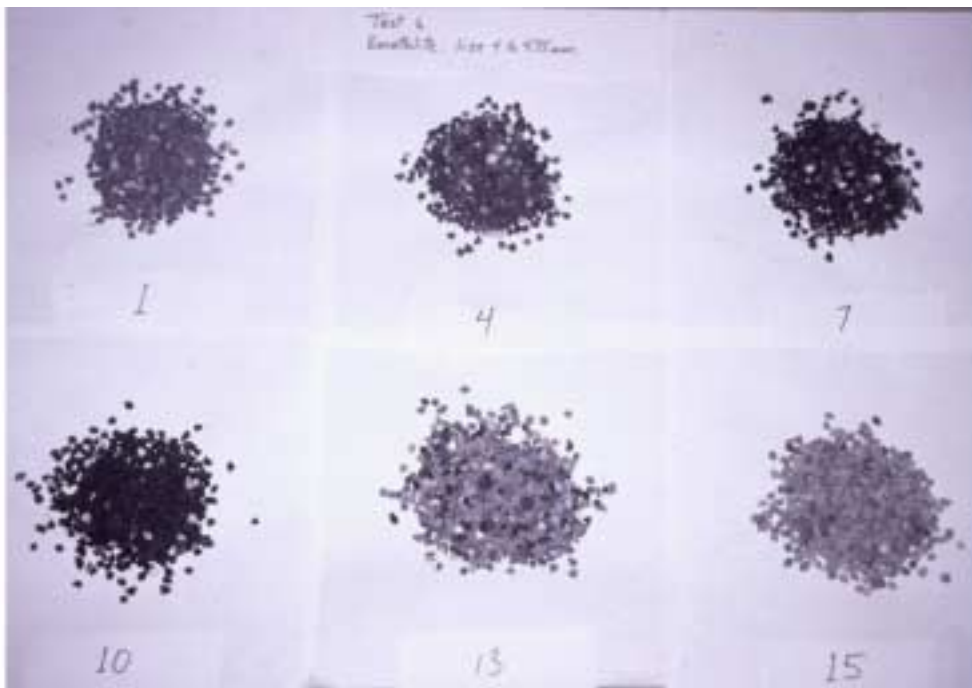


Figure 29. Samples of emathlite recovered from the alkali getter reactor after test 51G-E-P. Numbers designate cell number within the reactor, with cell 1 at the inlet and cell 15 at the outlet.

#### 4.6.2.3 Getter Material Bulk Analyses

Table 12 includes concentrations of K, Na, and Cl in the getter material in the first two cells of the reactor, which have been corrected using the analyses of the respective getter materials after a 4-h exposure to 750°C (see Table 11). The element mass recovered from the getter material in each getter reactor cell is plotted in Figures 30 through 34 for each test. Figure data have also been corrected for background element concentrations using the analyses of the getter material after 4 h at 750°C (see Table 9). Data from Table 12 and the figures indicate that most of the elemental mass of K and Na was removed in the first cell of the getter reactor in each test; cell 2 mass represented  $\leq 15\%$  of the mass in cell 1 in all cases. This pattern differs from the visual observation of C deposition described above. Carbon was deposited most heavily over the first four cells in the activated bauxite tests, but concentrated in the mid-depth cells when emathlite was tested, suggesting that in the case of emathlite, alkali may serve as an inhibitor to C deposition. Over all tests, K and Na concentrations in the getter material of the first cell were 1 to 5 mg K g<sup>-1</sup> sorbent and 0.3 to 1.4 mg Na g<sup>-1</sup> sorbent, respectively. Based on the gas-phase alkali content, temperature, and duration of exposure, the alkali loading rates are generally consistent with Figures 1 and 2 for emathlite, and Figure 6 for activated bauxite. Higher number cells, those located lower in the reactor, contained less of either analyte than was found in cell 1, and, with few exceptions, this was true of cell 2 as well. Net negative values of element mass were computed for several cells as shown in Figures 30 through 34. These result from applying a background correction to samples that have adsorbed little or no analyte, and may be interpreted as a zero value. The final test, 51G-E-P, exhibits larger negative values for K (-0.02 to -0.08 g). Getter material used in this test was from a different size class (4.0-4.8 mm) than the first four tests, and a pretest sample from this lot was not analyzed. It seems unlikely that the pretest composition of the two size classes would be drastically different since both were screened from a larger material lot.

Chlorine was found in greater concentrations than Na and K in nearly all cells, and whereas alkali concentrations were greatly reduced following the second cell, elevated Cl concentrations were measured in all reactor cells. Test results for 76G-AB, 51G-E, and 51G-AB (Figures 30 to 32) show an increase in captured Cl in the last cells in the reactor near the gas exit. This increase may be due in part to a reduction in temperature in this region resulting from ill-fitting insulation at the reactor exit from the tube furnace. This was improved for tests 76G-E and 51G-E-P. The Cl captured by the getter material in the latter stages of the reactor, as shown in Figures 33 and 34, reflects that.

The molar ratios of total alkali (K+Na) to Cl in cells 1 and 2 are included in Table 12. Assuming that the alkali is expected to be in the form of chlorides, a molar ratio of  $\sim 1$  would indicate that the alkali chloride was removed from the gas stream as a molecule, a molar ratio  $\gg 1$  would indicate that the molecule has dissociated and the Cl has dispersed to the gas phase. A molar ratio  $\ll 1$  can be interpreted as Cl being present in the getter in a form other than alkali chloride. The concentrations of alkali and Cl measured in the gas phase (Table 9) indicate that Cl is present in form(s) other than alkali chloride. This affects data interpretation in that the origin of Cl present in the getter material is indistinguishable and thus the form of adsorption, chemisorption, or physical adsorption is also difficult to distinguish. Only when the alkali to Cl molar ratio  $\gg 1$ , is it apparent that the alkali chloride has been chemisorbed and the Cl released as a gas. Literature studies concluded that emathlite and activated bauxite adsorb alkali by chemisorption ( $[(K+Na)/Cl] \gg 1$ ) and physical adsorption ( $[(K+Na)/Cl] \approx 1$ ), respectively. Molar ratios of total alkali to Cl in the first cells of the reactor for the two activated bauxite tests, 76G-AB and 51G-AB, were 1.2 and 2.3, respectively.

The three emahlite getter tests, 51G-E, 76G-E, and 51G-E-P, yielded ratios less than unity, 0.87, 0.20, and 0.50, respectively. Interpretation of the results for both materials is difficult because of the obvious presence of Cl from sources other than alkali chlorides.

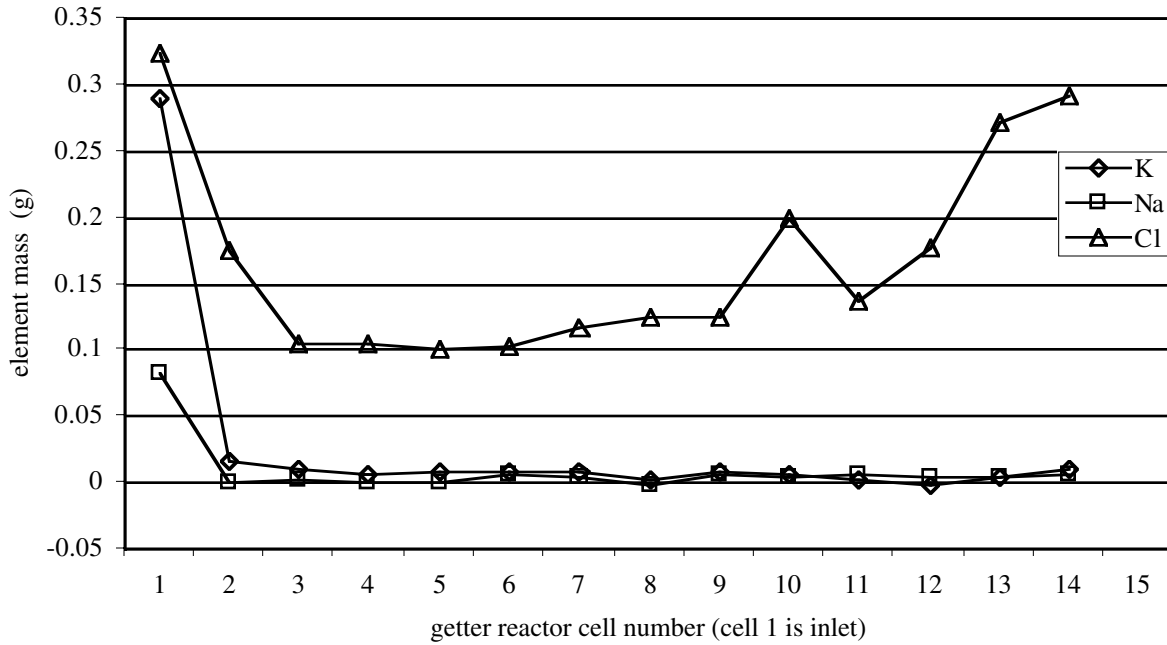


Figure 30. Distribution of K, Na, and Cl in the activated bauxite from test 76G-AB as a function of cell location within the reactor. Cell 1 is at the reactor inlet and cell 14 is at the reactor outlet and cell depth is 5.2 cm. Element mass values have been corrected for background levels present in the getter material heated to 750°C for 4 h.

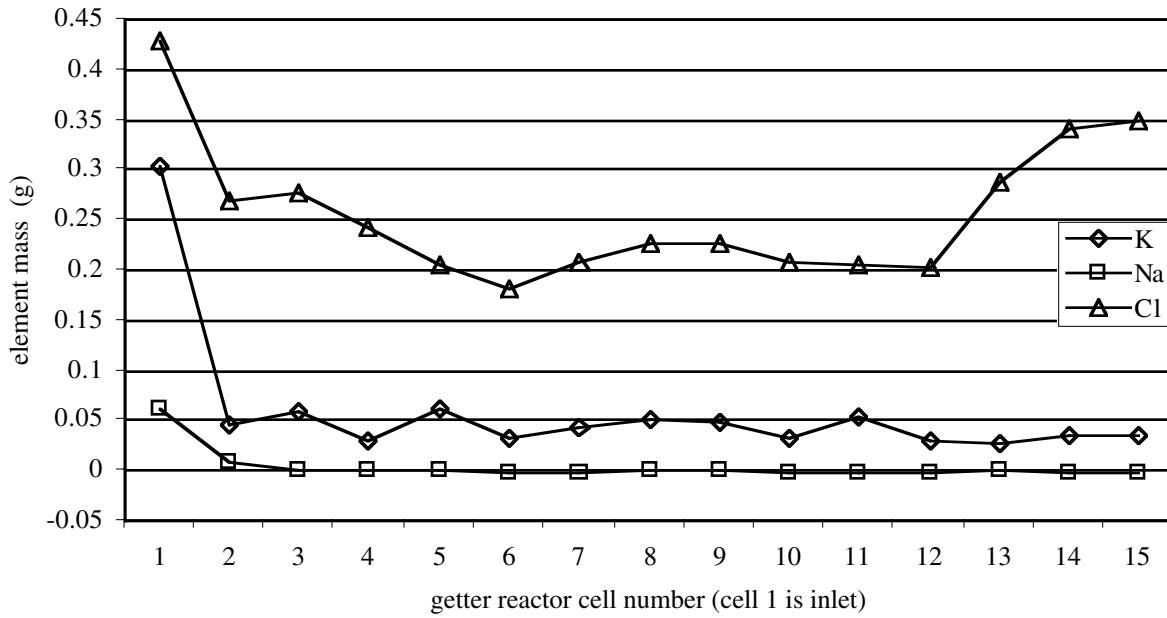


Figure 31. Distribution of K, Na, and Cl in the emathlite from test 51G-E as a function of cell location within the reactor. Cell 1 is at the reactor inlet and cell 15 is at the reactor outlet and cell depth is 5.4 cm. Element mass values have been corrected for background levels present in the getter material heated to 750°C for 4 h.

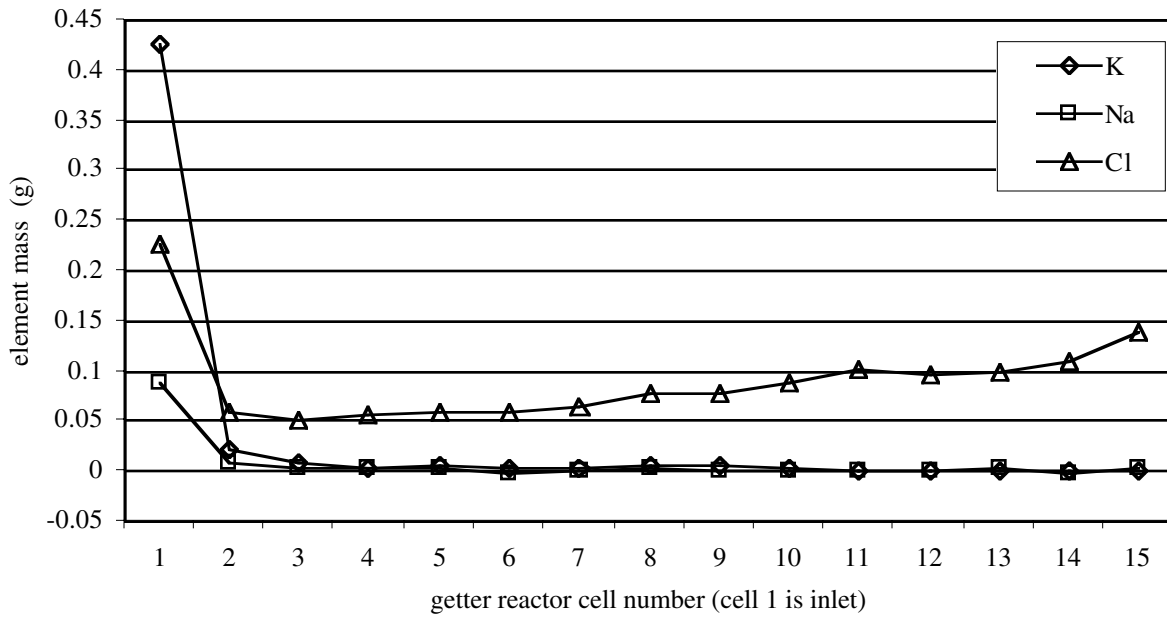


Figure 32. Distribution of K, Na, and Cl in the activated bauxite from test 51G-AB as a function of cell location within the reactor. Cell 1 is at the reactor inlet and cell 15 is at the reactor outlet and cell depth is 5.4 cm. Element mass values have been corrected for background levels present in the getter material heated to 750°C for 4 h.

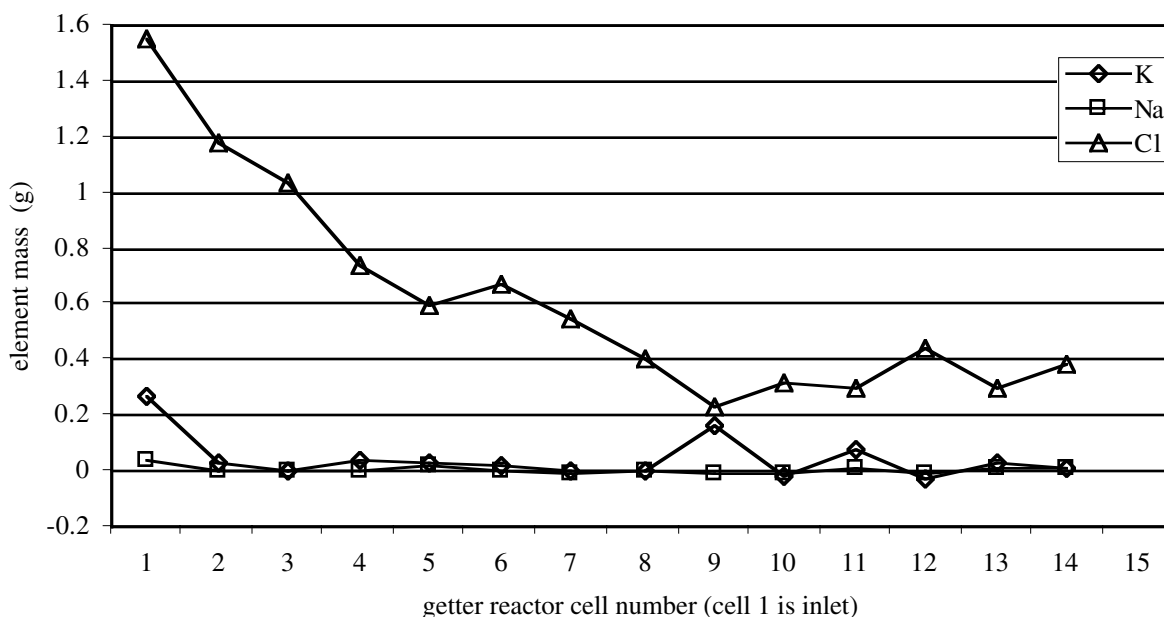


Figure 33. Distribution of K, Na, and Cl in the emathlite from test 76G-E as a function of cell location within the reactor. Cell 1 is at the reactor inlet and cell 14 is at the reactor outlet and cell depth is 5.2 cm. Element mass values have been corrected for background levels present in the getter material heated to 750°C for four hours.

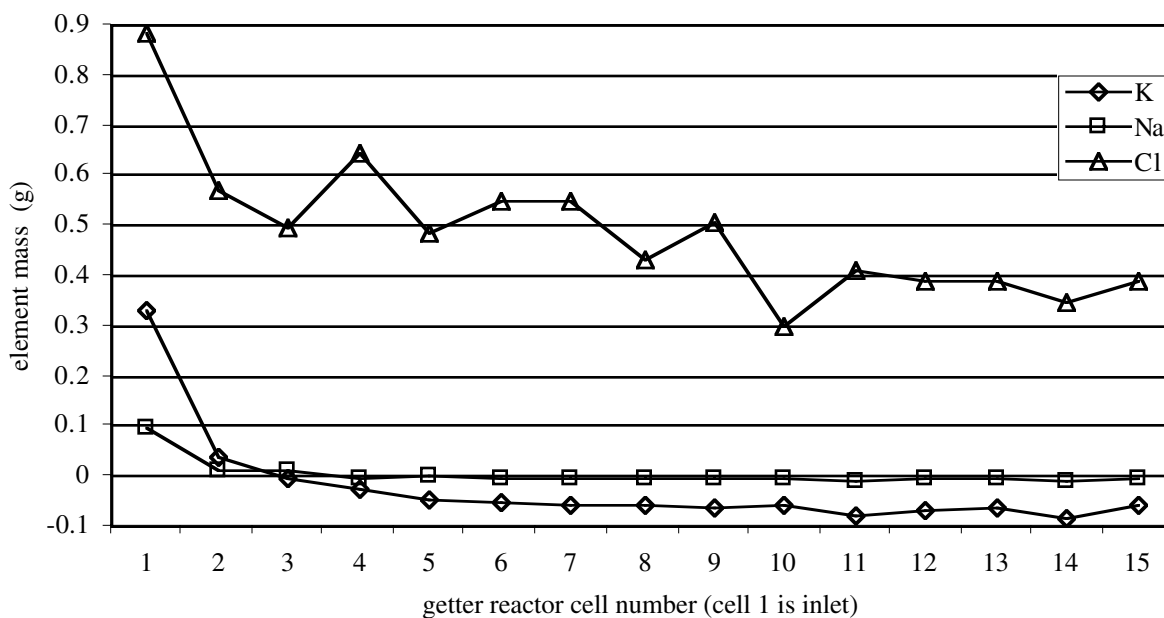


Figure 34. Distribution of K, Na, and Cl in the emathlite from test 51G-E-P as a function of cell location within the reactor. Cell 1 is at the reactor inlet and cell 15 is at the reactor outlet and cell depth is 5.4 cm. Element mass values have been corrected for background levels present in the getter material heated to 750°C for 4 h.

#### 4.6.2.4 Getter Material Surface Analyses

Table 13 contains a summary of SEM/XRF analyses of the surfaces of alkali getter particles from the oven-heated samples and from the first two getter reactor cells of tests 51G-E and 51G-AB. The results are averages of surface scans of 10 particles and may be viewed only as semiquantitative indicators because of particle surface nonuniformities that affect the analysis. Oxygen, Al, Si, Cl, Ti, and Fe were identified as being present in the heated emathlite and activated bauxite. Magnesium, K, and Ca were also identified in the heated emathlite sample, and S was present in the heated activate bauxite. Neither heated getter material surface contained Na. These results agree with the bulk getter analyses presented in Table 11.

Both the emathlite and activated bauxite getter reactor samples exhibited an increase in surface concentrations of K and Cl. Small amounts of Na were also detected on the particles from the first cell of the reactor for each test. Oxygen, Mg, Al, Si, P, Ca, Ti, and Fe concentrations on the emathlite particle surfaces decreased in the 51G-E sample compared to the heated sample, supporting evidence of surface adsorption. The opposite was true for activated bauxite, with the greater concentrations of Al, Si, Ti, and Fe and lower O concentrations in the 51G-AB, first cell sample compared to the heated activated bauxite sample. Examination of activated bauxite in the SEM was complicated because of the amount of getter particle charging experienced during the analysis, and this may contribute to the differences seen in the results since the C deposited on the getter particles exposed to product gas may have reduced charging in those samples. Limited analysis of the heated samples with careful site selection to minimize charging yielded results comparable to those for the exposed samples, but consequently reduced the "randomness" of the analysis. The analyses of the first and second cell activated bauxite particles are in agreement for O, Al, Si, Ti, and Fe, indicating consistency of the analysis. A second possible explanation would be that the heated activated bauxite particles examined in the SEM were contaminated. The reduction in surface O concentration in the getter-exposed samples was about 10% compared to the heated sample, indicating that the contaminant may have been an O-bearing compound.

Element maps of a site on the surface of a single particle from each heated emathlite and activated bauxite sample, and emathlite and activated bauxite first cell samples from Table 13 were obtained from the SEM analysis. At the alkali loading rates obtained, the element maps showed no apparent difference between the heated samples and the corresponding samples recovered from the alkali getter reactor after testing.

#### 4.6.2.5 Getter Reactor Exit Gas

Measurements of K, Na, and Cl in the process stream exiting the reactor were made using the same methods that were applied during the test conducted without alkali getter material present in the reactor, i.e. the blank run. Results are presented in Figure 35 for each getter test, with the blank run (76G-B) included as a comparator. Gas-phase concentrations of the principal alkali component, K, were reduced by as much as three orders of magnitude, ranging from 0.03 ppmw (76G-AB) to 0.1 ppmw (51G-E-P) compared to the blank run concentration of 28 ppmw. Sodium concentrations were reduced by an order of magnitude from the blank run concentration of 11 ppmw to a range varying from 0.2 to 0.9 ppmw over the getter experiments. The reduction in gas-phase alkali concentrations substantiates the analyses of the getter material. Chlorine concentrations of 650 to 1650 ppmw were measured in the getter tests compared to the value of 1,309 ppmw determined in the blank run test, indicating variability of the input stream Cl content or possibly sampling or measurement error.

Table 13. Summary of semiquantitative elemental analyses of alkali getter material surfaces by SEM/XRF.

	Heated Emathlite		Heated Activated Bauxite		51G-E				51G-AB			
	Mean	S.D.	Mean	S.D.	Cell 1		Cell 2		Cell 1		Cell 2	
					Mean	S.D.	Mean	S.D.	Mean	S.D.	Mean	S.D.
<u>Mass %</u>												
O	47.12	5.61	52.48	4.93	45.64	3.11	42.89	5.48	37.26	3.26	38.91	2.51
Na	*		*		0.11	0.17	*		0.21	0.29	*	
Mg	3.33	0.51	*		3.25	1.08	2.97	0.78	*		*	
Al	3.52	0.61	25.59	2.15	2.78	0.62	3.07	0.91	31.92	3.16	33.61	2.56
Si	24.78	3.44	2.68	0.75	22.56	2.77	23.34	6.40	3.55	1.65	3.84	2.06
P	0.72	0.10	*		0.62	0.11	0.67	0.20	*		*	
S	*		0.13	0.03	*		*		0.15	0.12	*	
Cl	0.15	0.05	0.48	0.07	0.62	0.25	1.19	2.13	0.94	0.45	0.65	0.10
K	0.74	0.20	*		2.40	1.63	1.22	0.84	1.59	1.08	*	
Ca	4.44	2.52	*		3.81	3.18	7.18	10.46	*		0.17	0.06
Ti	0.28	0.14	0.90	0.46	0.17	0.05	0.23	0.09	1.99	0.51	1.99	0.69
Fe	2.97	3.02	0.49	0.55	2.85	1.21	2.37	1.36	3.07	1.20	2.33	2.31
<u>Molar Ratio</u>												
(K+Na)/Cl	4.5		*		3.8		0.9		1.9		*	

\* sample concentration is &lt;0.1%

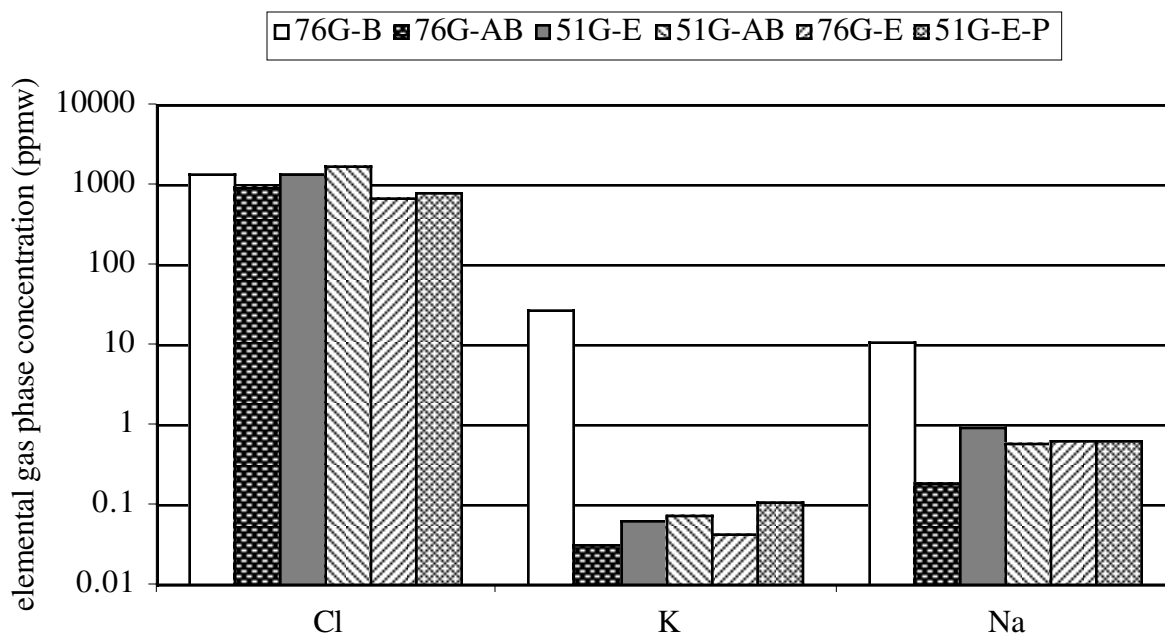


Figure 35. Gas-phase concentration of K, Na, and Cl with an empty alkali getter reactor (blank) and with activated bauxite and emathlite used as getter materials in the 76-mm and 51-mm diameter getter reactors.

#### 4.6.2.6 Mass Balances

Results of mass balances performed around the getter reactor for the elements Cl, K, and Na are presented in Figures 36, 37, and 38, respectively. Element masses measured in the exit stream from the blank run, 76G-B, were used as input conditions for the runs performed with the various getter materials. Element masses recovered from the getter material and removed from the gas stream in the sample conditioning system downstream of the getter reactor are presented as fractions of the input mass. Chlorine balances around the getter reactor (Figure 36) are 90% to 150%. In the first three tests, Cl was found predominantly in the gas phase in contrast to the last two tests in which the Cl mass in the getter material was larger. This may be related to the lower getter reactor temperatures (645° and 605°C) of the last two tests compared to the first three tests, 670°-700°C. Potassium balances around the getter reactor (Figure 37) were generally poor, ranging from a negative value to >400% of the input value. The elemental mass in the getter material accounted for nearly the entire amount of K recovered. Sodium balances (Figure 37) were in a range similar to that of Cl, 80% to 150%, but the bulk of the elemental mass was found in the getter material.

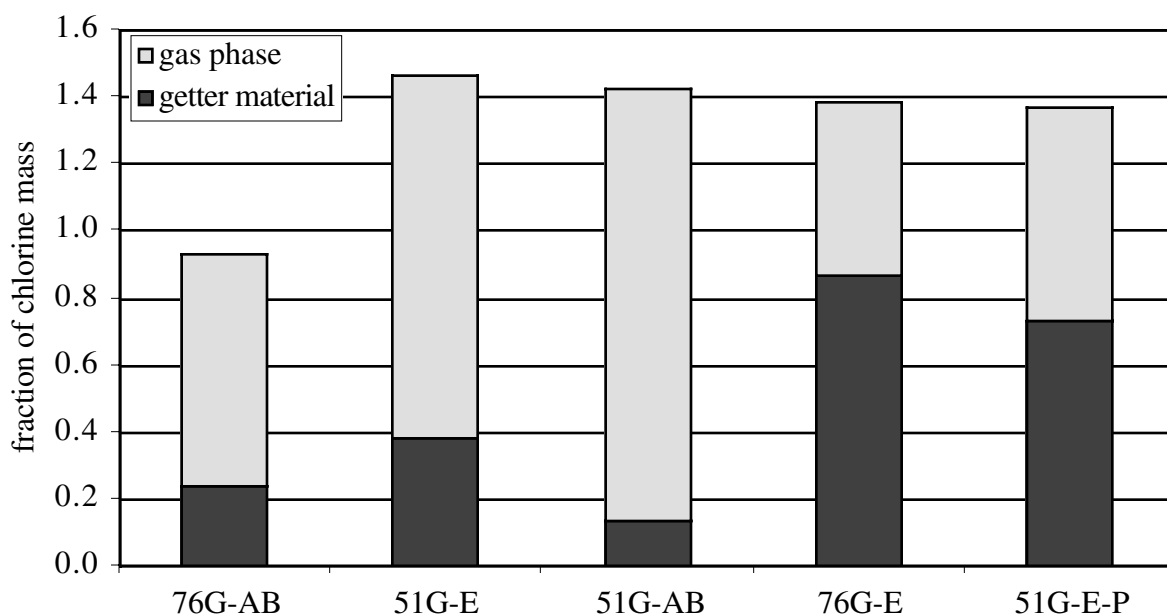


Figure 36. Distribution of input stream gas-phase Cl between the getter material and the output gas stream. Input gas stream Cl mass based on measurements from the blank run, 76G-B.

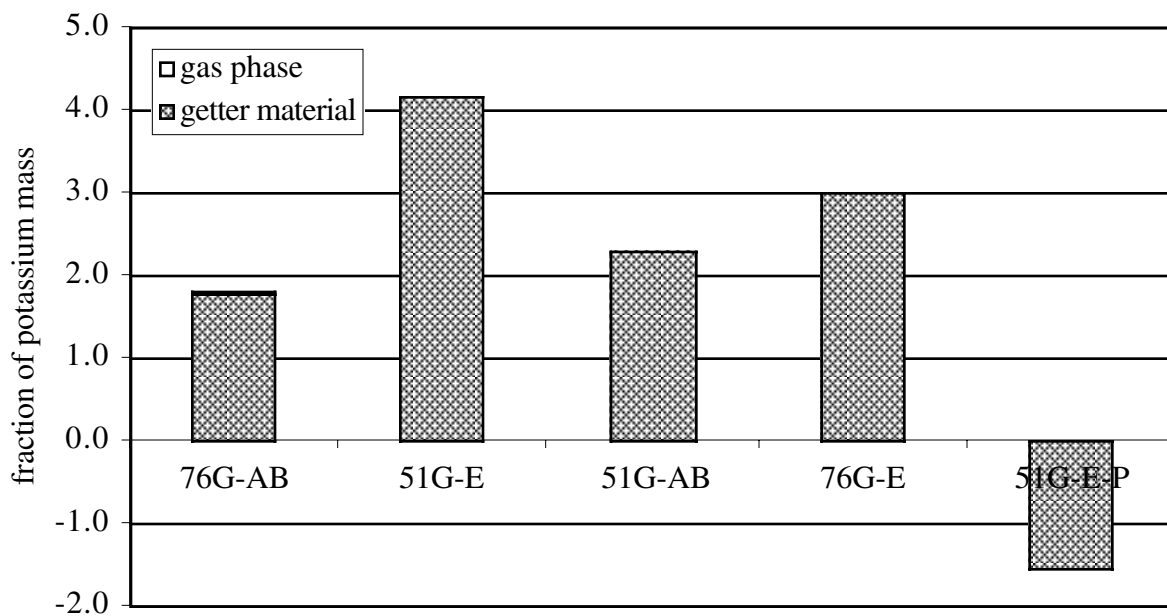


Figure 37. Distribution of input stream gas-phase K between the getter material and the output gas stream. Input gas stream K mass based on measurements from the blank run, 76G-B. Note that the output gas stream contained <0.5% of the total K recovered.

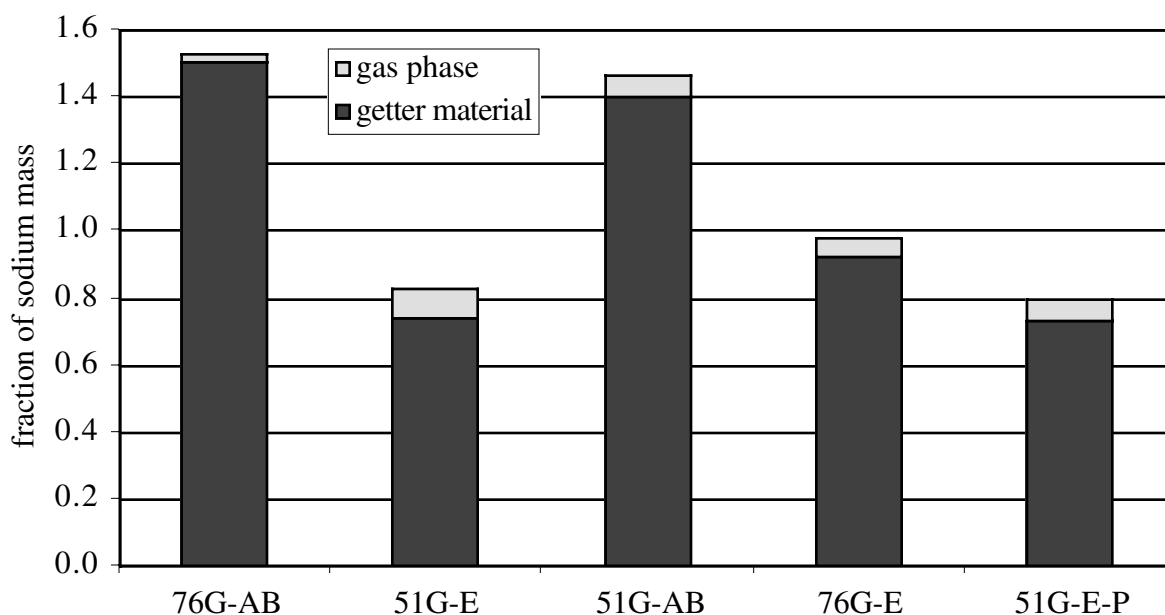


Figure 38. Distribution of input stream gas-phase Na between the getter material and the output gas stream. Input gas stream Na mass based on measurements from the blank run, 76G-B.

Element mass balances for Cl, K, and Na for the gasifier-filter-getter system are presented in Figures 39 through 41, respectively. Element mass recovered from the gasifier bed, filter char, getter material, and gas phase are shown as the fraction of the element mass contained in the fuel. Gasifier bed and filter char masses were prorated using the ratio of the time duration that flow passed through the getter reactor to the time duration of the test. As was the case in a previous study,<sup>12</sup> the degree of closure is linked to the abundance of the element, i.e., elements present in larger quantities generally yield more complete balances. Balances for K, which was present as ~1% of fuel mass, varied from 75% to 91% of closure. Balances for Cl (~0.6% of fuel mass) showed a wider range from 63% to 93% of full closure. Sodium was present as ~0.1% of fuel mass, and elemental balances ranged from 63% to 150%. As noted earlier, Cl was found predominantly in the gas phase for the first four tests, but substantial amounts were recovered from the getter material in the two final tests (76G-E and 51G-E-P) where getter reactor temperatures were lower. Most fuel K and Na were sequestered in the gasifier bed material, as was found in earlier work,<sup>12</sup> with roughly 10% to 15% in the filter char. The Na balance for test 51G-E-P was much higher than the other tests (150%) and this large value results from a higher value for Na in the bed material analysis. In general, the degree of closure obtained for the elemental balances of interest, Cl, K, and Na, indicates that the tests and measurements produced consistent results.

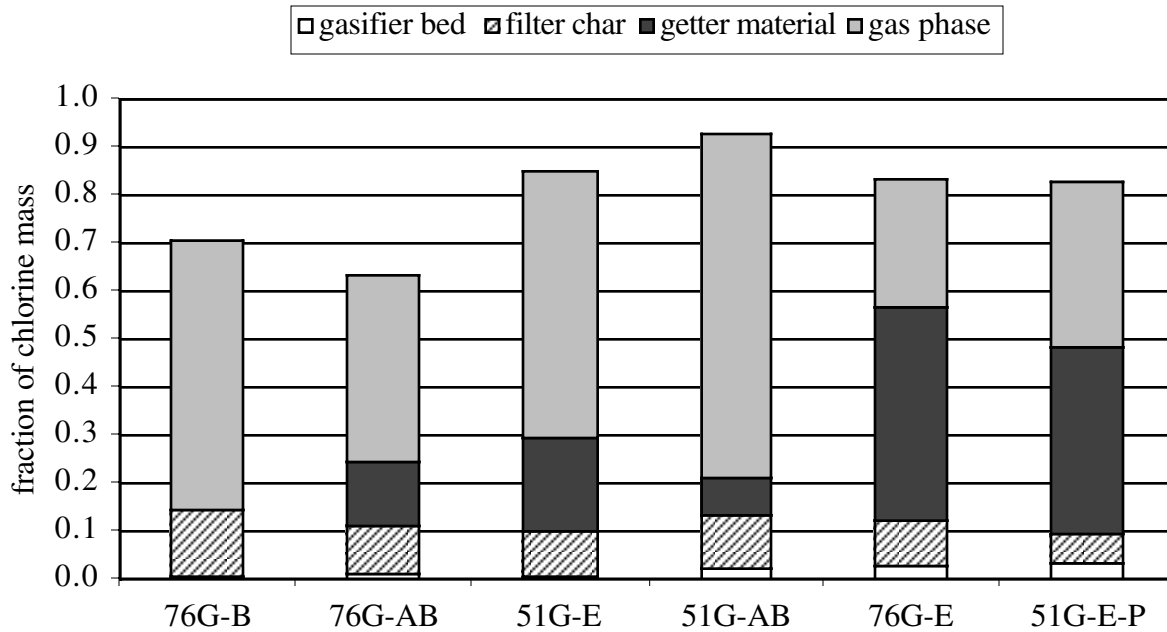


Figure 39. Distribution of the Cl mass present in the input fuel among the outputs: gasifier bed, filter char, getter material, and gas phase.

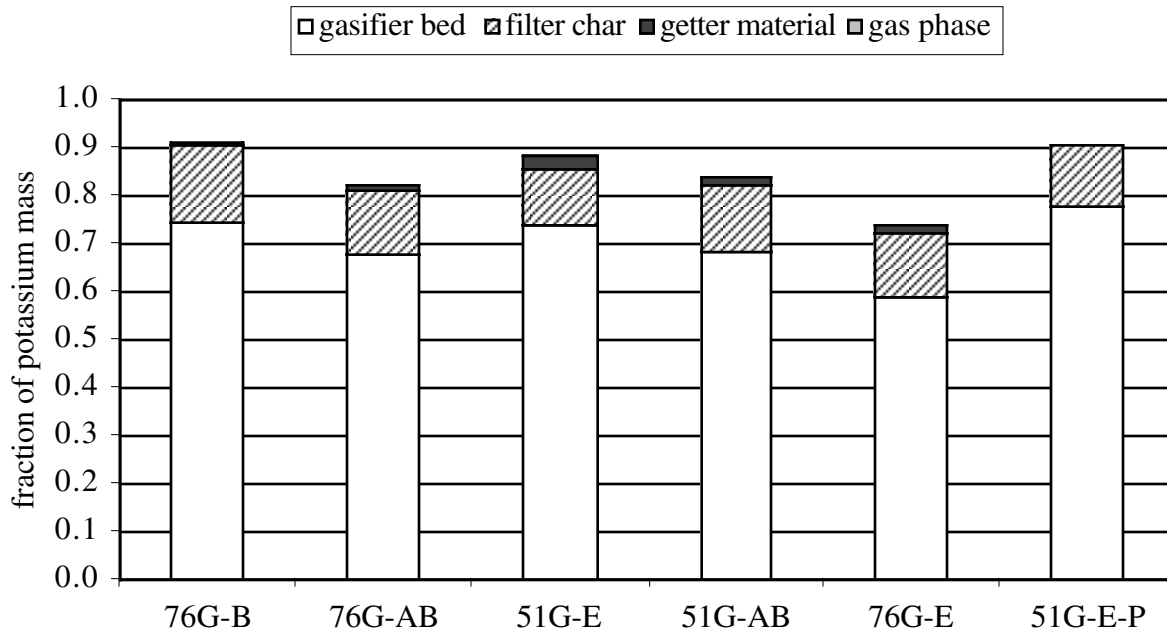


Figure 40. Distribution of the K mass present in the input fuel among the outputs: gasifier bed, filter char, getter material, and gas phase.

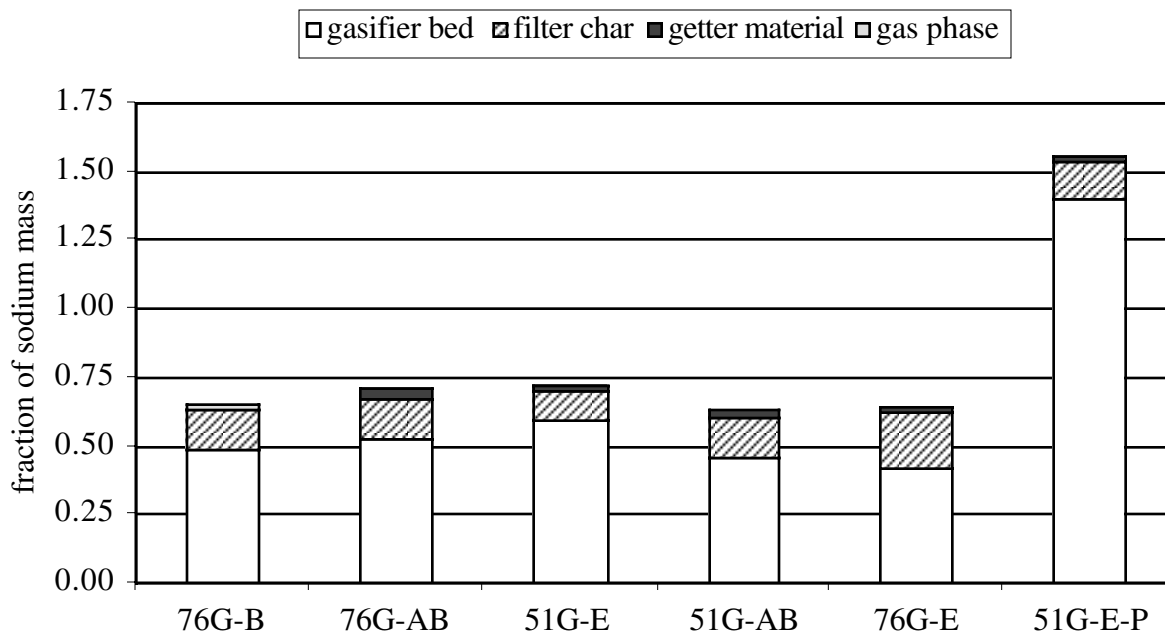


Figure 41. Distribution of the Na mass present in the input fuel among the outputs: gasifier bed, filter char, getter material, and gas phase.

#### 4.6.2.7 Comparison of Treatments

The test matrix of the present investigation was designed to explore differences between the getter materials, emathlite, and activated bauxite, and the dependencies of getting activity on space time, or residence time of the gas within the reactor. The latter was accomplished using two reactor bodies with different diameters, and hence, different superficial gas velocities and residence times. The results from the four tests (76G-AB, 51G-E, 51G-AB, and 76G-E) showed no apparent differences between the getter materials or the residence times (~0.7 s versus ~1.4 s). In all cases, the gas stream exiting the getter reactor had a total alkali content one to two orders of magnitude lower than the inlet stream, and the first cell within the getter reactor contained >80% of the alkali captured by the reactor as a whole. Getter reactor inlet concentrations of K and Na in the gas phase were ~28 ppmw and 11 ppmw, respectively, with corresponding average concentrations at the getter reactor outlet on the order of 0.05 and 0.6 ppmw, indicating that K was preferentially removed over Na.

The fifth test (51G-E-P) used 4.0- to 4.8-mm emathlite particles in the getter reactor where the initial four test used particles in a 2.4- to 3.4-mm size class. Respective concentrations of K and Na in the reactor exit gas streams were 0.06 and 0.9 ppmw for the smaller getter particle test and 0.1 and 0.6 ppmw for the larger getter particle size. No apparent difference was found between the results of the two particle size tests.

## 5. SUMMARY AND CONCLUSIONS

Air-dried banagrass was used as fuel in a bench-scale fluidized bed gasification reactor to generate an alkali-laden product gas stream to study adsorption of alkali compounds in packed beds of solid sorbents. The gasifier was operated at  $\sim 820^{\circ}\text{C}$  and equivalence ratio of  $\sim 0.3$ . Exiting the gasifier, the product stream was hot filtered using a ceramic filter unit, then passed through a packed bed of sorbent material, either emathlite or activated bauxite. Emathlite is composed of roughly 60%  $\text{SiO}_2$  and 10%  $\text{Al}_2\text{O}_3$ , with smaller amounts of Ca, Mg, Fe, and titanium oxides and trace levels of P, K, Na, Cl, and S. Activated bauxite contains roughly 90%  $\text{Al}_2\text{O}_3$ , 6%  $\text{SiO}_2$ , 2% each of iron and titanium oxides, and trace elements similar to emathlite. In addition to testing these two sorbent materials, two reactor bodies, one 51 mm in diameter, the other 76 mm in diameter, were employed to investigate the effects of product gas space time on the alkali adsorption process. The two reactor bodies resulted in experimental space time values of 0.7 and 1.5 s, respectively. The initial square matrix of tests using sorbent materials and space time were conducted with getter particles in a size class from 2.4 to 3.4 mm. A final test was performed using emathlite particles in a size range from 4.0 to 4.8 mm to explore the effects of getter particle size on alkali removal.

A preliminary test was conducted to obtain baseline data on the alkali content of the hot filtered gas stream for the gasifier and filter operating conditions used for all subsequent alkali getter tests. Potassium, Na, and Cl concentrations in the post-filter product gas were 28, 11, and 1,309 ppmw, respectively, and the alkali concentrations were in excellent agreement with concentrations predicted by alkali chloride vapor pressure data available in the literature. Molar ratios of total alkali (K+Na) to chlorine were  $\sim 0.03$ , indicating that Cl is present in a form other than alkali chloride, possibly as HCl.

Visual inspection of the getter materials recovered from the reactor after each test showed evidence of C deposition on the surface of the particles. The location of heaviest deposition was at the inlet of the reactor for activated bauxite, and in the middle depths of the packed bed for emathlite. The relationship between C deposition and alkali removal efficiency merits further study to better understand potential C poisoning or deactivation of the getter material. Alkali removal in all tests, regardless of getter material, space time, or particle size employed, was concentrated in the first cell at the inlet of the reactor, containing  $>80\%$  of the total alkali mass captured in the entire bed. The second cell in the reactor captured  $\sim 15\%$  of the total alkali mass captured in the bed, with the remaining cells containing amounts near the background levels of alkali present in the pretest oven-heated sorbent material. Future experiments should include pretest heat treating of sorbent materials to improve analytical clarity. Potassium and Na concentrations in the getter materials recovered from the first cell in the 51-mm diameter reactor tests averaged  $4.6 \text{ mg K g}^{-1}$  sorbent and  $1.1 \text{ mg Na g}^{-1}$  sorbent, respectively. Concentrations were lower in the 76-mm test, averaging  $1.5 \text{ mg K g}^{-1}$  sorbent and  $0.4 \text{ mg Na g}^{-1}$  sorbent, respectively, because of the greater amounts of sorbent present. Future sorbent testing would be better served by incorporating a bed of smaller diameter to obtain better penetration of alkali and higher concentrations in the sorbent materials. Chlorine was distributed throughout the bed in concentrations of 0.5 to  $13 \text{ mg Cl g}^{-1}$  sorbent. Over all tests, calculated molar ratios of total alkali to Cl in the first cell of the reactor varied from 0.2 to 2.3 but did not permit firm conclusions regarding the form of adsorption (chemisorption versus physical adsorption) because of the presence of high Cl concentrations in gas phase from forms other than alkali chloride.

Gas-phase concentrations of K, Na, and Cl were measured in the outlet gas stream from the getter reactor. Potassium concentrations, measured at 28 ppmw from the hot filter exit, were reduced by as much as three orders of magnitude, ranging from 0.03 to 0.1 ppmw in the getter reactor exit gas stream. Sodium was also removed in the getter bed ranging from 0.2 to 0.9 ppmw in the exit gas stream compared to an inlet concentration of ~11 ppmw.

Element balances around the getter reactor for K, Na, and Cl were generally poor due to the small analyte masses compared to the total getter mass in the reactor. Element balances which included the contributions of the input fuel were generally acceptable. Carbon balances ranged from 93% to 103% of complete closure, with carbon conversion efficiencies on the order of 93%. Balances for K, which were present as ~1% of fuel mass, varied from 75% to 91% of closure. Balances for Cl (~0.6% of fuel mass) showed a wider range from 63% to 93% of full closure. Sodium was present as ~0.1% of fuel mass, and elemental balances ranged from 63% to 150%. Chlorine was found predominantly in the gas phase; K and Na were concentrated in the gasifier bed material.

In general, the tests to examine the effects of getter material (emathlite versus activated bauxite), space time (0.5 versus 1.2 s), and getter particle size class (2.4-3.4 mm versus 4.0-4.8 mm) on alkali capture showed no apparent differences in gas-phase alkali removal efficiency. Potassium and Na removal efficiency for all of the tests was greater than 99% and 92%, respectively. Chlorine concentrations in the product stream exiting the hot ceramic filter were ~1,300 ppmw and were reduced in the getter bed by roughly half in the best case, yielding a gas-phase concentration of 650 ppmw. Chlorine's well established role in high-temperature corrosion warrants further research to determine the forms of Cl in product gas and high-temperature gas conditioning for Cl control.

## 6. REFERENCES

1. Jenkins, B.M., R.R. Bakker, and J.B. Wei. On the properties of washed straw. *Biomass and Bioenergy*, 1996, 10(4), pp. 177-200.
2. Turn, S.Q., C.M. Kinoshita, and D.M. Ishimura. Removal of inorganic constituents of biomass feedstocks by mechanical dewatering and leaching. *Biomass and Bioenergy*, 1997, 12(4), PP. 241-252.
3. Baxter, L.L., T.R. Miles, T.R. Miles, Jr., B.M. Jenkins, G.H. Richards, and L.L. Oden. Transformations and deposition of inorganic material in biomass boilers. In M.G. Carvalho (ed.) *Second International Conference on Combustion Technologies for a Clean Environment*. Commission of the European Communities. Lisbon, Portugal. 1993. pp. 9-15.
4. Jenkins, B.M., L.L. Baxter, T.R. Miles, T.R. Miles, Jr., L.L. Oden, R.W. Bryers, and E. Winther. Composition of ash deposits in biomass fueled boilers: results of full-scale experiments and laboratory simulations. Paper No. 946007. Presented at the 1994 International Summer Meeting Sponsored by ASAE, Kansas City, Kansas, June 19-24, 1994.
5. Baxter, L.L. Ash deposition during biomass and coal combustion: a mechanistic approach. *Biomass and Bioenergy*, 1993, (4)2, pp. 85-102.
6. Miles, T.R., T.R. Miles, Jr., L.L. Baxter, R.W. Bryers, B.M. Jenkins, and L.L. Oden. 1995. Alkali deposits found in biomass power plants, a preliminary investigation of their extent and nature. Summary report for the National Renewable Energy Laboratory. NREL Subcontract TZ-2-11226-1.
7. Ergudenler, A. and A.E. Ghaly. Agglomeration of alumina sand in a fluidized bed straw gasifier at elevated temperatures. *Bioresource Technology*, 1993a, 43, pp. 259-268.
8. Ergudenler, A. and A.E. Ghaly. Agglomeration of silica sand in a fluidized bed gasifier operating on wheat straw. *Biomass and Bioenergy*, 1993b, 4(2), pp. 135-147.
9. Padban, N., S. Kiuru, and A.L. Hallgren. Bed material agglomeration in PFB biomass gasification. Preprints of papers presented at the 210th ACS National Meeting. Volume 40, No. 3. Chicago Illinois, August 20-25, 1995.
10. Mojtahedi, W., E. Kurkela, and M. Nieminen. Release of sodium and potassium in the PFB gasification of peat. *Journal of the Institute of Energy*, 1990, 63, pp. 95-100.
11. Mojtahedi, W. and R. Backman. The fate of sodium and potassium in the pressurised fluidised-bed combustion and gasification of peat. *Journal of the Institute of Energy*, 1989, 62, pp. 189-196.
12. Turn, S.Q., C.M. Kinoshita, D.M. Ishimura, and J. Zhou. The fate of inorganic constituents of biomass in fluidized bed gasification. *Fuel*, 1998, 77(3), pp. 135-146

13. Onischak, M., R.H. Carty, and R.A. Knight. 1995. Hot gas cleanup for operation of a gas turbine with a fluidized bed air blown biomass gasifier, Filter performance short duration tests. Volume III – PDU operations and analytical results, Topical Report – Task 2.9, National Renewable Energy Laboratory Contract Number XAZ-3-12092-01-106794. pp. 41. Westinghouse Electric Corporation.
14. Lee, S.H.D. and I. Johnson. Removal of gaseous alkali metal compounds from hot flue gas by particulate sorbents. *Journal of Engineering for Power*, Transactions of the ASME, 1980, 102, pp. 397-402.
15. Scandrett, L.A. and R. Clift. The thermodynamics of alkali removal from coal-derived gases. *Journal of the Institute of Energy*, 1984, 57(433), pp. 391-397.
16. Luthra, K.L. and O.H. LeBlanc, Jr. Adsorption of NaCl and KCl on Al<sub>2</sub>O<sub>3</sub> at 800-900°C. *Journal of Physical Chemistry*, 1984, 88(9), pp. 1896-1901.
17. Lee, S.H.D., R.F. Henry, and K.M. Myles. Removal of alkali vapors by a fixed granular-bed sorber using activated bauxite as a sorbent. 1985. USDOE Report CONF-850351-3. Argonne National Laboratory.
18. Jain, R.C. and S.C. Young. Laboratory/Bench Scale Testing and Evaluation of A.P.T. Dry Plate Scrubber. 1985. Report No. DOE/ET/15492--2030. Air Pollution Technology, Inc.
19. Bachovchin, D.M., M.A. Alvin, E.A. DeZubay, and P.R. Mulik. A study of high temperature removal of alkali in a pressurized gasification system. 1986. Report No. DOE/MC/20050-2226. Westinghouse Electric Corporation, Research and Development Center.
20. Punjak, W.A. and F. Shadman. Aluminosilicate sorbents for control of alkali vapors during coal combustion and gasification. *Energy & Fuels*, 1988, 2(5), pp. 702-708.
21. Punjak, W.A., M. Uberoi, and F. Shadman. High-temperature adsorption of alkali vapors on solid sorbents. *AIChE Journal*, 1989, 35(7), pp. 1186-1194.
22. Uberoi, M., W.A. Punjak, and F. Shadman. The kinetics and mechanism of alkali removal from flue gases by solid sorbents. *Progress in Energy and Combustion Science*, 1990, 16, pp. 205-211.
23. Mulik, P.R., D.F. Ciliberti, M.A. Alvin, M.M. Ahmed, D.M. Bachovchin, and D.L. Kearns. Simultaneous high-temperature removal of alkali and particulates in a pressurized gasification system. 1981. Report No. DOE/ET/11026--T1. Westinghouse Electric Corporation, Research and Development Center.
24. Szekeley, J., J.W. Evans, and H.Y. Sohn. *Gas-Solid Reactions*. Academic Press, San Francisco. 1976.
25. Adamson, A.W. *Physical Chemistry of Surfaces*. John Wiley and Sons, Inc. New York. 1990.

26. Worrall, W.E. *Clays and Ceramic Raw Materials, Second Edition*. Elsevier Applied Sciences Publishers, New York. 1986.
27. Grim, R.E. *Applied Clay Mineralogy*. McGraw-Hill Book Co., Inc. New York. 1962.
28. Cotton, F.A. and G. Wilkinson. *Advanced Inorganic Chemistry*. Interscience Publishers, New York. 1962.
29. Salmenoja, K., K. Makela, M. Hupa, and R. Backman. Superheater corrosion in environments containing potassium and chlorine. *Journal of the Institute of Energy*, 1996, 69, pp 155-162.
30. Vaughan, D.A., H.H. Krause, and W.K. Boyd. Chloride corrosion and its inhibition in refuse firing. In R.W. Bryers (ed.), *Ash Deposits and Corrosion Due to Impurities in Combustion Gases*. Hemisphere Publishing Corporation, Washington. 1977.
31. Reid, W.T. *External Corrosion and Deposits, Boilers and Gas Turbines*. American Elsevier Publishing Company, Inc. New York. 1971.
32. Daijou, Y., S.H.D. Lee, K. Suzuki, T. Ishinomori, T. Yanagisawa, and Y. Tsumita. Alkali-vapor measurements in the Wakamatsu PFBC Plant. Presented at the Third Hot Gas Symposium—Gas Cleaning at High Temperatures, University of Karlsruhe, Germany, September 18-20, 1996.
33. Lee, S.H.D., W.M. Swift, and I. Johnson. Regeneration of activated bauxite used as a granular sorbent for removing gaseous alkali metal compounds from hot flue gas. Gas Turbine Division of ASME. New Orleans, LA, March 10-13, 1980.
34. Kunii, D. and O. Levenspiel. *Fluidization Engineering*. Robert F. Krieger Publishing Co., Huntington, N.Y. 1977.
35. Kinoshita, C.M. Cogeneration in the Hawaiian sugar industry. *Bioresource Technology*, 1991, 35, pp. 231-237.
36. Zimm, B.H. and J.E. Mayer. Vapor pressures, heats of vaporization, and entropies of some alkali halides. *The Journal of Chemical Physics*, 1944, 12(9), pp 362-369.

## **Appendix A – TEST DATA**

Traces of temperature at locations in the gasifier, ceramic filter, and alkali getter reactor and of major gas species in the product gas recorded during tests 76G-B, 76G-AB, 51G-E, 51G-AB, 76G-E, and 51G-E-P.

**Test 76G-B**

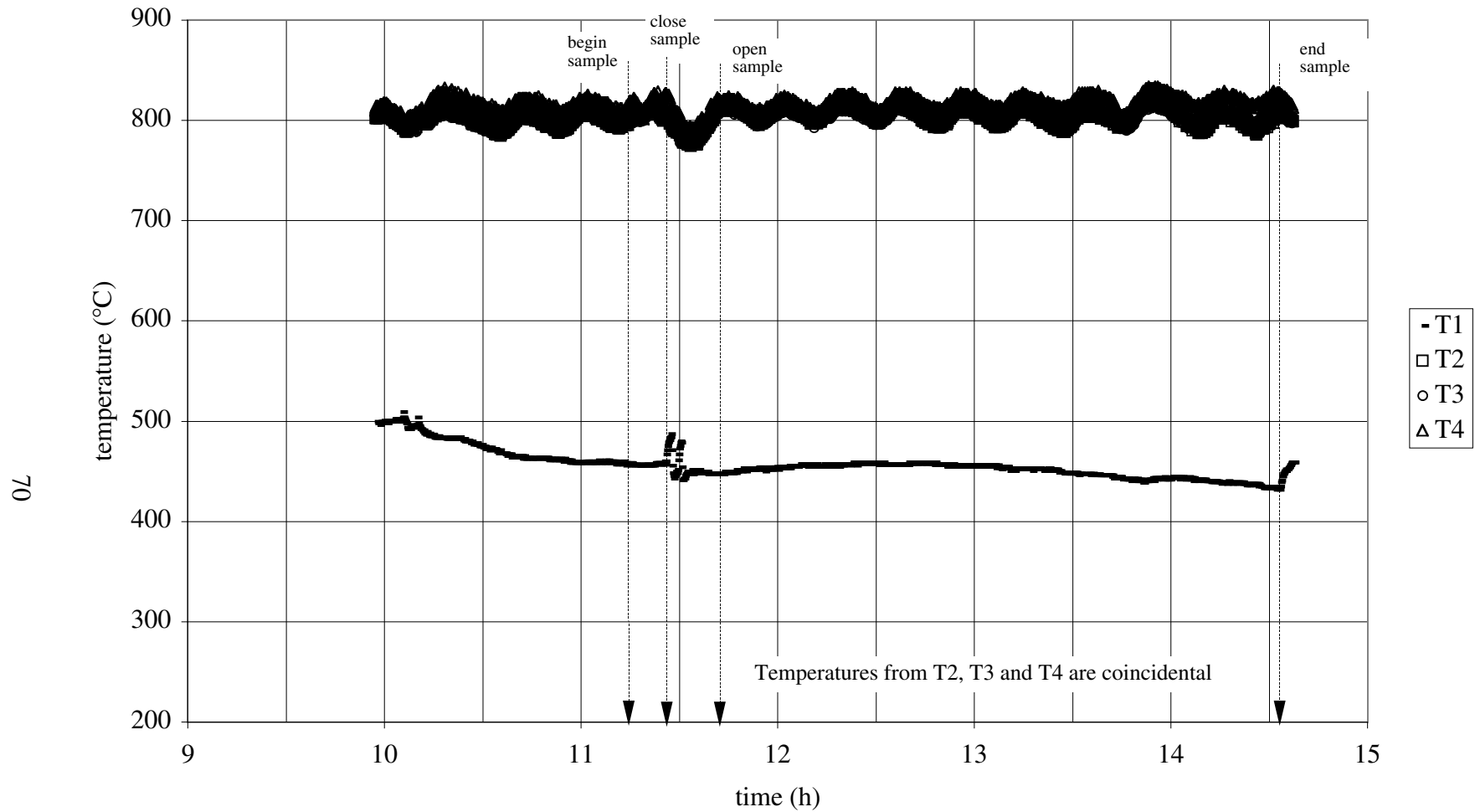


Figure A1. Thermocouple measurements of gasifier temperature below the distributor (T1), above the distributor (T2), and in the dense bed (T3 and T4) during Test 76G-B.

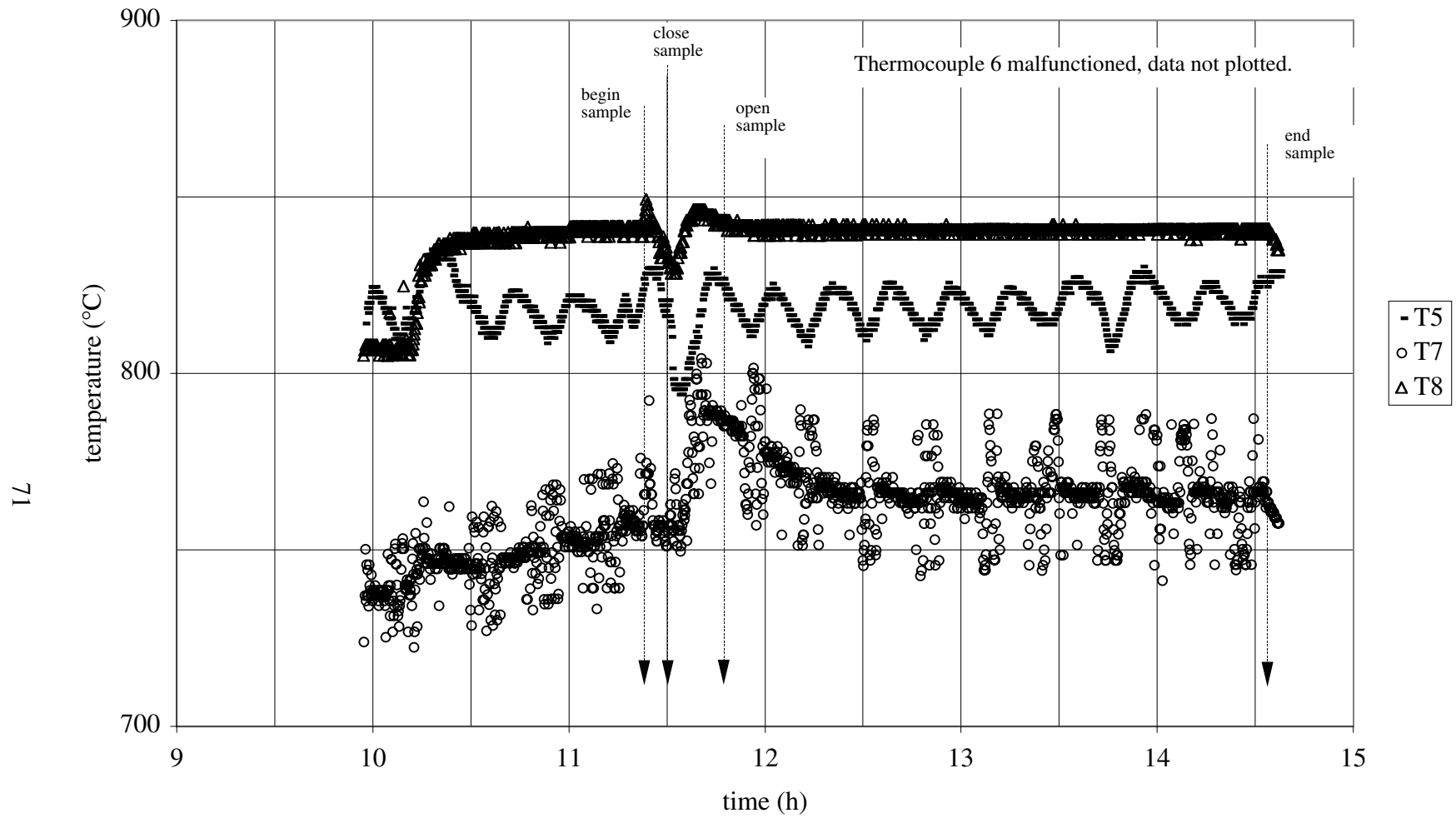


Figure A2. Thermocouple measurements of gasifier temperature in the dense bed (T5 and T6) and in the transition (T7) and disengagement zone (T8) during Test 76G-B.

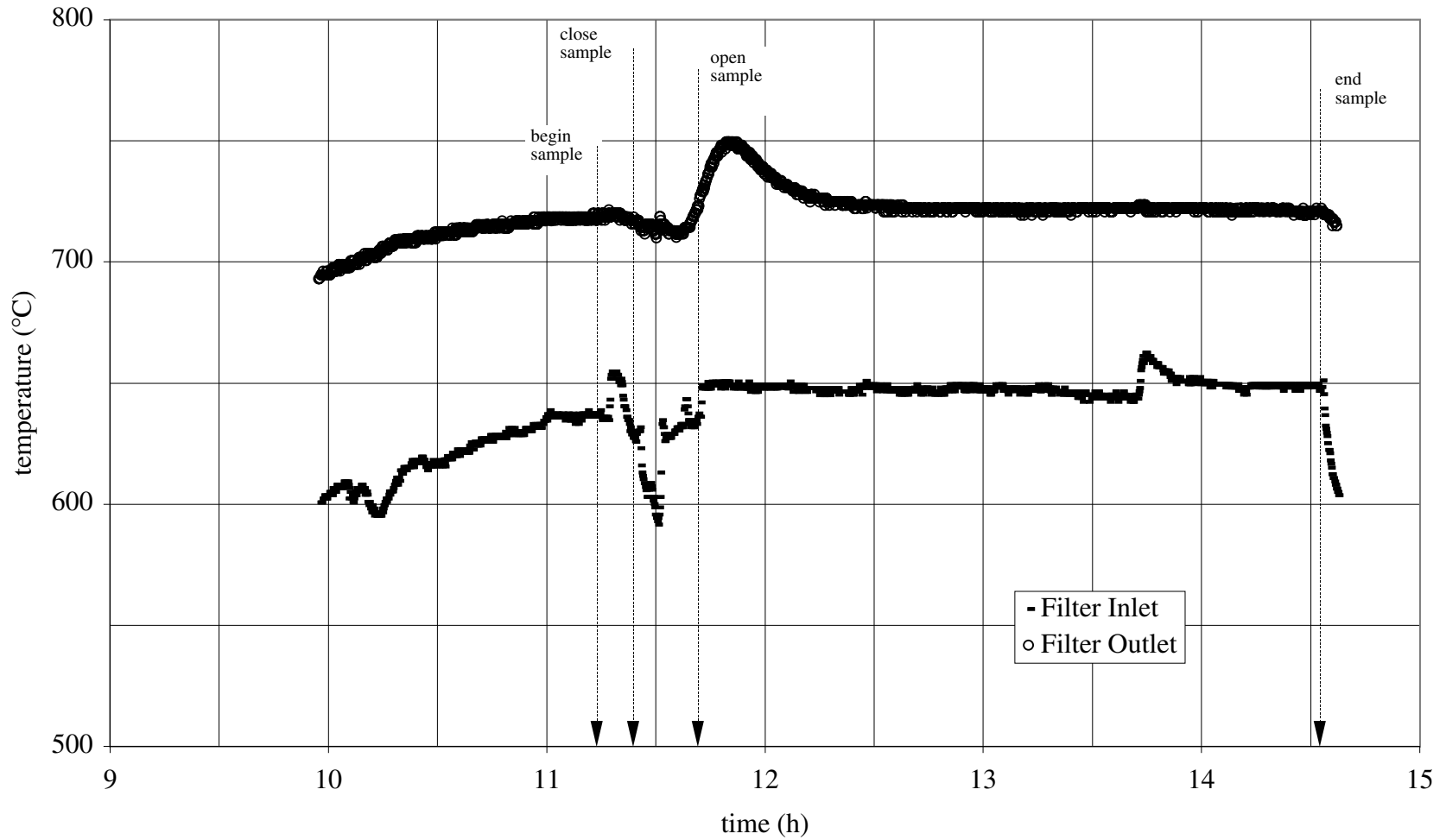


Figure A3. Thermocouple measurements of inlet and outlet temperatures in the heated ceramic filter unit during Test 76G-B.

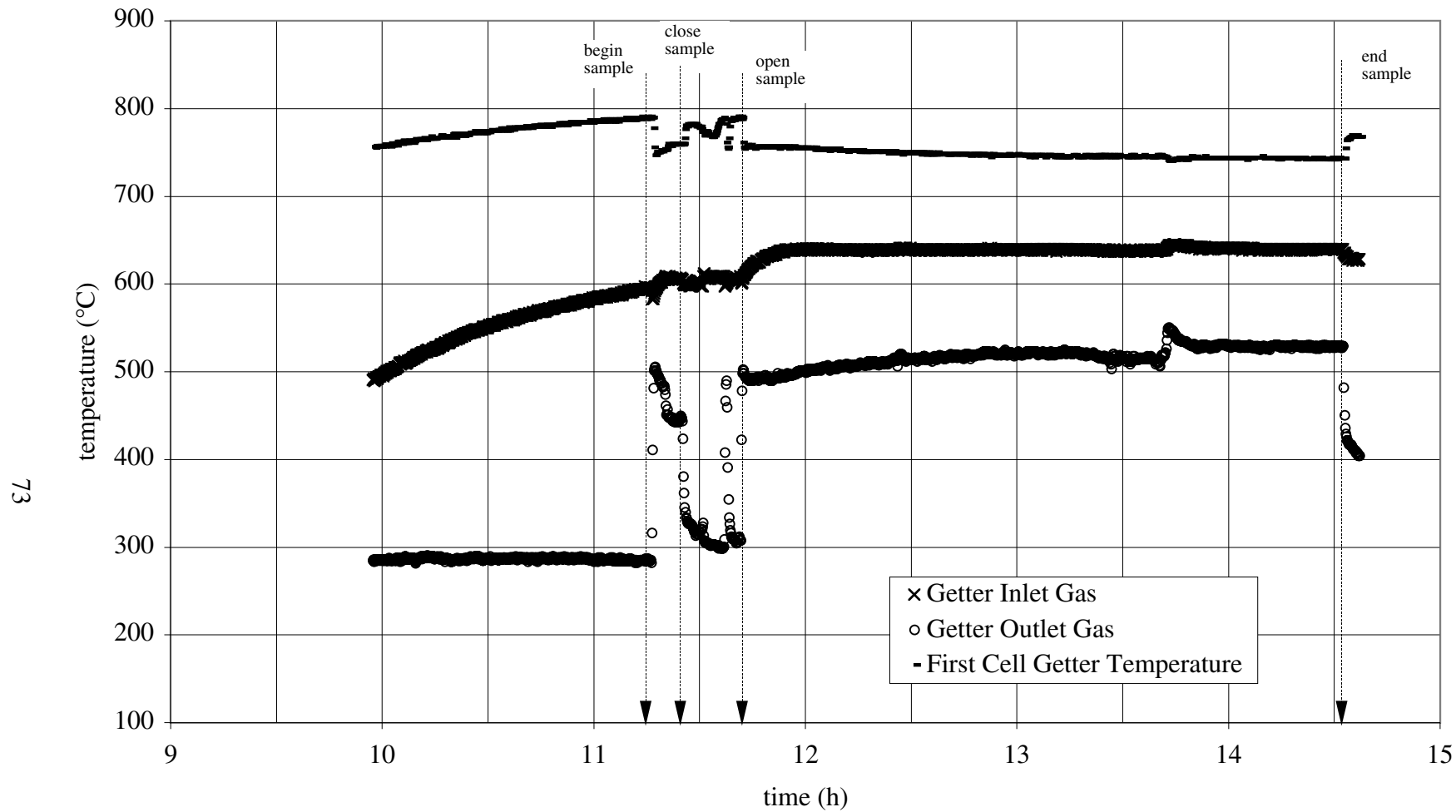


Figure A4. Thermocouple measurements of inlet gas stream, upper getter material surface, and outlet gas stream temperatures in the empty alkali getter reactor during Test 76G-B.

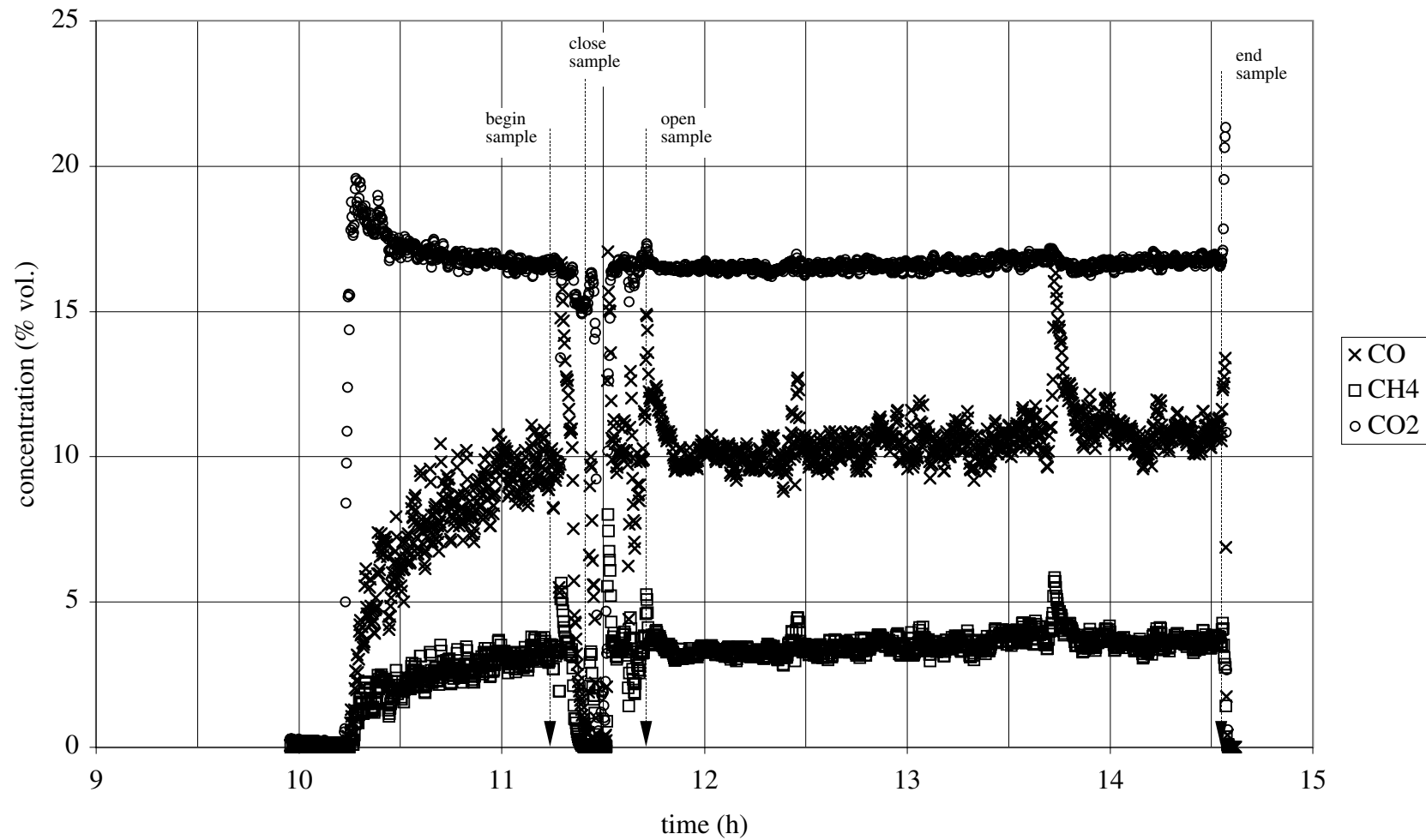


Figure A5. Product gas concentrations of CO, CO<sub>2</sub>, and CH<sub>4</sub> measured at the outlet of the empty alkali getter reactor during Test 76G-B.

**Test 76G-AB**

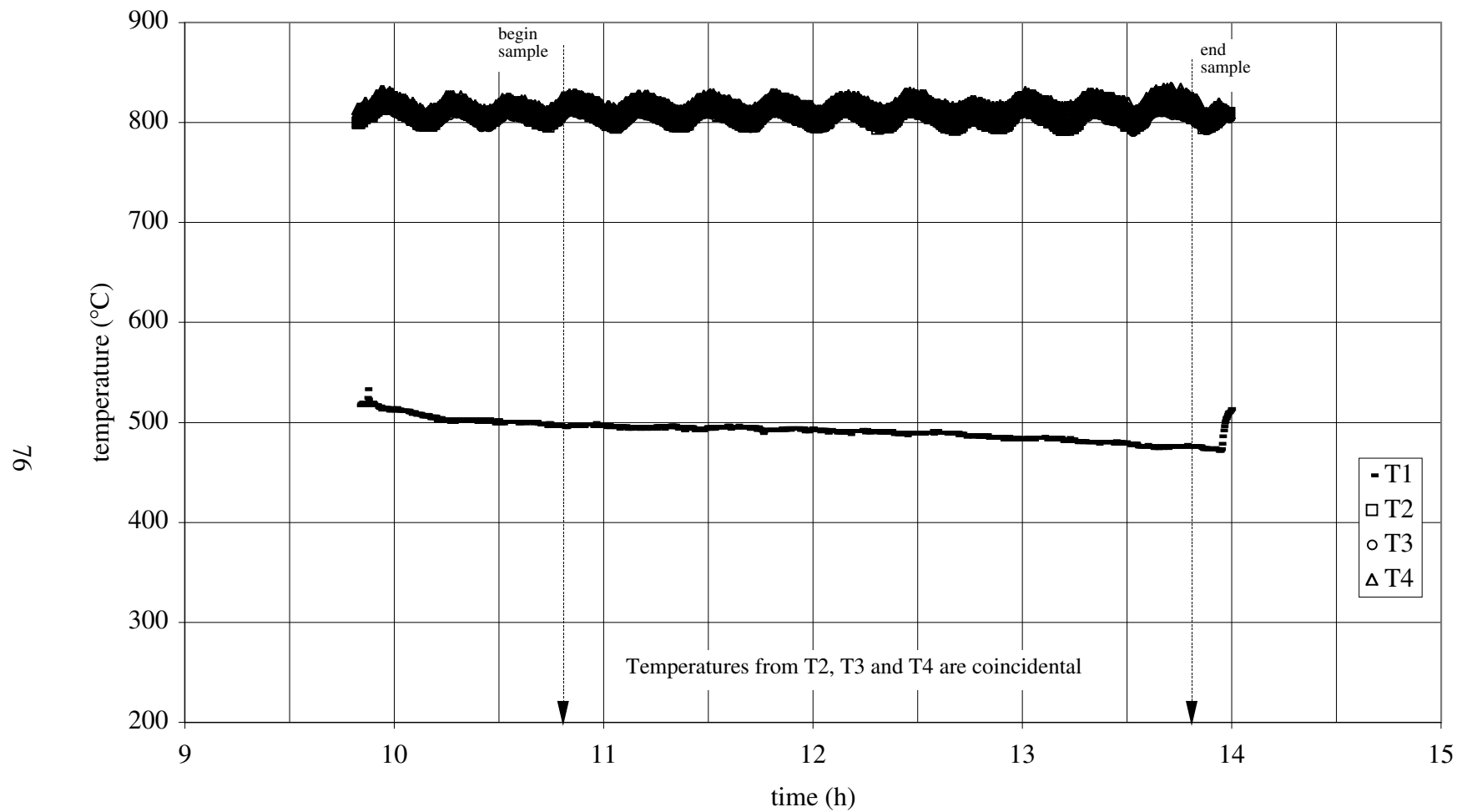


Figure A6. Thermocouple measurements of gasifier temperature below the distributor (T1), above the distributor (T2), and in the dense bed (T3 and T4) during Test 76G-AB.

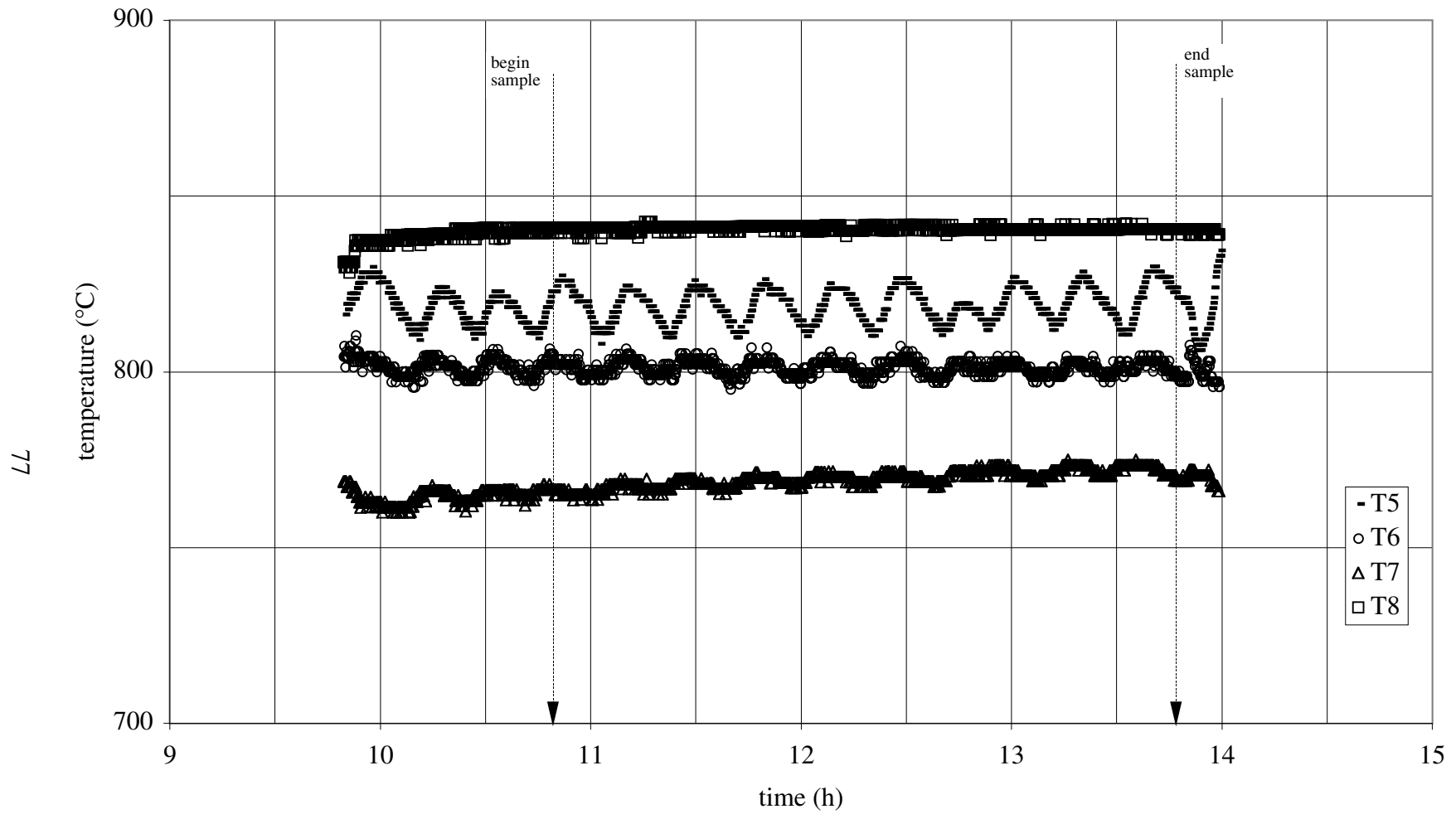


Figure A7. Thermocouple measurements of gasifier temperature in the dense bed (T5 and T6) and in the transition (T7) and disengagement zone (T8) during Test 76G-AB.

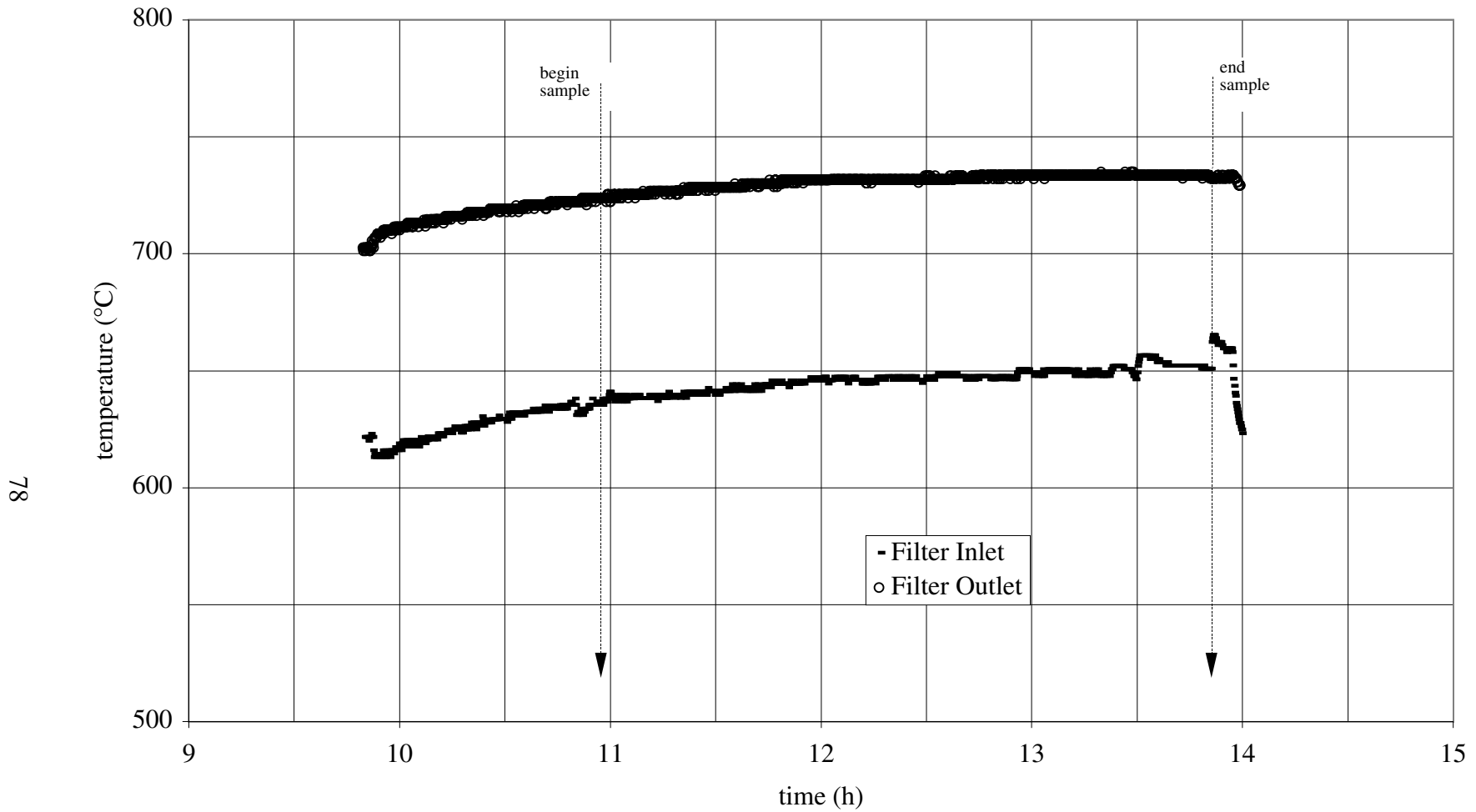


Figure A8. Thermocouple measurements of inlet and outlet temperatures in the heated ceramic filter unit during Test 76G-AB.

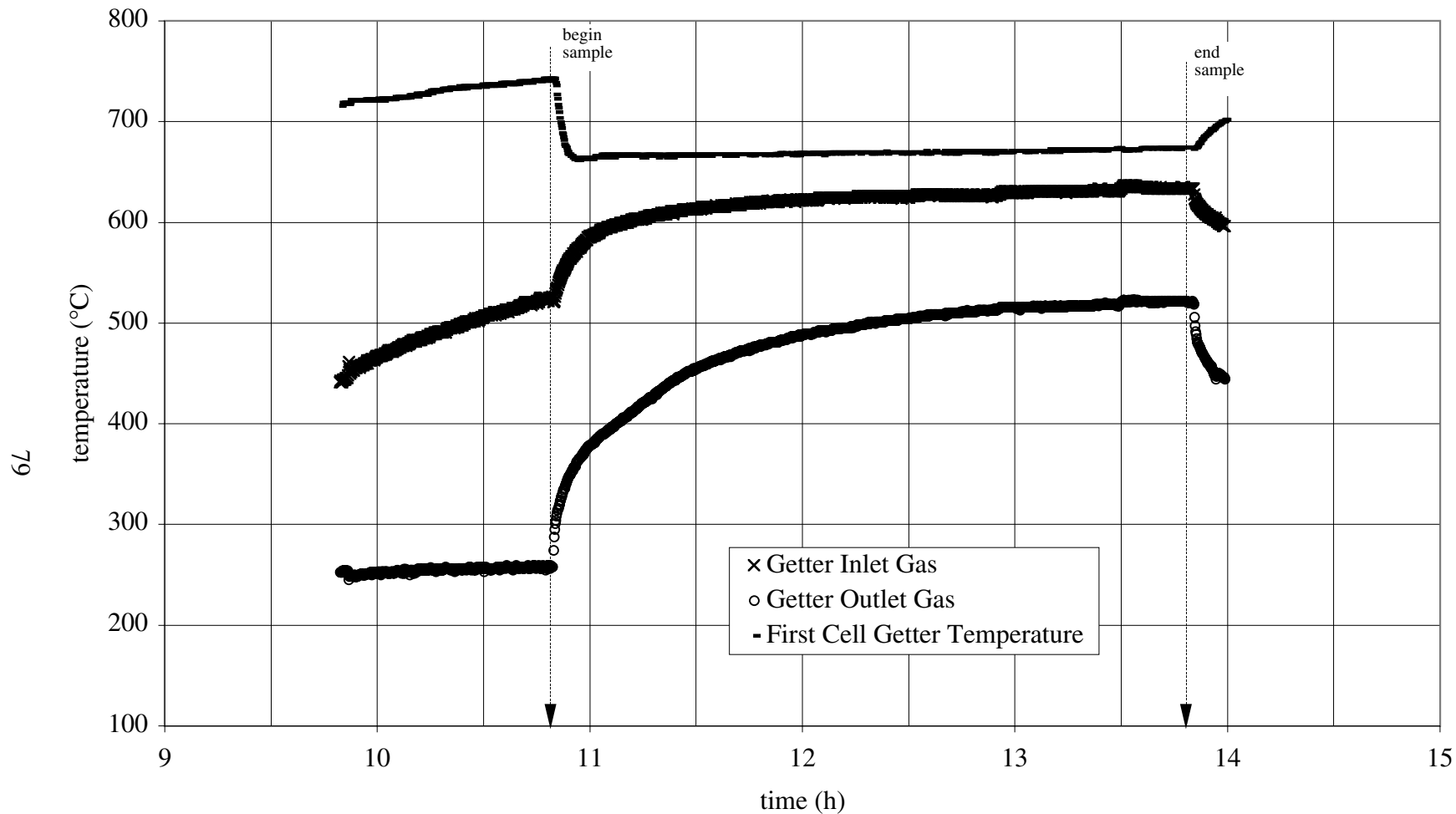


Figure A9. Thermocouple measurements of inlet gas stream, upper getter material surface, and outlet gas stream temperatures in the packed bed alkali getter reactor during Test 76G-AB.

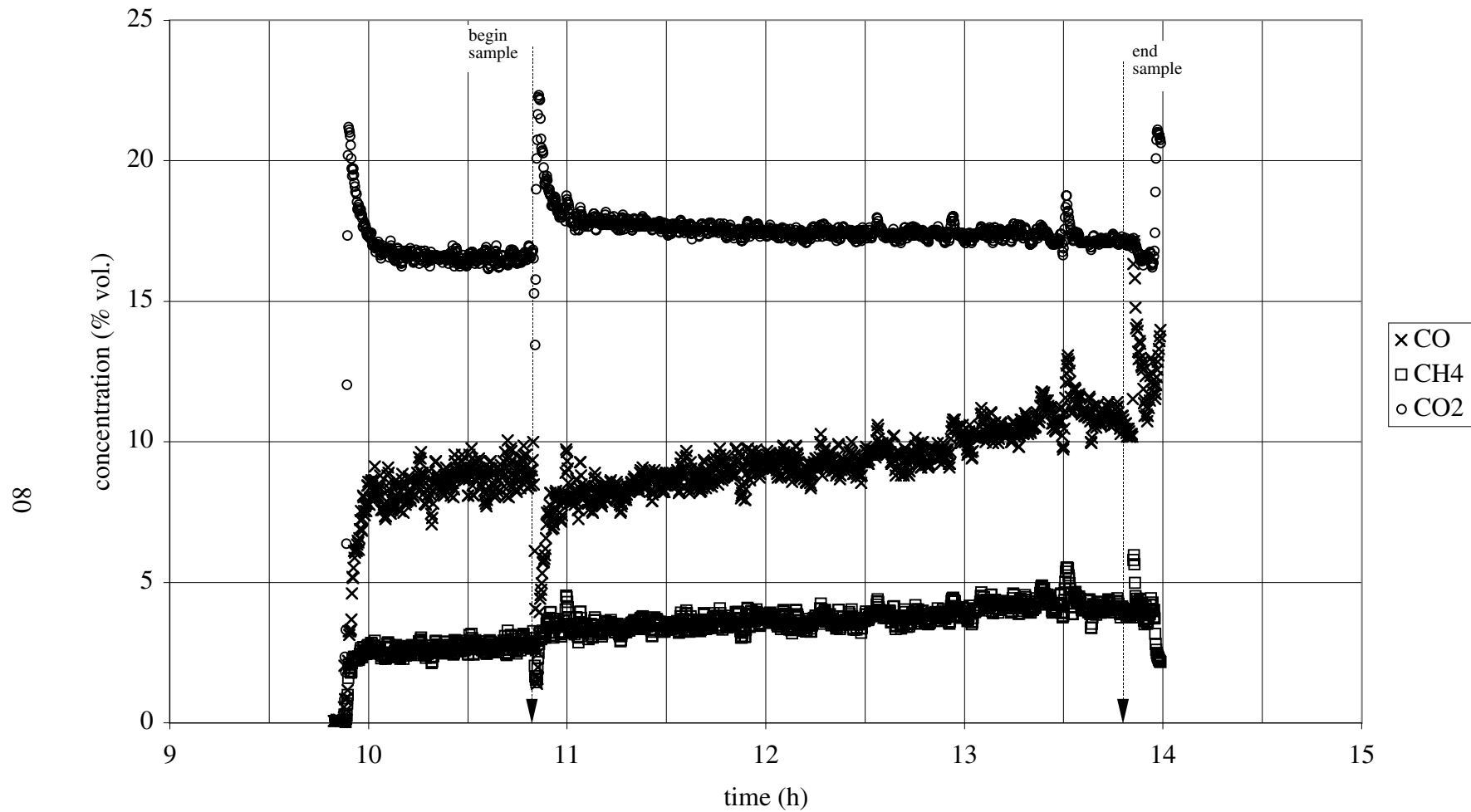


Figure A10. Product gas concentrations of CO, CO<sub>2</sub>, and CH<sub>4</sub> measured at the outlet of the packed bed alkali getter reactor during Test 76G-AB.

## **Test 51G-E**

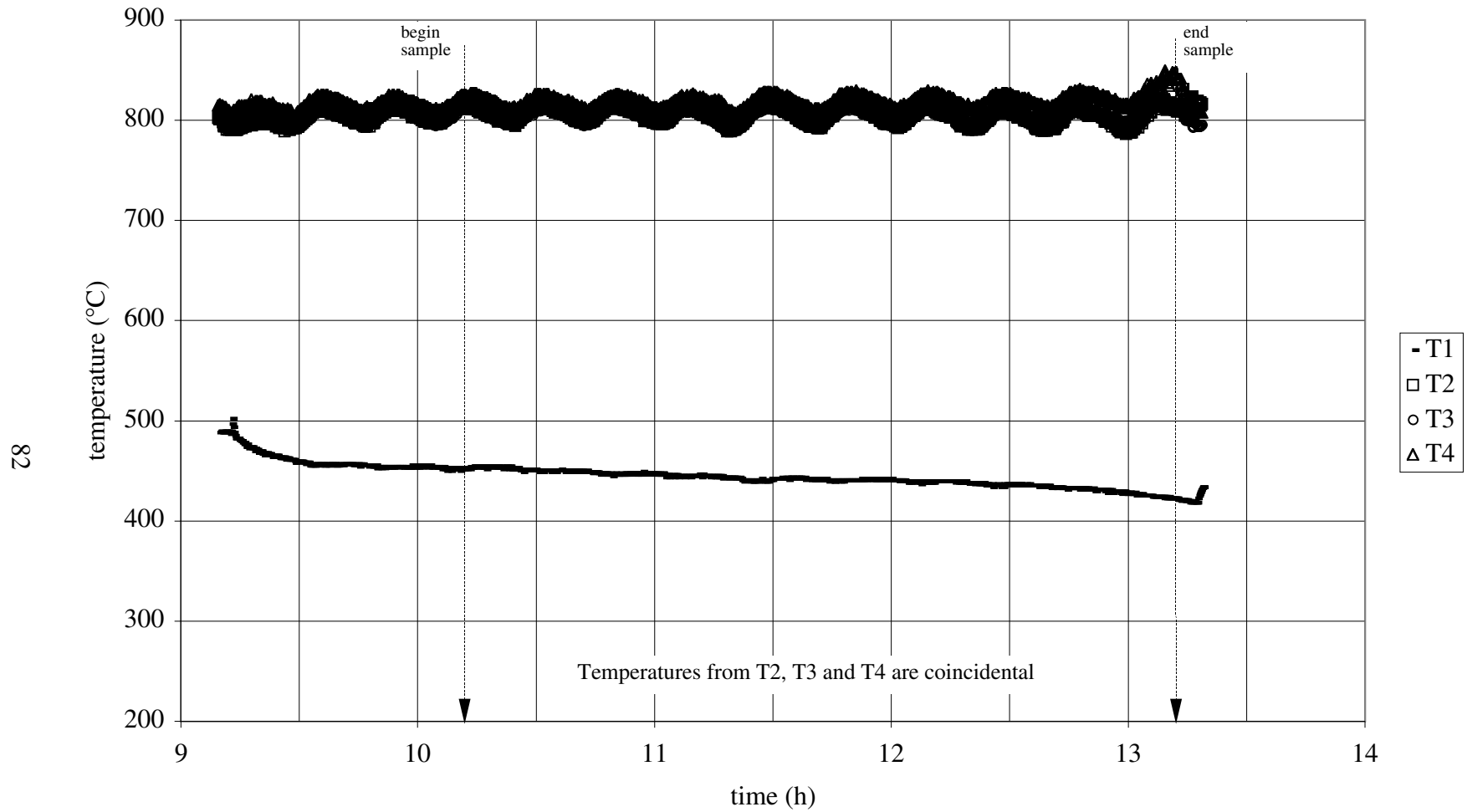


Figure A11. Thermocouple measurements of gasifier temperature below the distributor (T1), above the distributor (T2), and in the dense bed (T3 and T4) during Test 51G-E.

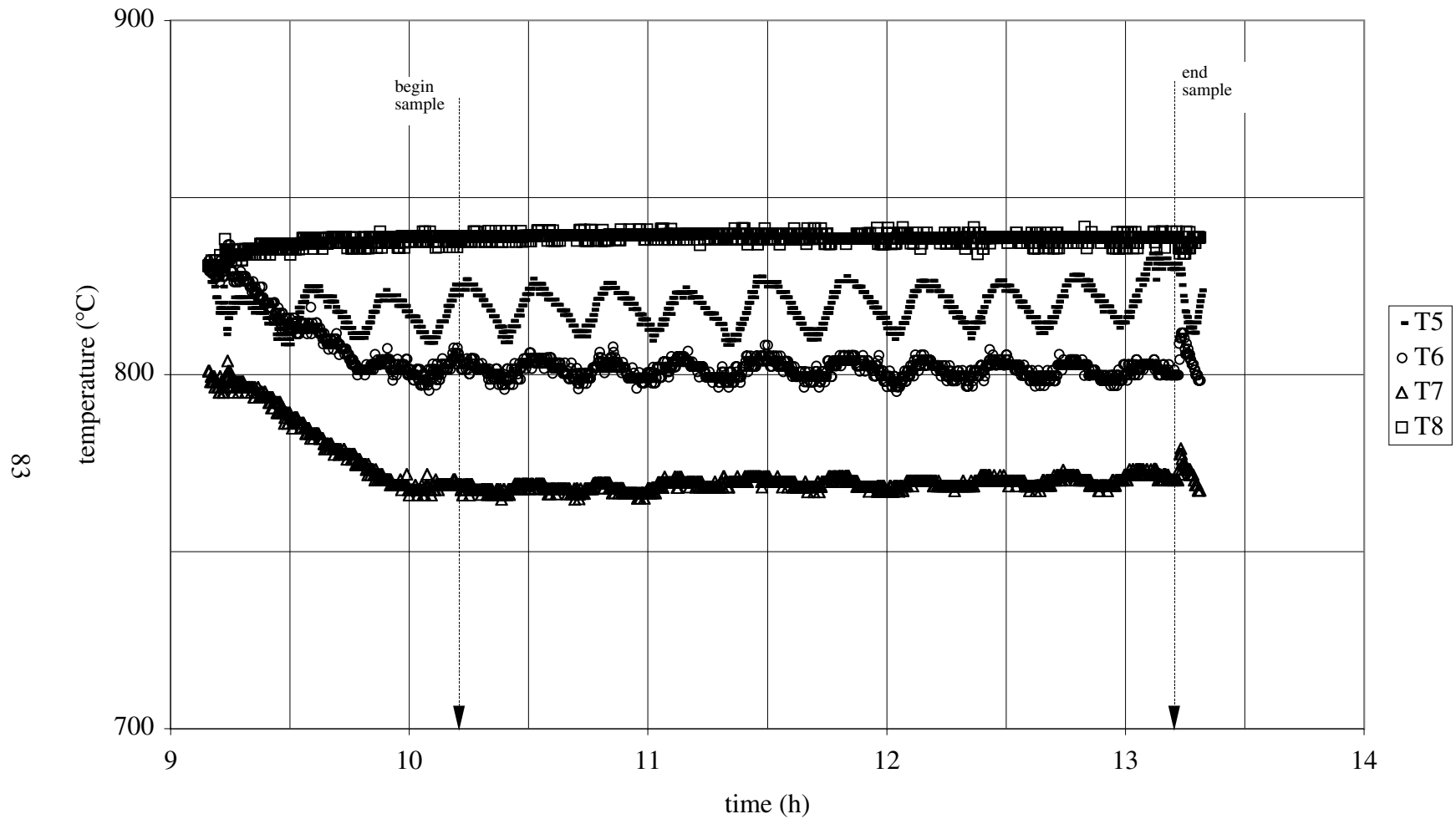


Figure A12. Thermocouple measurements of gasifier temperature in the dense bed (T5 and T6) and in the transition (T7) and disengagement zone (T8) during Test 51G-E.

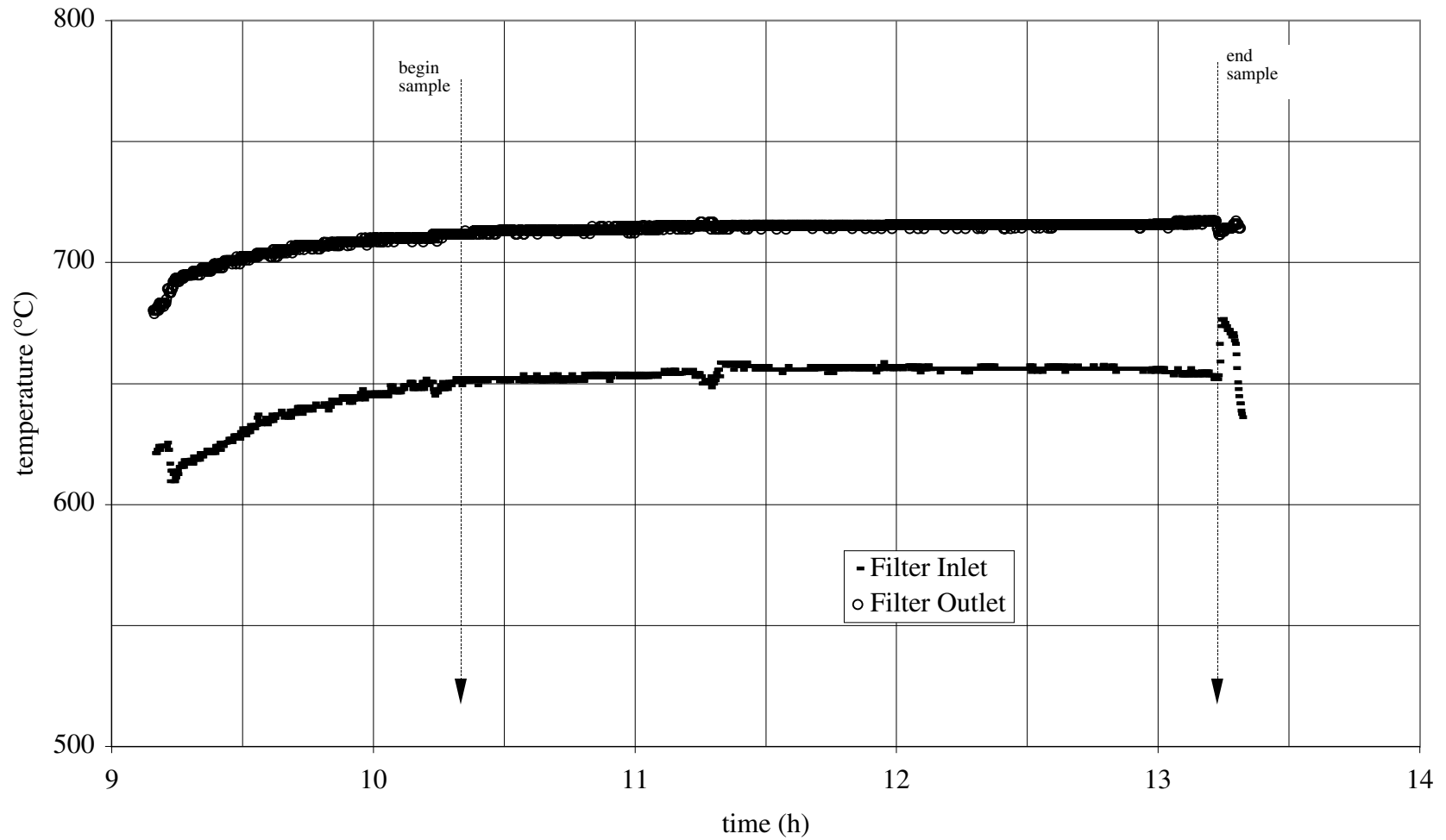


Figure A13. Thermocouple measurements of inlet and outlet temperatures in the heated ceramic filter unit during Test 51G-E.

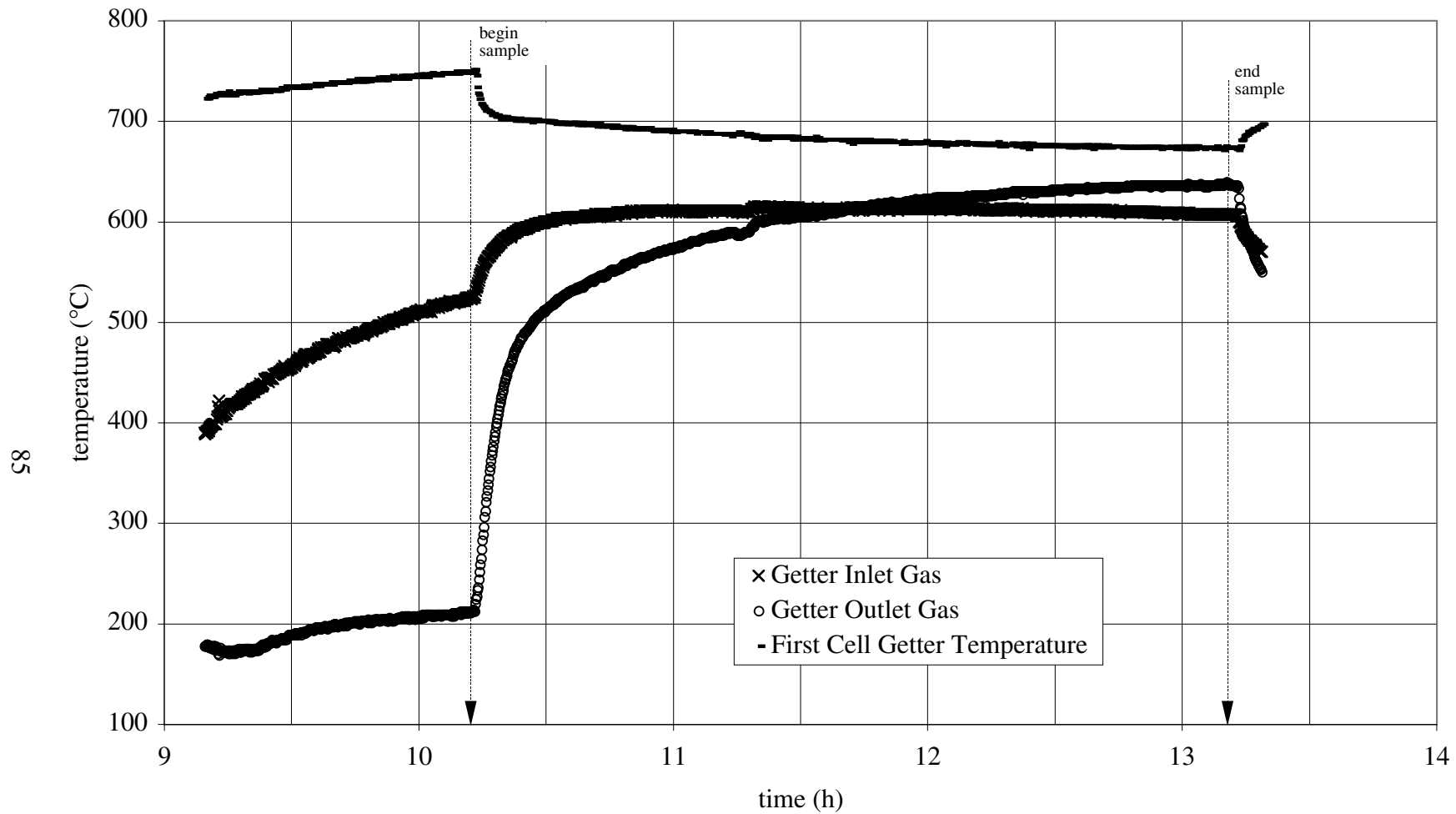


Figure A14. Thermocouple measurements of inlet gas stream, upper getter material surface, and outlet gas stream temperatures in the packed bed alkali getter reactor during 51G-E.

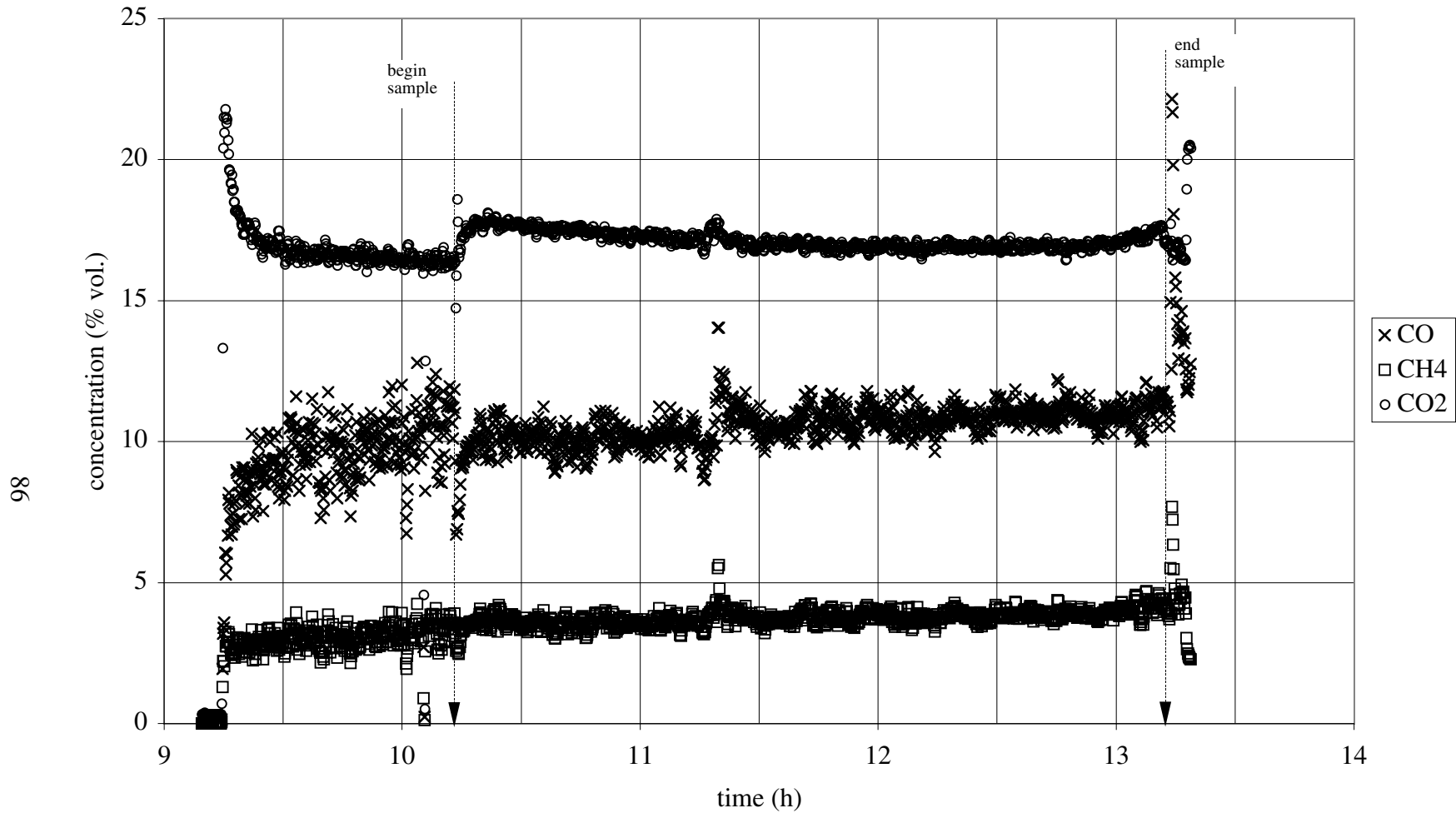


Figure A15. Product gas concentrations of CO, CO<sub>2</sub>, and CH<sub>4</sub> measured at the outlet of the packed bed alkali getter reactor during Test 51G-E.

## **Test 51G-AB**

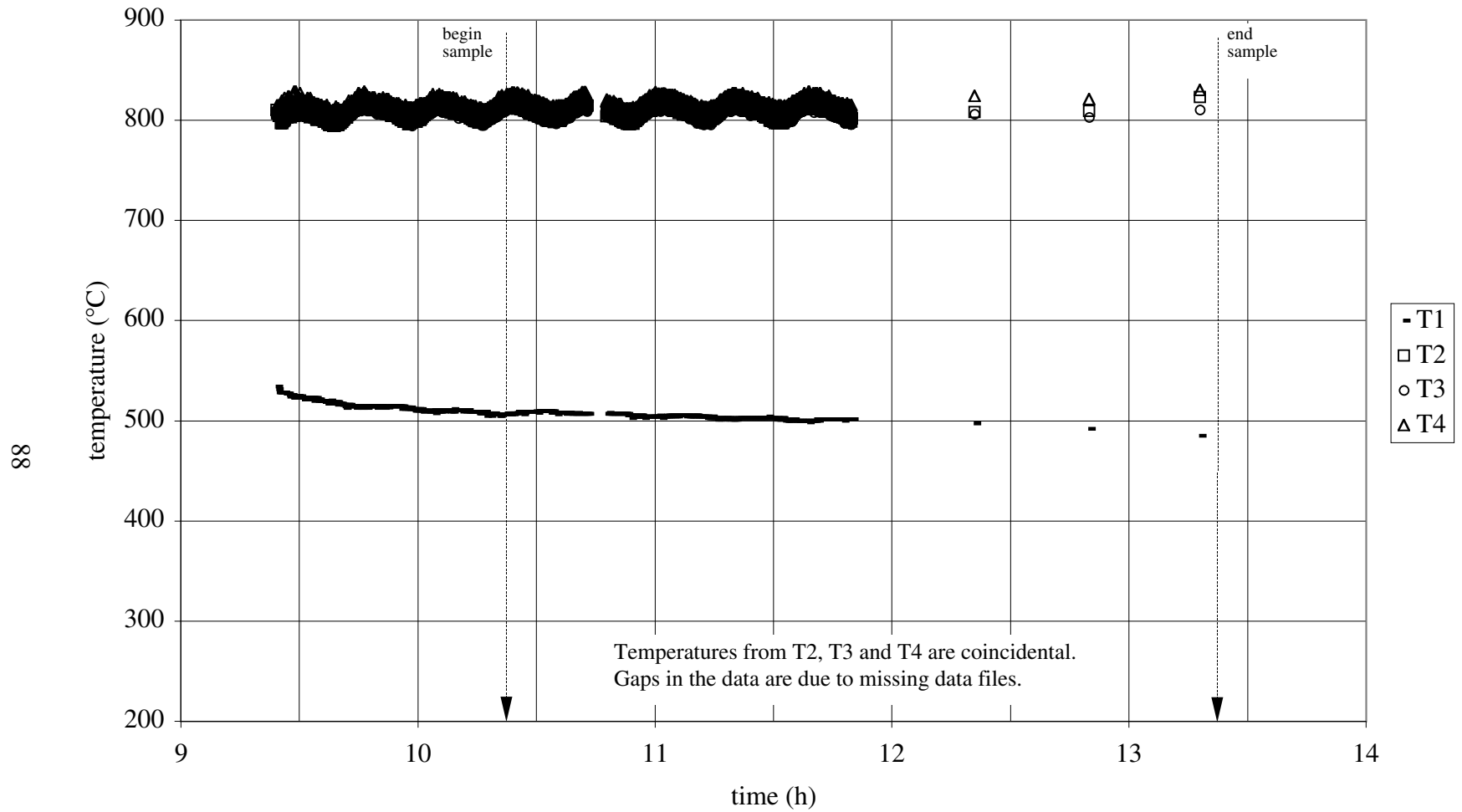


Figure A16. Thermocouple measurements of gasifier temperature below the distributor (T1), above the distributor (T2), and in the dense bed (T3 and T4) during Test 51G-AB.

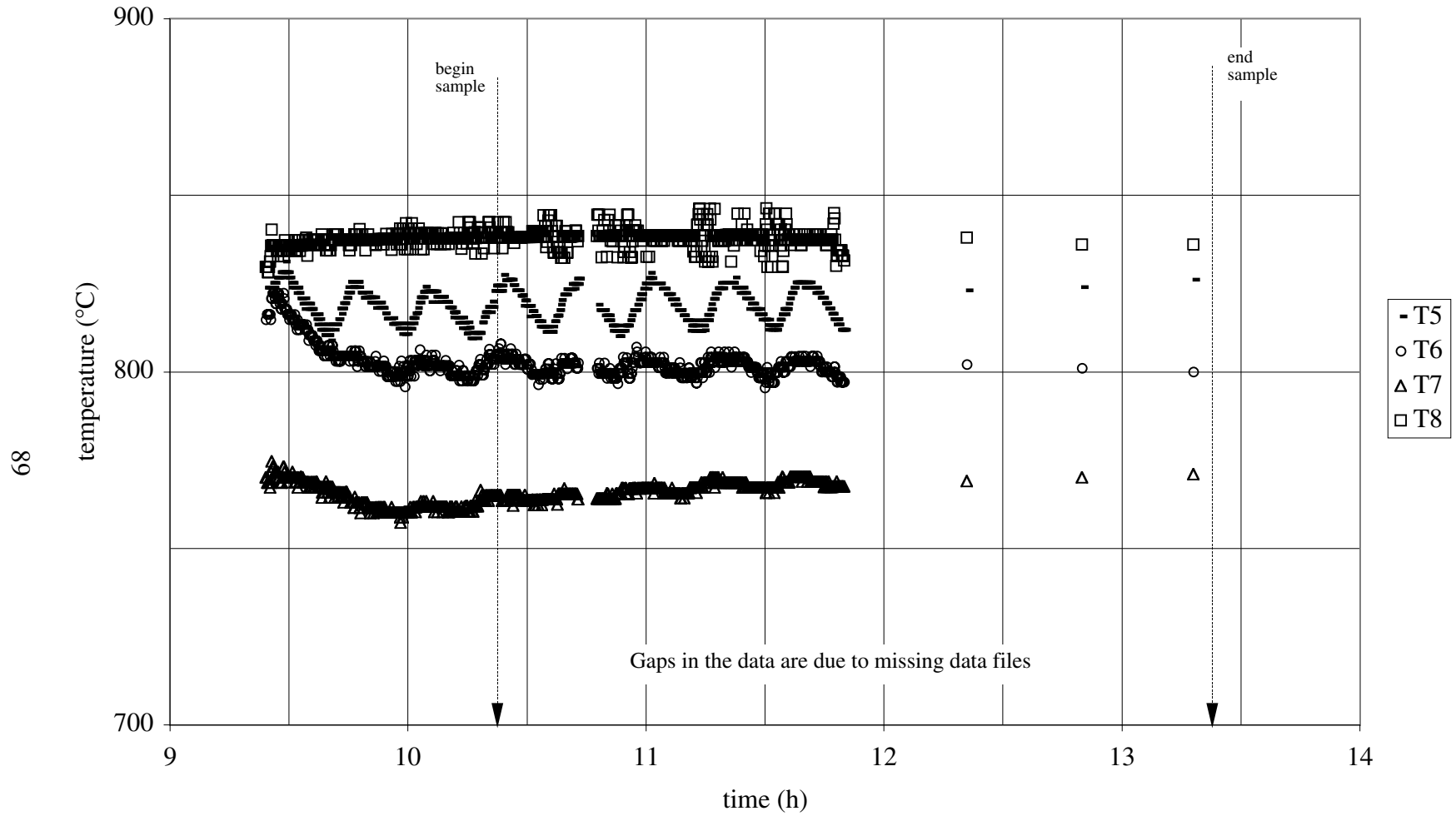


Figure A17. Thermocouple measurements of gasifier temperature in the dense bed (T5 and T6) and in the transition (T7) and disengagement zone (T8) during Test 51G-AB.

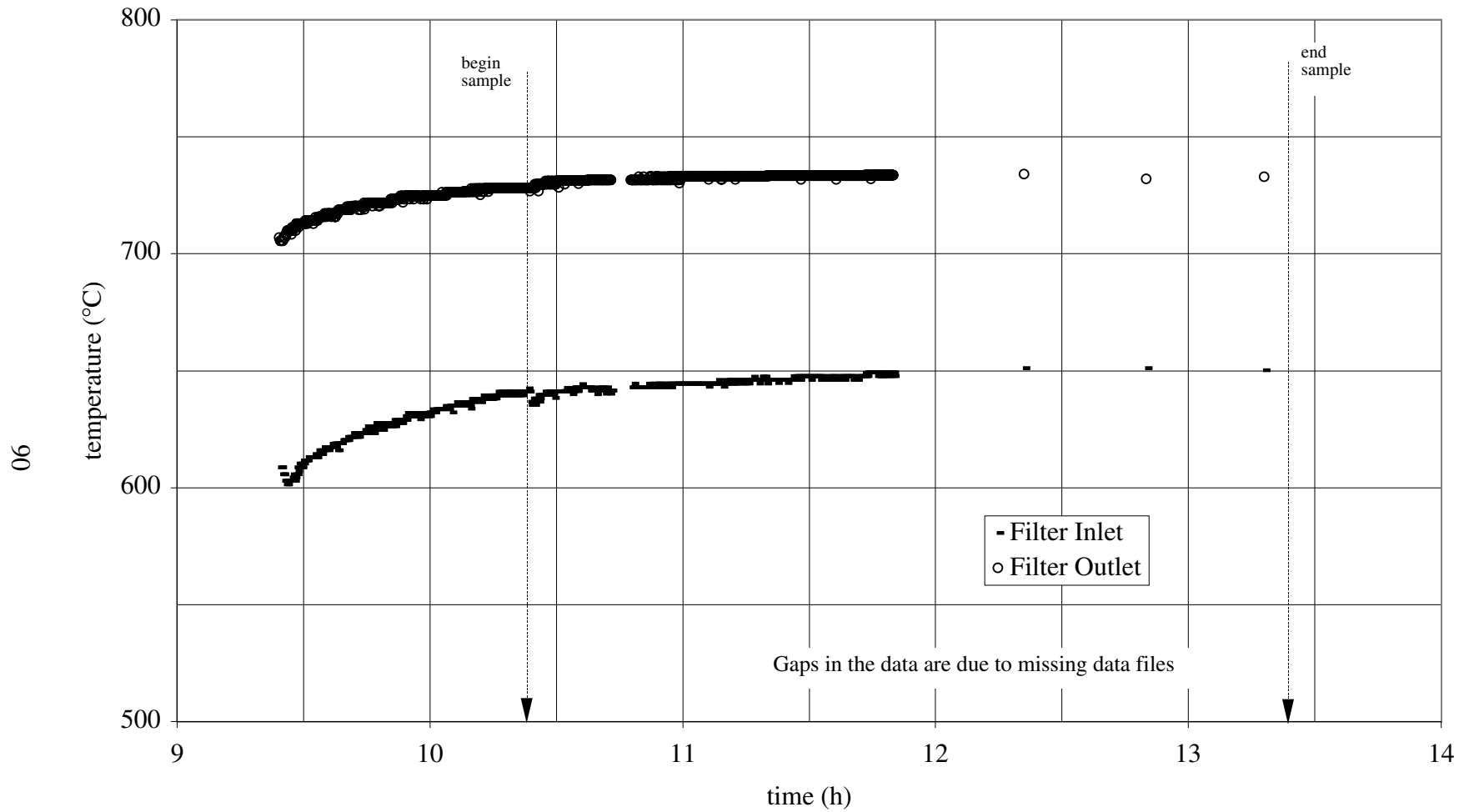


Figure A18. Thermocouple measurements of inlet and outlet temperatures in the heated ceramic filter unit during Test 51G-AB.

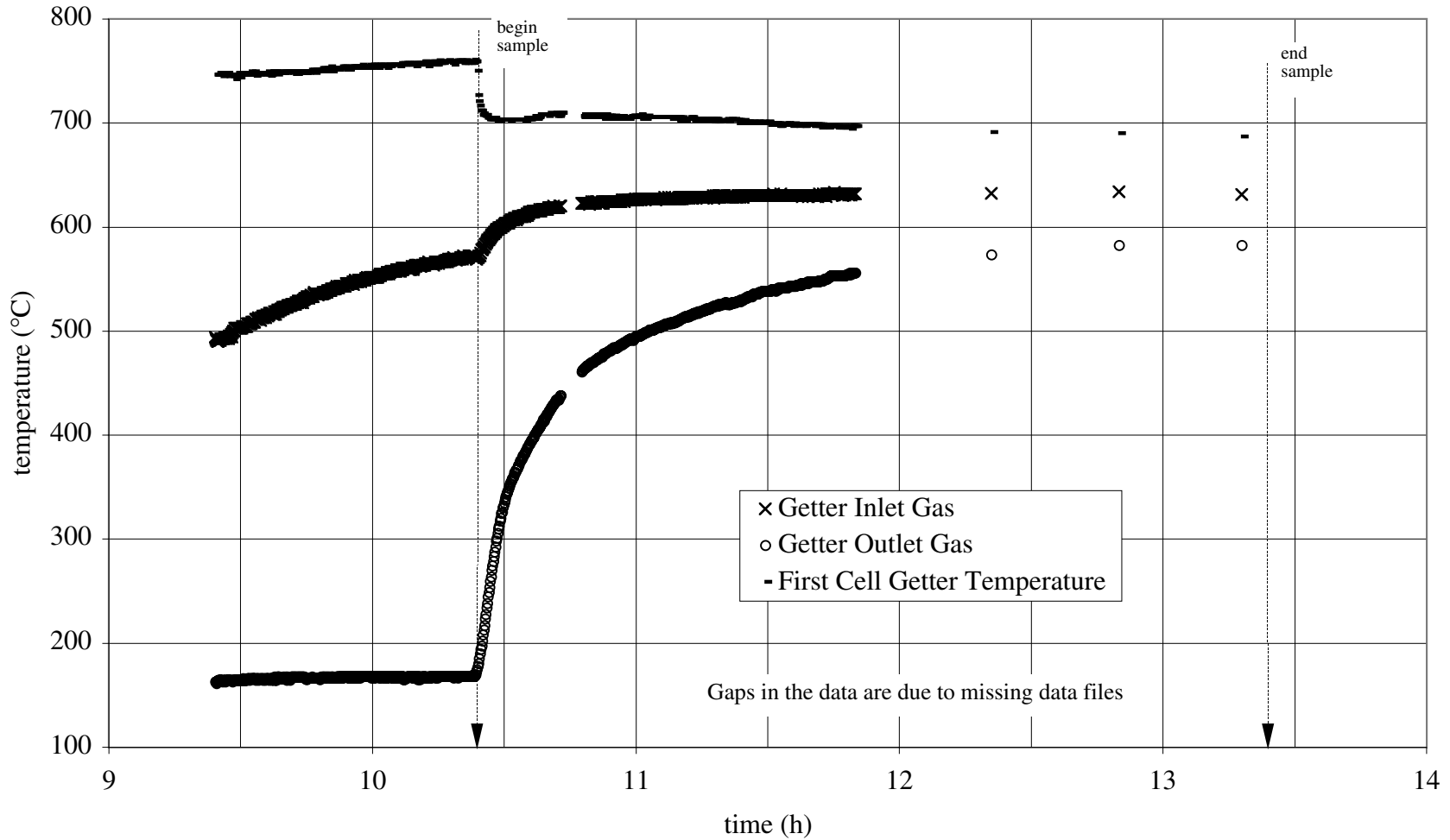


Figure A19. Thermocouple measurements of inlet gas stream, upper getter material surface, and outlet gas stream temperatures in the packed bed alkali getter reactor during Test 51G-AB.

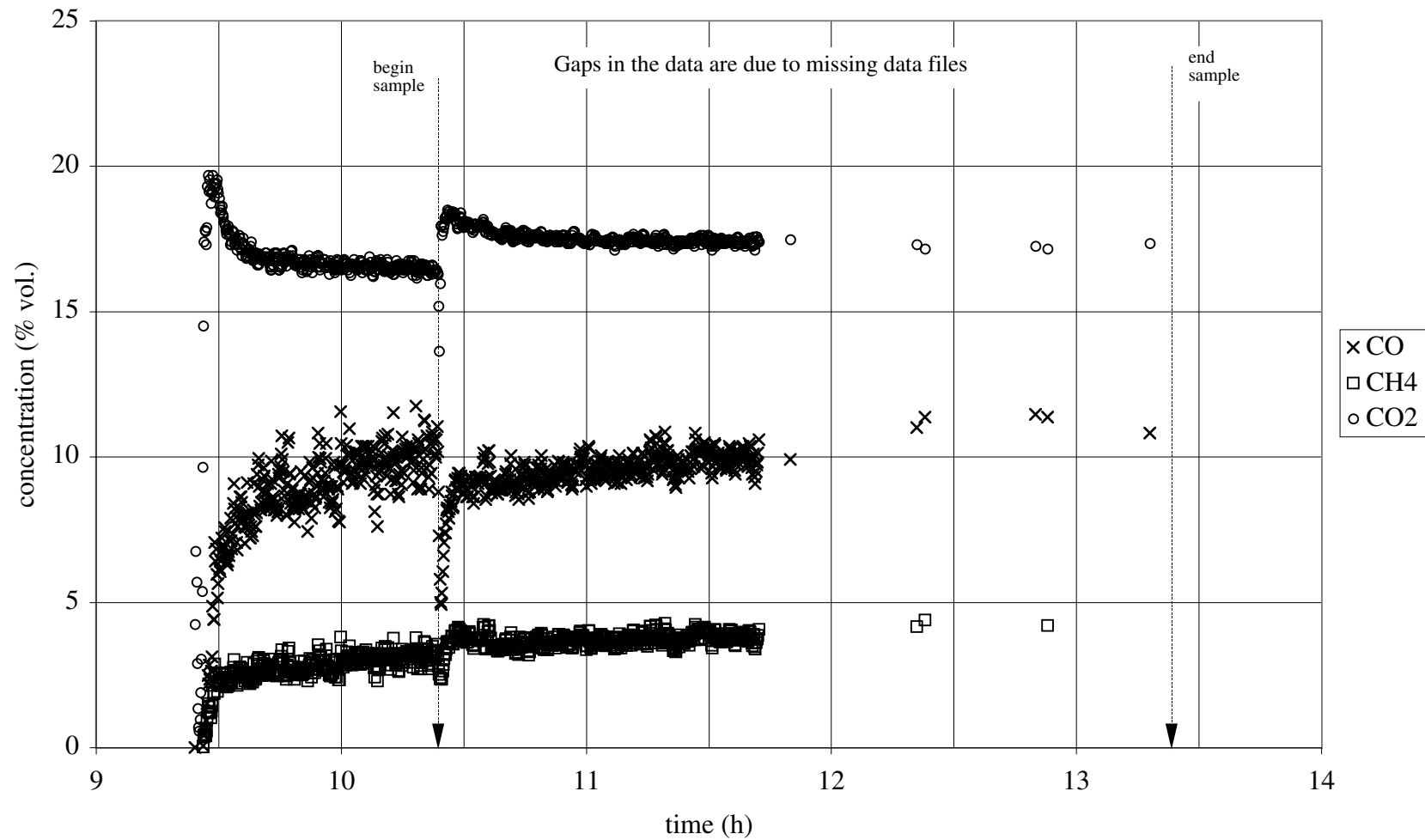


Figure A20. Product gas concentrations of CO, CO<sub>2</sub>, and CH<sub>4</sub> measured at the outlet of the packed bed alkali getter reactor during Test 51G-AB.

**Test 76G-E**

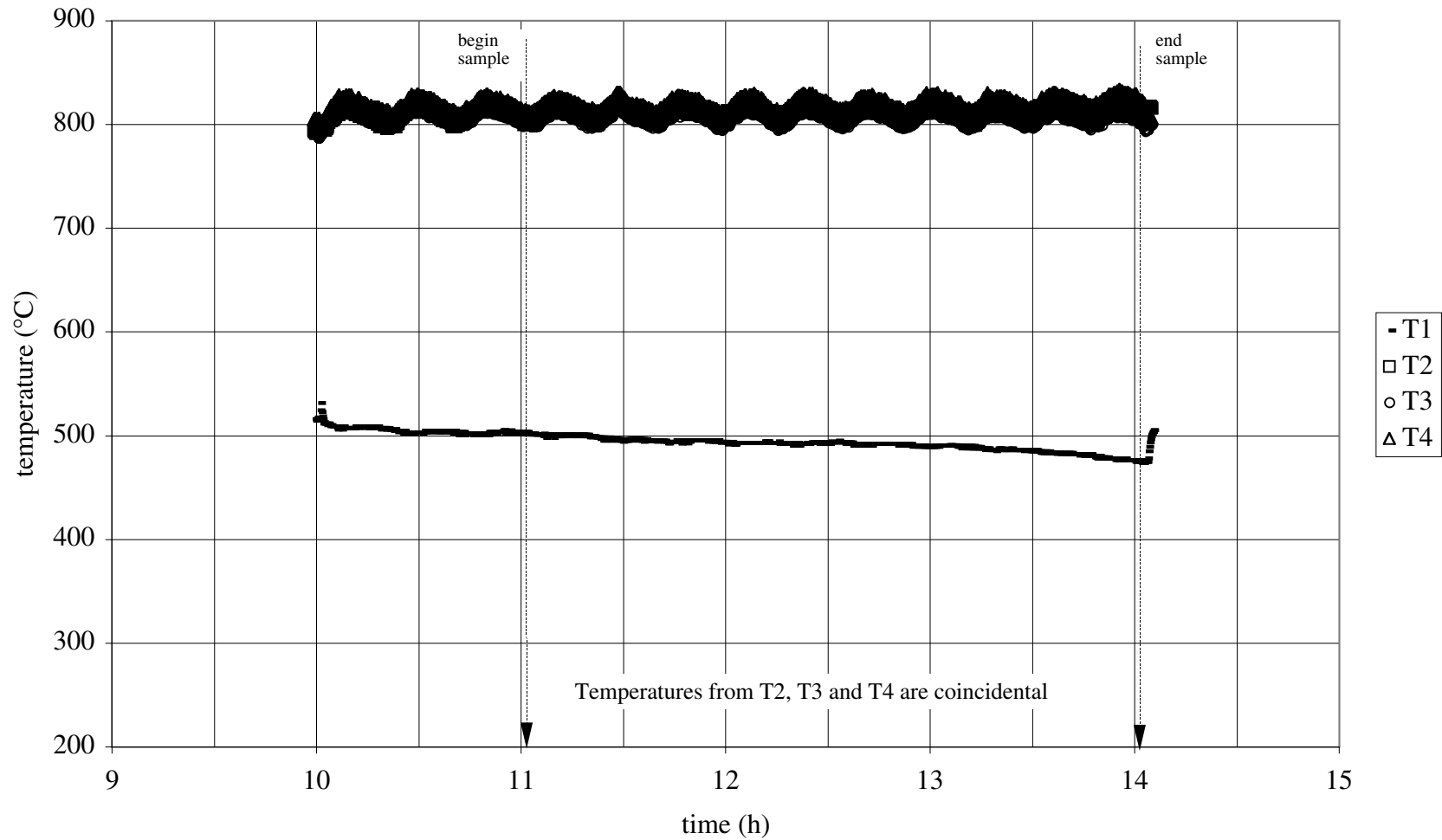


Figure A21. Thermocouple measurements of gasifier temperature below the distributor (T1), above the distributor (T2), and in the dense bed (T3 and T4) during Test 76G-E.

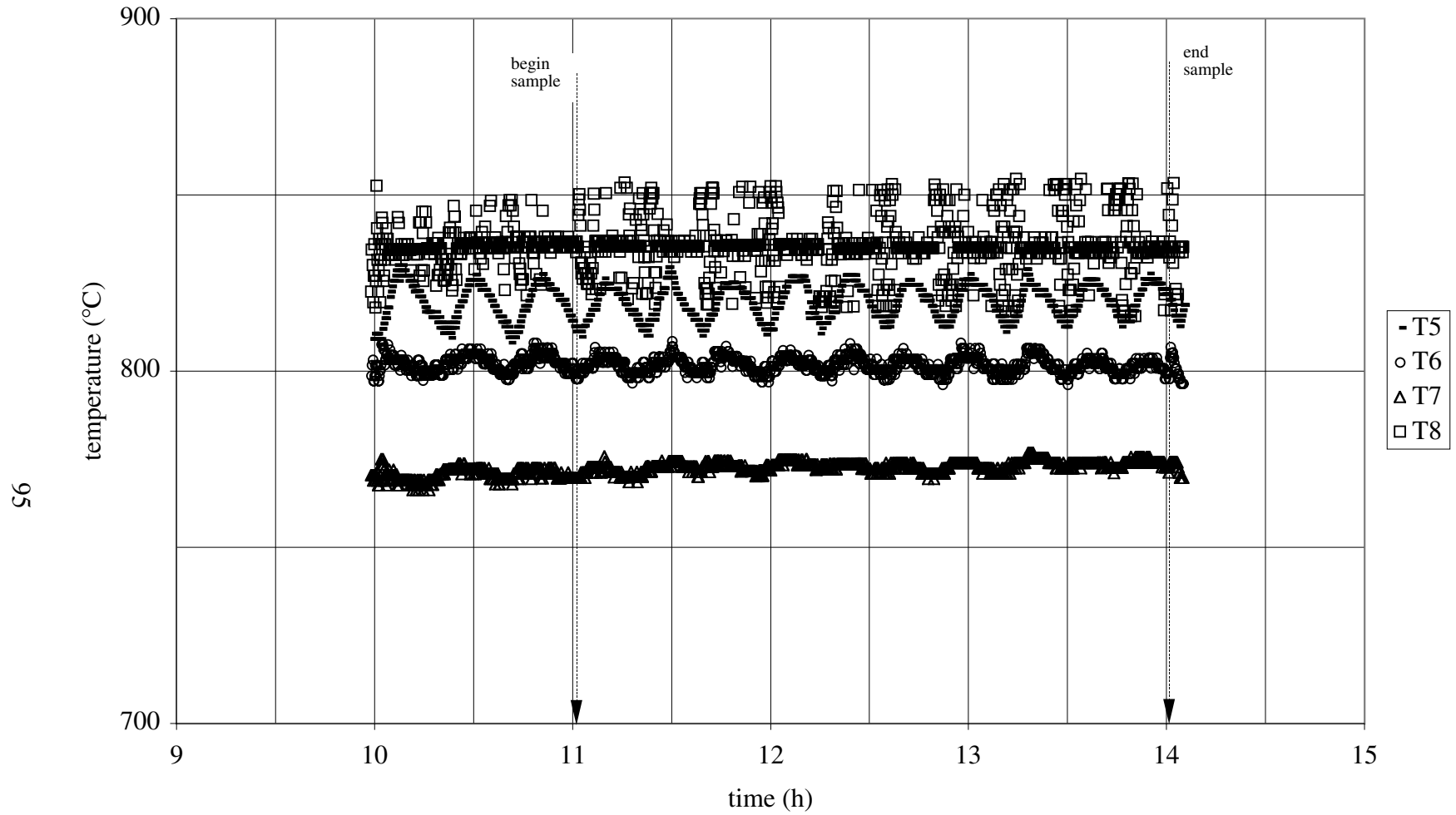


Figure A22. Thermocouple measurements of gasifier temperature in the dense bed (T5 and T6) and in the transition (T7) and disengagement zone (T8) during Test 76G-E.

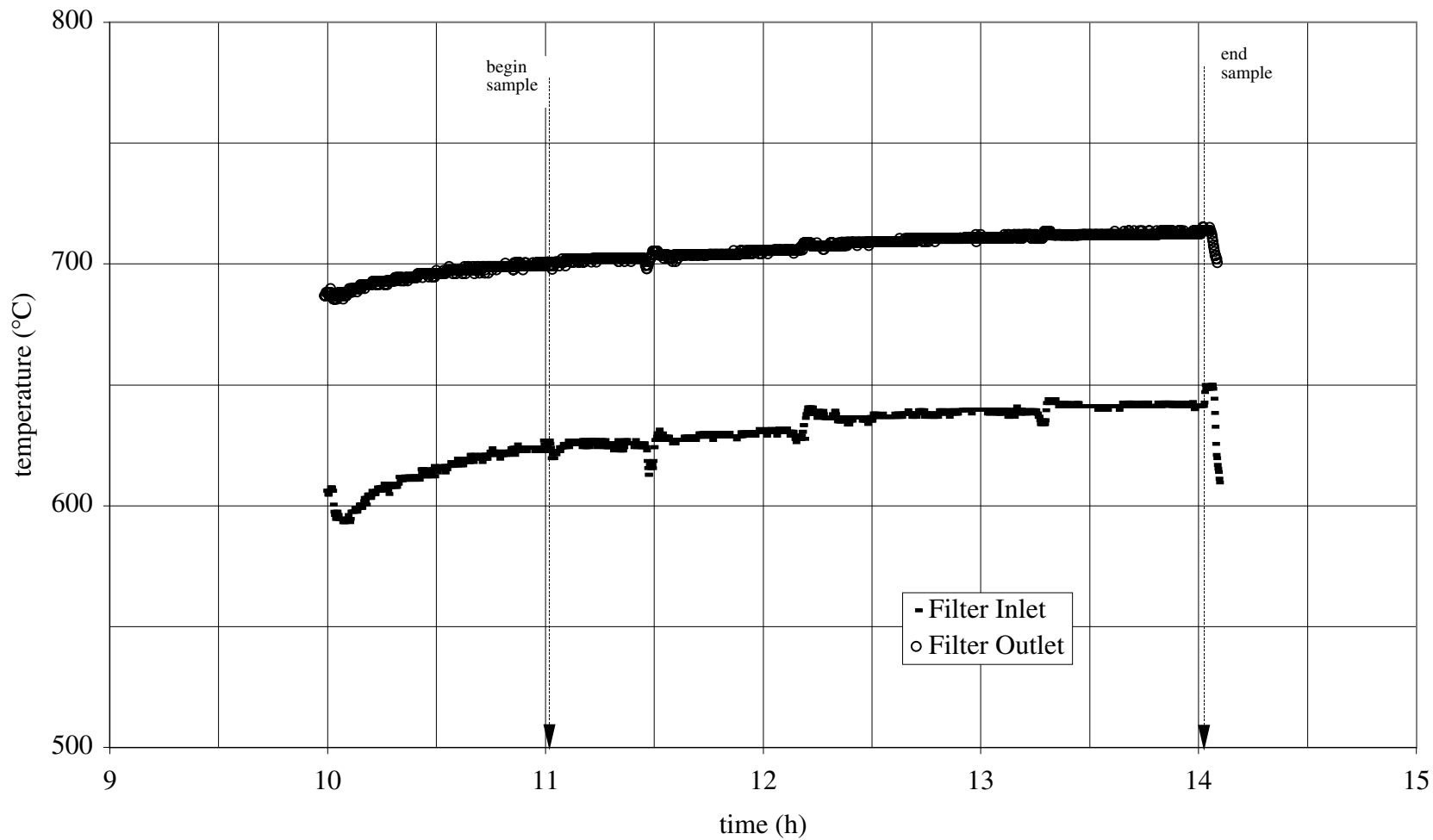


Figure A23. Thermocouple measurements of inlet and outlet temperatures in the heated ceramic filter unit during Test 76G-E.

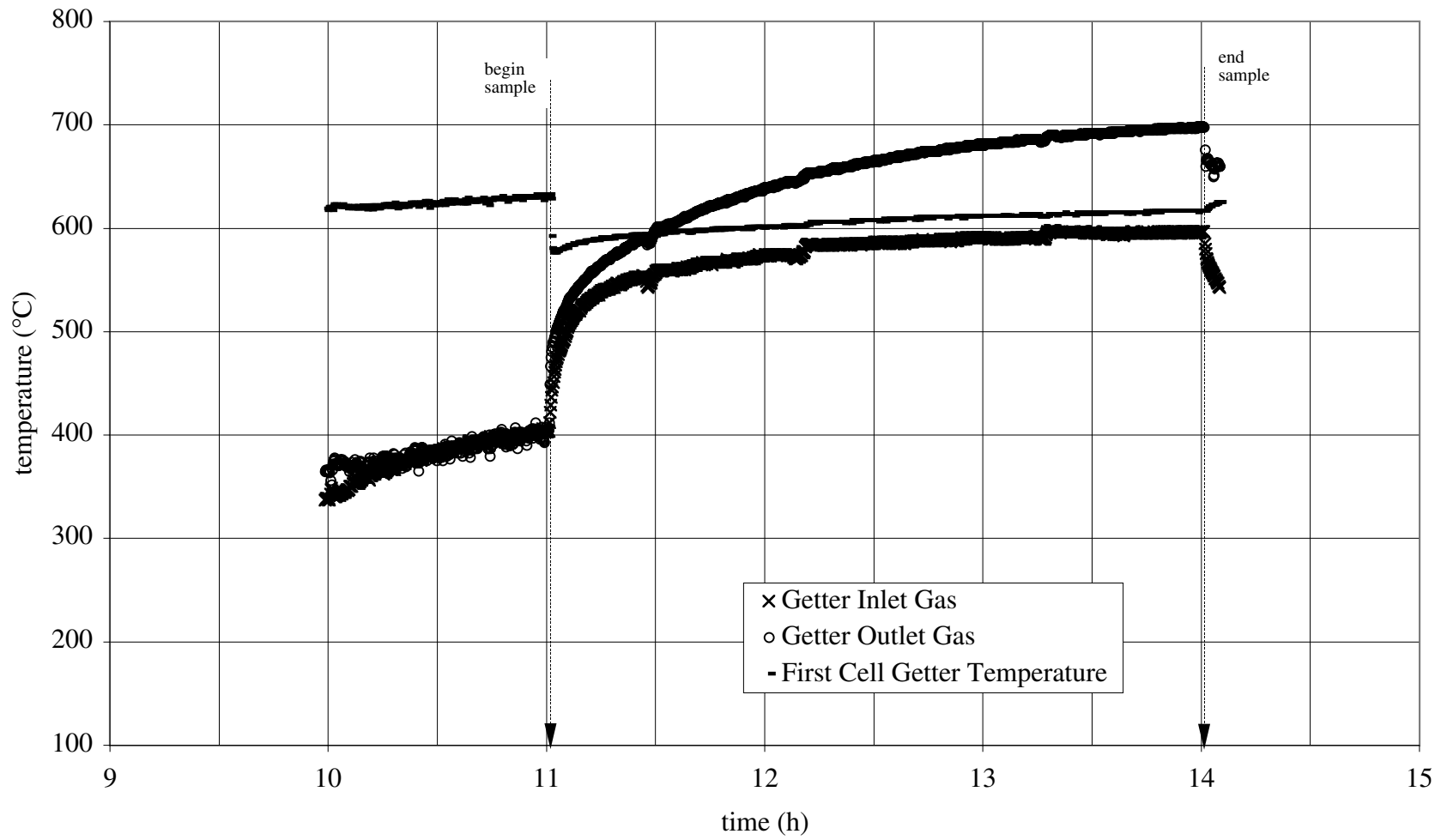


Figure A24. Thermocouple measurements of inlet gas stream, upper getter material surface, and outlet gas stream temperatures in the packed bed alkali getter reactor during 76G-E.

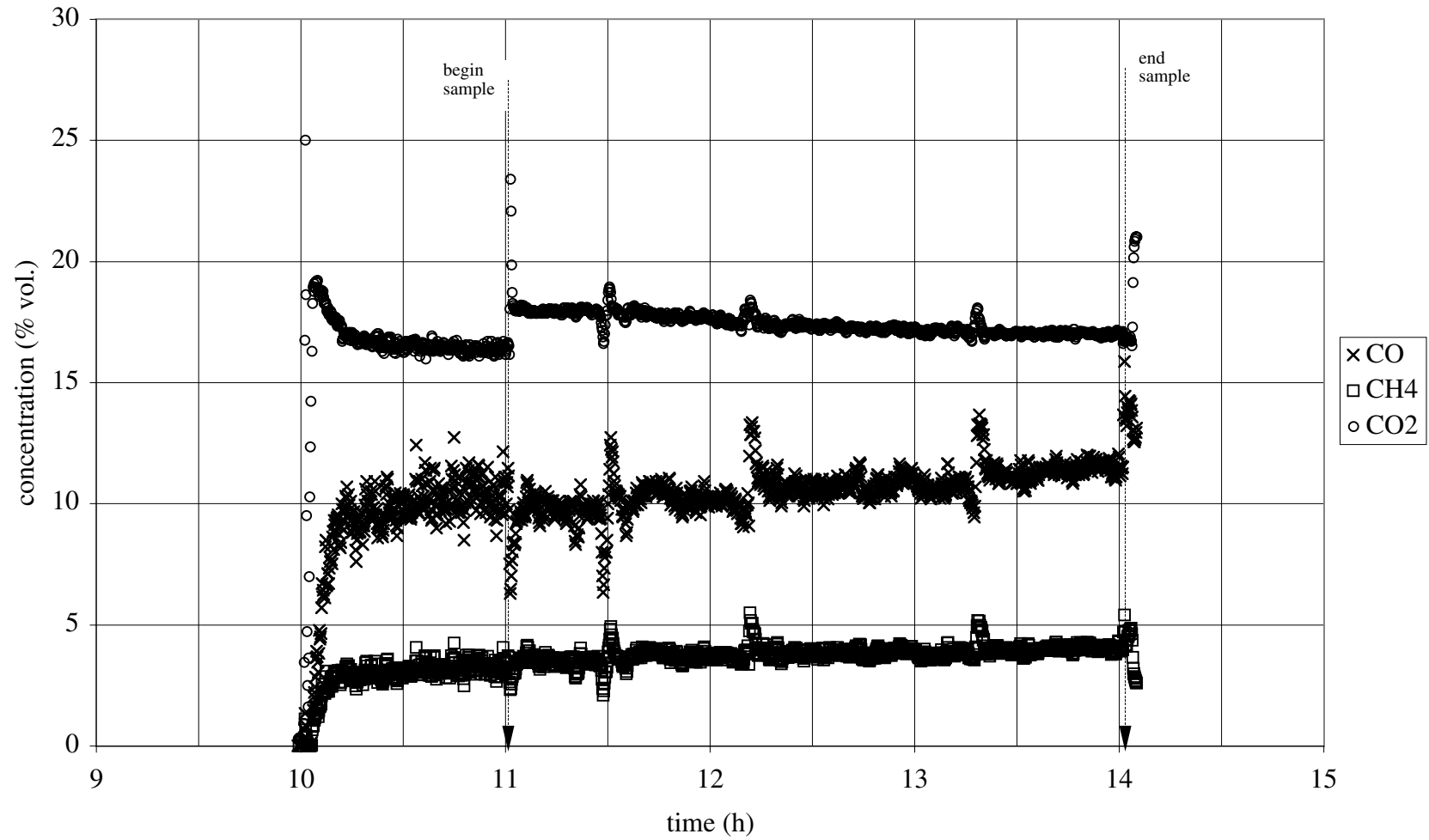


Figure A25. Product gas concentrations of CO, CO<sub>2</sub>, and CH<sub>4</sub> measured at the outlet of the packed bed alkali getter reactor during Test 76G-E.

**Test 51G-E-P**

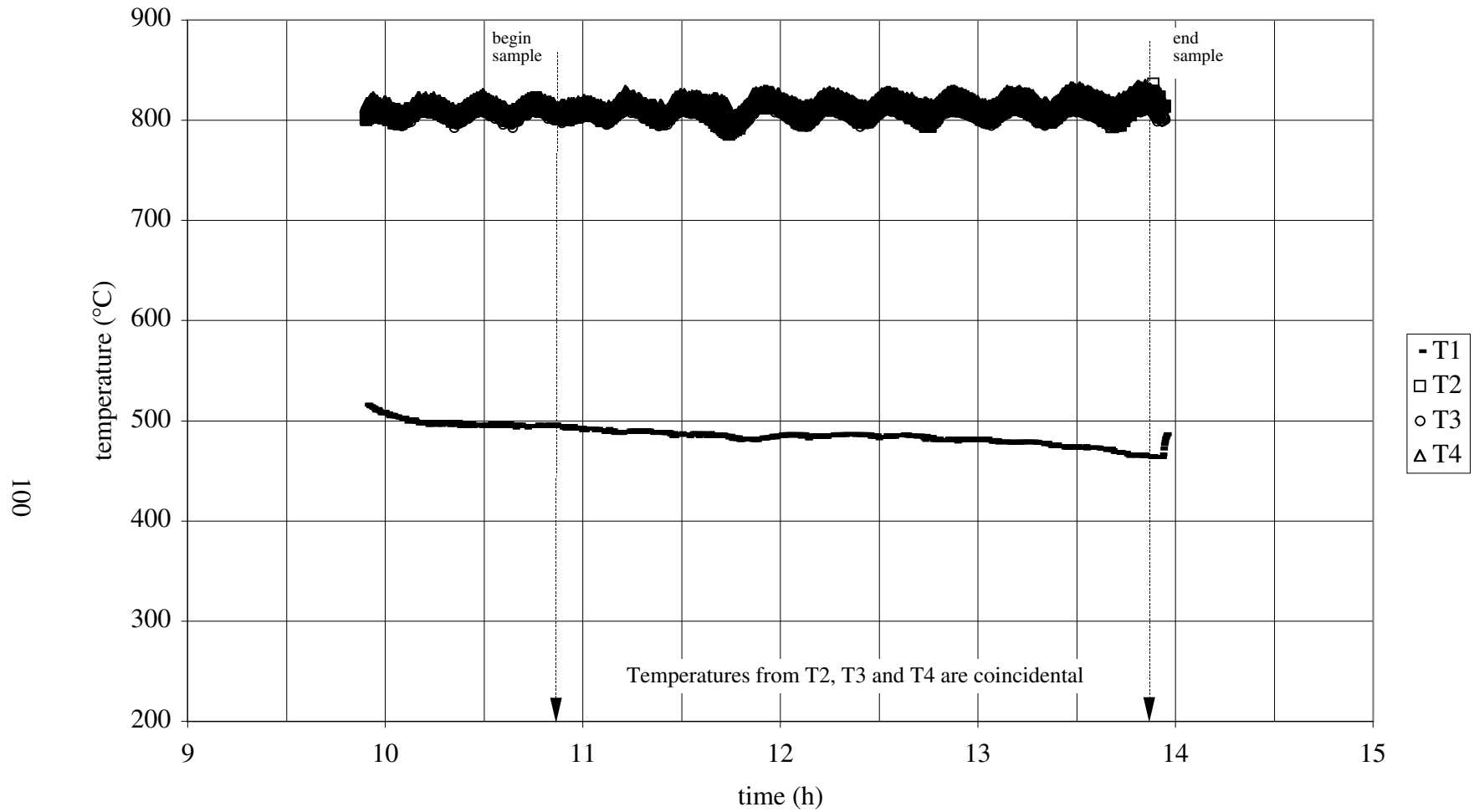


Figure A26. Thermocouple measurements of gasifier temperature below the distributor (T1), above the distributor (T2), and in the dense bed (T3 and T4) during Test 51G-E-P.

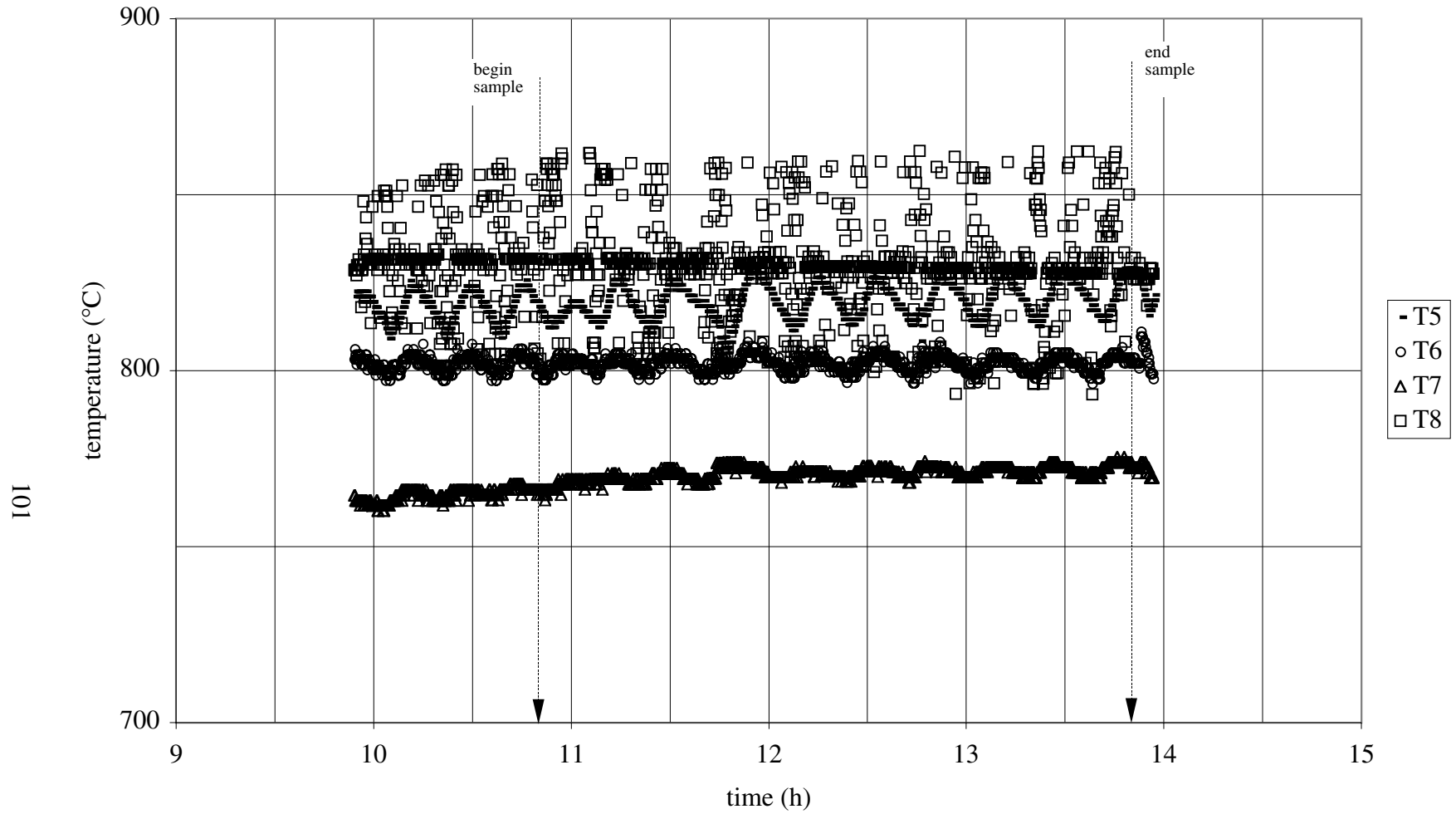


Figure A27. Thermocouple measurements of gasifier temperature in the dense bed (T5 and T6) and in the transition (T7) and disengagement zone (T8) during Test 51G-E-P.

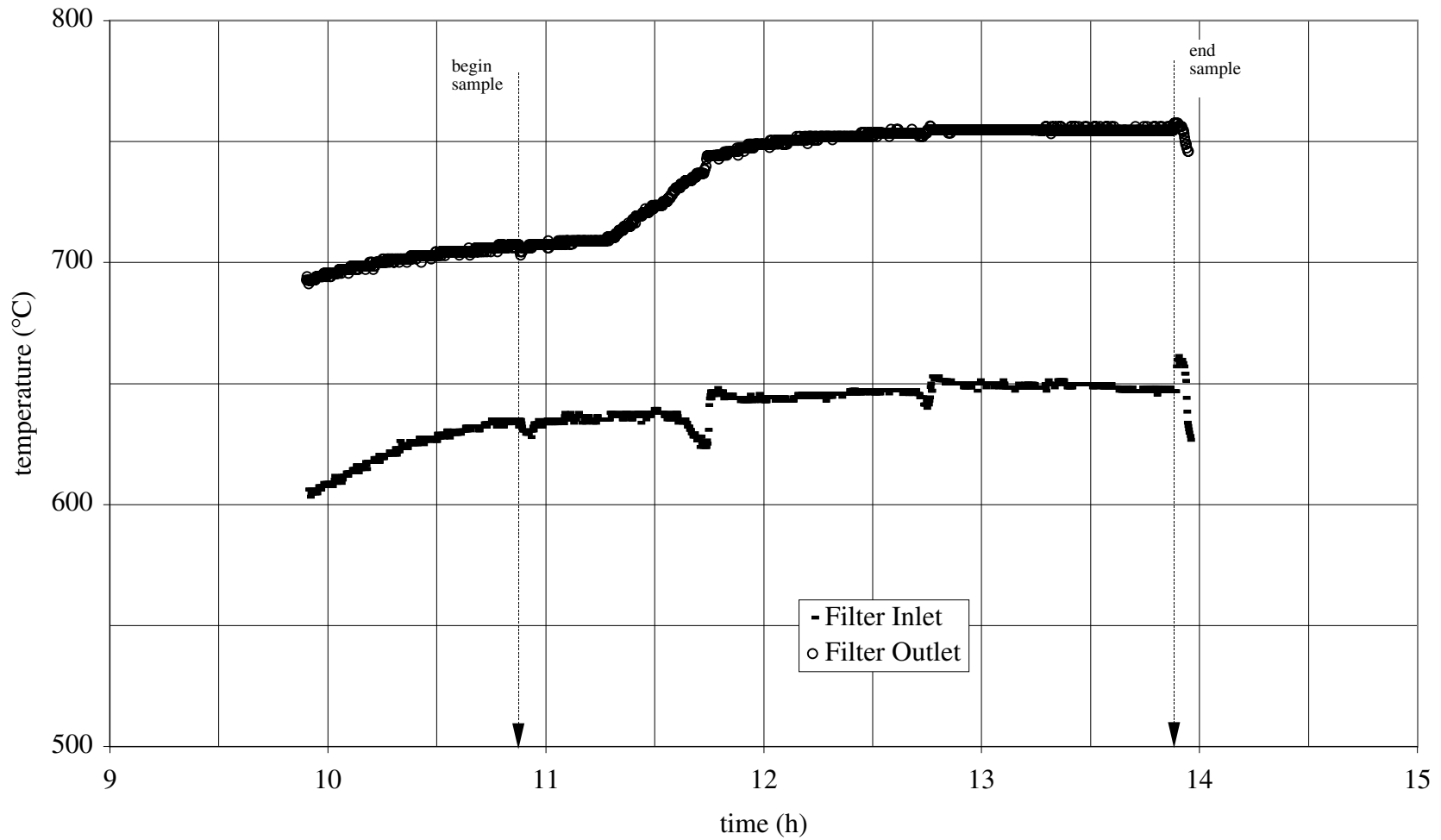


Figure A28. Thermocouple measurements of inlet and outlet temperatures in the heated ceramic filter unit during Test 51G-E-P.

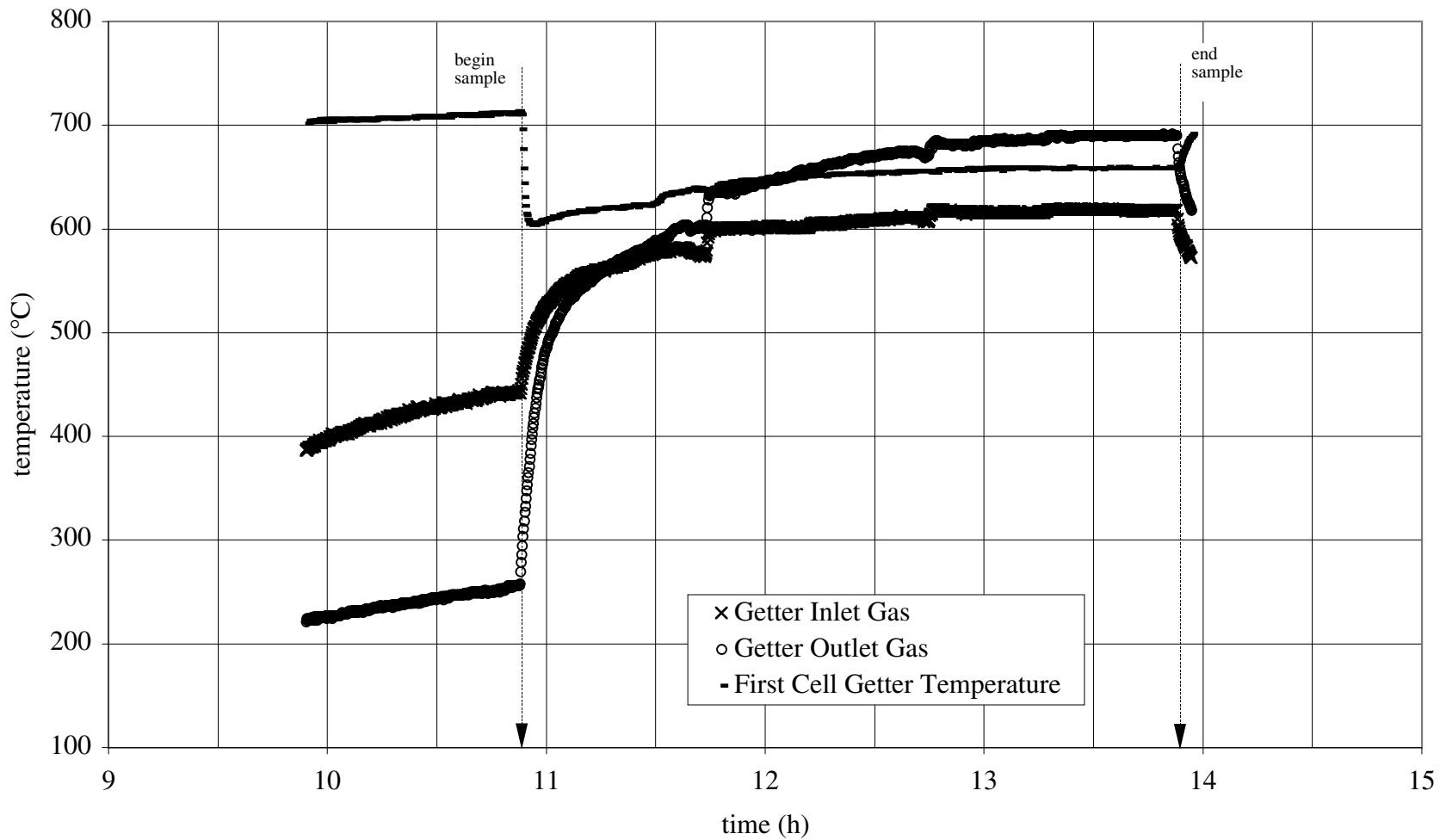


Figure A29. Thermocouple measurements of inlet gas stream, upper getter material surface, and outlet gas stream temperatures in the packed bed alkali getter reactor during Test 51G-E-P.

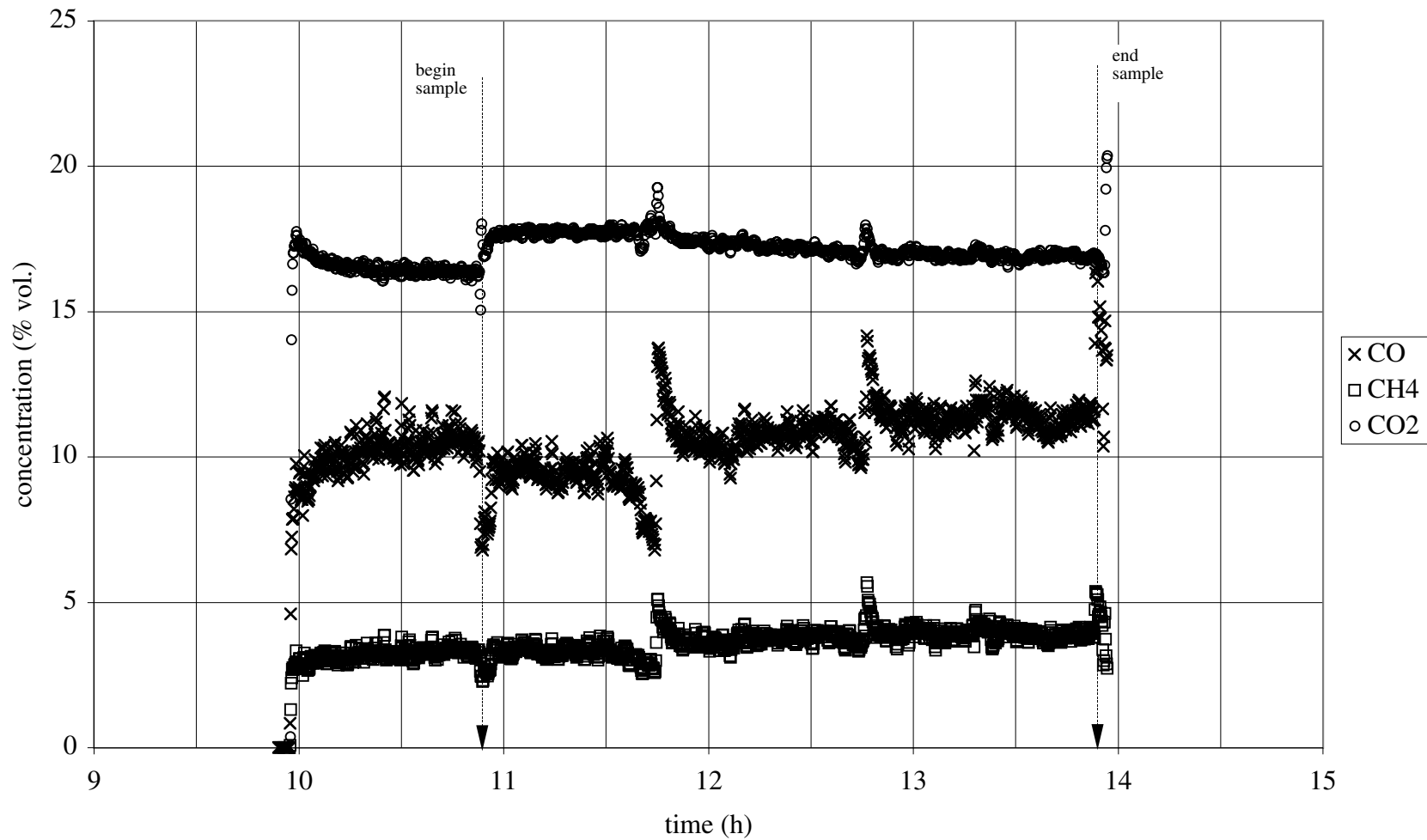


Figure A30. Product gas concentrations of CO, CO<sub>2</sub>, and CH<sub>4</sub> measured at the outlet of the packed bed alkali getter reactor during Test 51G-E-P.

REPORT DOCUMENTATION PAGE			Form Approved OMB NO. 0704-0188	
Public reporting burden for this collection of information is estimated to average 1 hour per response, including the time for reviewing instructions, searching existing data sources, gathering and maintaining the data needed, and completing and reviewing the collection of information. Send comments regarding this burden estimate or any other aspect of this collection of information, including suggestions for reducing this burden, to Washington Headquarters Services, Directorate for Information Operations and Reports, 1215 Jefferson Davis Highway, Suite 1204, Arlington, VA 22202-4302, and to the Office of Management and Budget, Paperwork Reduction Project (0704-0188), Washington, DC 20503.				
1. AGENCY USE ONLY (Leave blank)	2. REPORT DATE  July 2000	3. REPORT TYPE AND DATES COVERED  Subcontract Report		
4. TITLE AND SUBTITLE  Control of Alkali Species in Gasification Systems: Final Report			5. FUNDING NUMBERS  T: BP91.1010 C: YCV-7-16662-01	
6. AUTHOR(S) S. Turn, C. Kinoshita, D. Ishimura, J. Zhou, T. Hiraki, S. Masutani				
7. PERFORMING ORGANIZATION NAME(S) AND ADDRESS(ES)  Hawaii Natural Energy Institute School of Ocean and Earth Science and Technology University of Hawaii at Manoa 2540 Dole Street, Holmes Hall #246 Honolulu, HI 96822 (808) 956-8890			8. PERFORMING ORGANIZATION REPORT NUMBER	
9. SPONSORING/MONITORING AGENCY NAME(S) AND ADDRESS(ES) National Renewable Energy Laboratory 1617 Cole Blvd. Golden, CO 80401-3393			10. SPONSORING/MONITORING AGENCY REPORT NUMBER  NREL/SR-570-26160	
11. SUPPLEMENTARY NOTES  NREL Technical Monitor: Richard Bain				
12a. DISTRIBUTION/AVAILABILITY STATEMENT National Technical Information Service U.S. Department of Commerce 5285 Port Royal Road Springfield, VA 22161			12b. DISTRIBUTION CODE	
13. ABSTRACT ( <i>Maximum 200 words</i> ) Gas-phase alkali metal compounds contribute to fouling, slagging, corrosion, and agglomeration problems in energy conversion facilities. One mitigation strategy applicable at high temperature is the pass the gas stream through a fixed bed sorbent or getter material, which preferentially absorbs alkali via physical adsorption or chemisorption. This report presents results of an experimental investigation of high-temperature alkali removal from a hot filtered gasifier product gas stream using a packed bed of sorbent material. Two getter materials, activated bauxite and emathlite, were tested at two levels of space time by using two interchangeable reactors of different internal diameters. The effect of getter particle size was also investigated.				
14. SUBJECT TERMS alkali, gasification, energy conversion facility, adsorption, chemisorption, getter material, bauxite, emathlite			15. NUMBER OF PAGES	
			16. PRICE CODE	
17. SECURITY CLASSIFICATION OF REPORT Unclassified	18. SECURITY CLASSIFICATION OF THIS PAGE Unclassified	19. SECURITY CLASSIFICATION OF ABSTRACT Unclassified	20. LIMITATION OF ABSTRACT  UL	